Nasa Technical Memorandum 78574

Absolute Measurements of the Electronic Transition Moments of Seven Band Systems of the C_2 Molecule

David M. Cooper

April 1979

National Aeronautics and Space Administration

NASA Technical Memorandum 78574

Absolute Measurements of the Electronic Transition Moments of Seven Band Systems of the C_2 Molecule

David M. Cooper, Ames Research Center, Moffett Field, California

NASA
National Aeronautics and
Space Administration

Ames Research Center
Moffett Field, California 94035

TABLE OF CONTENTS

TABLE OF CONTENTS
(Continued)

TABLE OF CONTENTS
(Continued)

TABLE OF CONTENTS
(Concluded)

ABSOLUTE MEASUREMENTS OF THE ELECTRONIC TRANSITION MOMENTS OF SEVEN BAND SYSTEMS OF THE C_2 MOLECULE*

David M. Cooper

Ames Research Center

*Submitted in partial fulfillment of the degree of Doctor of Philosophy, York University, Toronto, Ontario.

Chapter 1

Introduction

1.1 Rationale for Study

The abundance of carbon on earth as well as its occurrence in celestial bodies has resulted in research over the past century that has determined many of the important physical and chemical properties of the C_2 molecule. In addition, the relative ease of exciting C_2 has led to the discovery of many of its spectroscopic features and molecular constants. However, the absolute strengths of the band systems of C_2 are virtually unknown. This thesis presents the results of a series of experimental tests designed to measure the electronic transition moments of the Ballik-Ramsay, Phillips, Swan, Deslandres-d'Azambuja, Fox-Herzberg, Mulliken, and Freymark systems of C_2.

The importance and usefulness of these measurements are stated in the following section. A brief description of the problem and the experimental technique chosen for its solution are also included. The last section of this chapter is a synopsis of the thesis.

1.1.1 C_2 Band Spectra Occurrences and Uses

The band systems of C_2 are easily observed in both absorption and emission in a wide variety of sources. These sources vary in sophistication from an ordinary candle flame to the bow shock wave formed on a multimillion dollar planetary entry probe. Several of the more important occurrences of C_2 band spectra are discussed below.

C_2 band systems are excited in virtually all combustion and explosion processes and are often used diagnostically in flame and combustion spectroscopy. Vibrational and rotational temperature

determinations from C_2 spectra not only indicate the temperature of the luminous source but also serve as a diagnostic of local thermodynamic equilibrium. Unknown C_2 concentrations in a flame or other source can be obtained from measurements of the spectral emission of C_2 lines or band systems if the absolute strength of the band system is known.

Band spectra of C_2 are easily excited by shock heating gases containing carbon compounds. This method produces large concentrations of C_2 in a local thermodynamic equilibrium environment. Consequently the shock tube is often used for spectroscopic investigations of C_2. An additional source of shock excited C_2 spectra is the bow shock wave on planetary entry probes. Whiting et al. (1973) have demonstrated the feasibility of determining the composition of planetary atmospheres by measuring the emission from the heated atmospheric gases in the region between the bow shock wave and the probe body. In this technique, a measurement of the emission of band systems in selected spectral regions can be used accurately to determine the composition of an unknown atmosphere. This is only possible if the electronic transition moment of the band system being measured is well established.

Carbon-containing compounds are candidate materials for the heat shield of outer planet entry probes. As a result of the high heating rates encountered by the probe, the outer surface of the heat shield material vaporizes and collects in the boundary layer. These ablation products in the boundary layer, of which C_2 is a major constituent, absorb radiation directed toward the body by the shock layer and can substantially reduce the radiative flux reaching the probe surface. The band systems of C_2 occur in the spectral region from below 0.2 to over

2.0 μ and thus they can play a major role in absorbing the radiation in this wavelength range directed toward the body. The amount of radiation absorbed is controlled by the relevant absorption coefficients which depend on the absolute strength of the respective band systems. Consequently, in order to evaluate the carbon heat shield effectively, the electronic transition moments of the C_2 systems must be accurately known.

Astrophysically, the C_2 molecule is very abundant and of great importance (Herzberg, 1950). The band systems of C_2 are so prominent in the atmospheres of the cooler type R and N stars that they are also known as carbon stars. Observed band intensities of the C_2 transitions can be used to obtain stellar abundances (Fujita, 1970). The intensity ratio of the isotopic bands $C^{12}C^{12}$ and $C^{12}C^{13}$ can be used to infer abundance ratios of isotopes in stellar atmospheres (Climenhaga, 1960). The relative intensities of individual rotational lines in a given vibrational sequence and different vibrational sequences of the same band have been used to determine temperatures of stellar atmospheres (Aller, 1964).

C_2 band systems have also been identified in the spectra of the photosphere of the sun, sunspots, and comet heads. Therefore, these band systems can be used as valuable diagnostic aids by astronomers and astrophysicists if the molecular constants are well documented.

Additional sources of C_2 spectra are discharge tubes containing CO and rare gases, electric furnaces, and carbon arc discharges. Phillips and Davis (1970) for example have used all three of these sources to produce spectra for an extensive analysis of 36 bands of the Swan

system. Similar extensive analyses of the other C_2 band systems are unfortunately not available.

Thus it is apparent that there is sufficient interest and need to justify a comprehensive experimental program to measure the absolute strengths of the band systems of the C_2 molecule. The program to accomplish this is described in detail below.

1.1.2 Definition of Problem

Simply stated, the goal of this thesis was to measure the absolute value of the electronic transition moments of C_2 band systems in the spectral region between 0.2 and 1.2 μ. Since several of these band systems are relatively weak, a source which supplies a high concentration (approximately 10^{17} particles/cm^3) of C_2 particles was required. An additional requirement (for ease of data reduction) is that the C_2 particles exist in a local thermodynamic equilibrium environment whose physical properties are well known. A shock tube is one source which fulfills these requirements and was selected because of the author's familiarity with shock-tube facilities and of the existence of a fine spectroscopic shock-tube laboratory at Ames Research Center. Gaseous C_2 was produced by shock heating a mixture of argon and acetylene (C_2H_2). The radiation from this heated gas was measured using spectrally and absolutely calibrated radiometers. The electronic transition moments of the band systems were obtained by the synthetic spectrum analysis of the absolute intensity data.

This project is a cooperative effort between Ames Research Center and York University. The experimental tests were supported by and done at Ames Research Center. This work continues the effort of R. W.

Nicholls and his colleagues and students at The University of Western Ontario and York University to determine basic spectroscopic radiation constants of selected molecules.

1.2 Synopsis of Thesis

1.2.1 Overview

Chapter 1 contains the introductory remarks. A synopsis of the current knowledge of the C_2 molecule including a brief review of the historical background of the band systems is found in Chapter 2.

The first five sections of Chapter 3 review the parts of shock-tube, thermochemistry, and equilibrium radiation theory necessary for the understanding of the experimental technique. The final section of Chapter 3 describes the synthetic spectrum analysis data reduction method.

Chapter 4 contains a description of the shock-tube facility and its operation. The instrumentation and calibration procedures required to make absolute intensity measurements of the spectral emission are also discussed there. Chapter 4 concludes by presenting a sample of the experimental data.

The measurements of the electronic transition moments of the Ballik-Ramsay, Phillips, Swan, Deslandres-d'Azambuja, Fox-Herzberg, Mulliken, and Freymark systems are given in Chapter 5. These measurements are compared with the previous results in Chapter 6. The latter part of Chapter 6 summarizes the results and presents final conclusions.

1.2.2 Sections Reporting New Results

The measurements of the electronic transition moments are presented in section 5.2. An error analysis leading to an estimate of the

accuracy of these results is given in section 5.3. A critical comparison of the results in section 5.2 with prior work is contained in section 6.1.

For the reader who desires a closer look at the results, Appendix E contains tables of the data for each experimental test. These tables also include the pertinent thermochemical quantities for each run. The spectroscopic constants and Franck-Condon factors used in the data reduction are given in section 2.1 and Appendix C, respectively.

Chapter 2

Synopsis of the Current Knowledge of the C_2 Molecule

As mentioned earlier, a vast amount of research and interest has been focused on the C_2 molecule. Consequently, many of the details of the spectrum including many of the spectroscopic constants have been reasonably well determined. This chapter gives a brief historical review of the current knowledge of the spectrum of the C_2 molecule.

2.1 Historical Background of C_2 Band Systems

C_2 was one of the first molecules to be studied spectroscopically. The first band system of this molecule was observed by Wollaston in 1802 in the spectrum from the base of a candle flame. Wollaston, however, was unable to identify the correct emitter. Consequently, the source of this band system, now known as the Swan system, remained a mystery for many years. Swan (1857), for whom the band was named, observed this same band system but concluded that the emitter must be acetylene since he could only obtain it by using hydrocarbon flames as sources. Shortly after Swan's hypothesis, Van der Willigen (1859) also observed this spectrum and properly identified C_2 as the emitter. In the years following Van der Willigen's work, several other workers agreed with his identification of C_2 as the emitter. Among his supporters were Schuster (1880), Deslandres (1888), and Kayser (1910). The matter was far from resolved however because authorities such as Angström and Thalén (1875) and Liveing and Dewar (1880) supported Swan's assertion that the emitter was a hydrocarbon. Smithells (1901) suggested that neither C_2 nor hydrocarbon were involved but that the proper emitter was actually CO. The controversy continued until 1930 when King and Birge,

128 years after the first observation of this band system, showed conclusively that the C_2 molecule was the emitter. This demonstration resulted from the identification of the $C^{12}C^{13}$ Swan bands with the correct isotope shift clearly resolving the long-term dispute.

Since the Swan bands were so easily observed in absorption, it was assumed that the lower state in the electronic transition was the ground state of the molecule. This assumption which was shown to be false several years later led to a rather confusing designation of the states of C_2. This problem too was resolved with time as will be discussed below.

While the controversy surrounding the nature of the emitter of the Swan bands was still in progress, Deslandres and d'Azambuja (1905) observed the second of the band systems of C_2 which now bears their name. Mulliken (1930) tentatively identified a third band system of C_2 in the ultraviolet. This identification was established in 1939 when both Mulliken and Landsverk properly identified the electronic states involved in the transition. This system was named for Mulliken.

Fox and Herzberg (1937) analyzed the fourth band system of the C_2 molecule. This band system has the same lower state as the Swan bands and was found to be strongly overlapped by the nearby Deslandres-d'Azambuja and Swan bands.

Phillips (1948), who perhaps has done more than anyone else to increase our knowledge of the C_2 molecule, discovered the fifth band system. The Phillips system as it is now known arises from a transition between the previously known lower states of the Deslandres-d'Azambuja and Mulliken systems.

Freymark (1951) observed the sixth C_2 band system. The upper level of this transition was a new electronic state which at its discovery was the highest lying state of C_2 yet discovered. The lower state is also the lower state of the Deslandres-d'Azambuja transition.

Ballik-Ramsay (1959) not only discovered a new band system, the seventh, but they showed that the lower state of the Swan transition previously assumed to be the ground state was not the ground state of C_2 at all. They discovered a new electronic state which lies 610 cm^{-1} below the lower state of the Swan transition. The Ballik-Ramsay system shares its lower state with the Swan and Fox-Herzberg systems.

The startling discovery of a "new" ground state by Ballik and Ramsay in addition to the new electronic state which is the upper state of the Ballik-Ramsay transition led to an inconsistency in the notation of the electronic states. Since the notation originally proposed by Herzberg (1950) was well accepted, Ballik and Ramsay were reluctant to propose a new notation. The situation became more confusing when in 1963 Ballik and Ramsay discovered a third electronic state lying between the upper and lower states of the Swan transition.

In 1967, Messerle and Krauss discovered the eighth band system. The lower state was the same as the Deslandres-d'Azambuja and Freymark transitions but the upper state was a new state which arose from perturbations on the Deslandres-d'Azambuja upper state.

Herzberg, Lagerqvist, and Malmberg (1969) identified three more electronic states which lie above all of the other previously identified states. The transitions from these new states to lower lying states are presently unnamed. With the discovery of these new states, Herzberg

et al. proposed a new notation for the electronic states of C_2. This new notation which is now widely in use will be used in this thesis. Table 2.1 in the next section which deals with the electronic states and their molecular constants contains both the old and new notations for reference.

2.2 Electronic States and Molecular Constants

A summary of the molecular constants of all of the known electronic states of C_2 was published by Ballik and Ramsay in 1963. Since then, a new state near the upper state of the Deslandres-d'Azambuja system and arising from perturbations on it has been observed by Messerle and Krauss (1967). Three more states lying above all of the previously identified states were documented by Herzberg, Lagerqvist, and Malmberg in 1969. Therefore at the present time there are 14 known electronic states of C_2. The various molecular constants of these states are given in table 2.1. A complete listing and bibliography of the data contained in table 2.1 are given in the book Spectroscopic Data Relative to Diatomic Molecules (1970) edited by Rosen.

Both the old notation (Herzberg, 1950) and the new notation (Herzberg et al., 1969) are given in table 2.1. A perceptive reader will notice that the letter B is missing from the singlet notation. This letter was reserved by Herzberg et al. for two predicted low lying singlet states that have not yet been observed.

The potential energy curves of the C_2 molecule are shown on figure 2.1. All of the electronic states listed in table 2.1 are included. The curves represented by the solid lines were constructed on the basis of Morse potential functions and were taken from

Table 2.1. Molecular Constants for the Known Electronic States of the C_2 Molecule

State	T_e*	ω_e*	$\omega_e x_e$*	$\omega_e y_e$*	B_e*	α_e*	γ_e*	r_e*	Reference	Old notation
E $^1\Sigma_g^+$	55034.6	1671.5	40.02	0.248	1.7930	0.0421		1.2517	Freymark (1951)	e $^1\Sigma_g^+$
D $^1\Sigma_u^+$	43240.23	1829.57	13.97		1.8334	.0204		1.2378	Herzberg (1950)	d $^1\Sigma_u^+$
e $^3\pi_g$	40796.65	1106.56	39.26	2.805	1.1922	.0242		1.5350	Herzberg (1950)	B $^3\pi_g$
C $^1\pi_g$	34261.9	1809.1	15.81	-4.02	1.783**	.0180		1.2552**	Herzberg (1950)	c $^1\pi_g$
d $^3\pi_g$	20022.50	1788.22	16.440	-.5067	1.7527	.01608	-0.001274	1.2660	Herzberg (1950)	A $^3\pi_g$
c $^3\Sigma_u^+$	13312.1	1961.6	13.65		1.87			1.23	Ballik & Ramsay (1963b)	A'' $^3\Sigma_u^+$
A $^1\pi_u$	8391.00	1608.35	12.078	-.010	1.61634	.01686	-.00005	1.31843	Ballik & Ramsay (1963b)	b $^1\pi_u$
b $^3\Sigma_g^-$	6434.27	1470.45	11.19	.02	1.49852	.01634		1.36928	Ballik & Ramsay (1963a)	A' $^3\pi_u$
a $^3\pi_u$	716.24	1641.35	11.67		1.63246	.01661		1.31190	Ballik & Ramsay (1963a)	X' $^3\pi_u$
X $^1\Sigma_g^+$	0	1854.71	13.340	-.172	1.81984	.01765	-.00023	1.2425	Ballik & Ramsay (1963b)	X $^1\Sigma_g^+$
F $^1\pi_u$	74550.	1557.5†			1.645	.019		1.307	Herzberg et al. (1969)	
g $^3\Delta_g$	72390.	1458.06†			1.5238	.0170		1.358	Herzberg et al. (1969)	
f $^3\Sigma_g^-$	70924.	1360.5	14.8		1.448	.040††		1.393	Herzberg et al. (1969)	

*All units are cm^{-1} except for r_e, which are given in Å units. To obtain the T_e values for the triplet states, it has been assumed that the "zero" level of the a $^3\pi_u$ state lies exactly 610.00 cm^{-1} above the zero level of the X $^1\Sigma_g^+$ state (Ballik and Ramsay, 1963a).

**Herzberg (1950) quotes different values, which are apparently in error.

†These are $\Delta G(1/2)$ values.

††$B_v = 1.448 - 0.040[v + (1/2)] + 0.006[v + (1/2)]^2$.

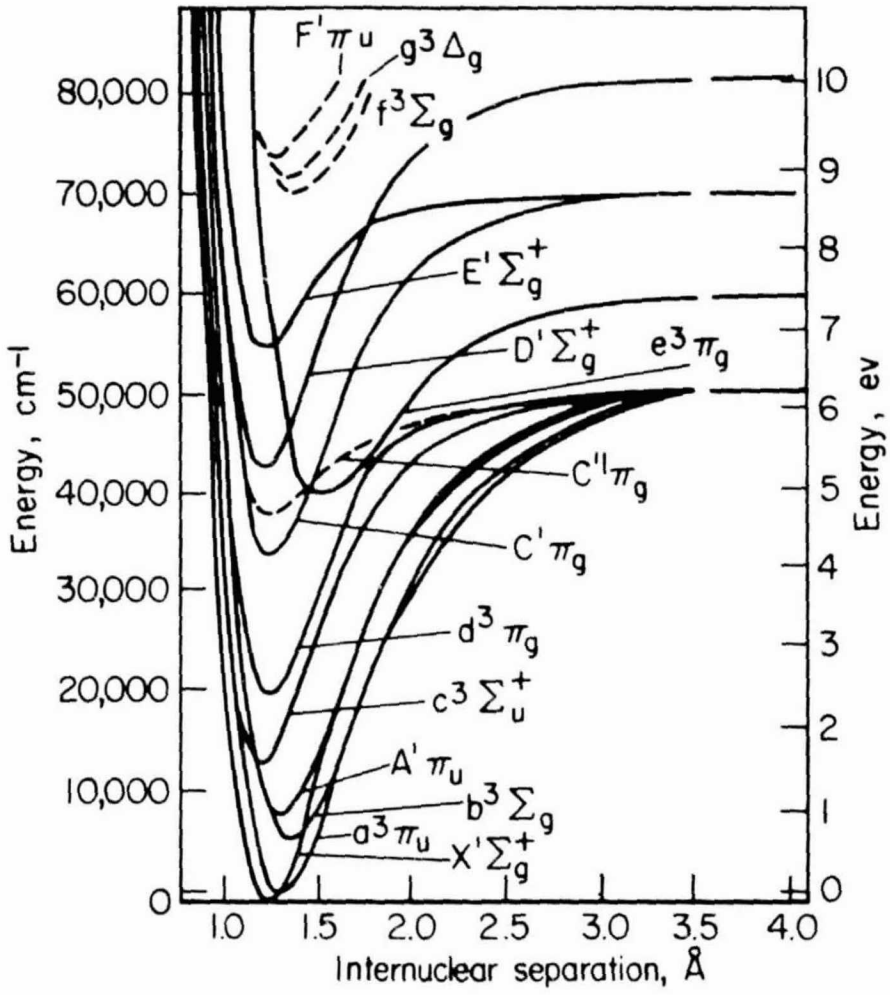

Figure 2.1.- Potential energy curves for the C_2 molecule. The curves given by the solid lines were constructed on the basis of Morse functions. The dashed curves were taken from Herzberg et al. (1969) and the dotted curve was taken from Messerle and Krauss (1967).

Ballik and Ramsay (1963). The dashed curve representing the C' $^1\pi_g$ state which results from perturbations of the C $^1\pi_g$ state was adopted from Messerle and Krauss (1967). The partial potential curves indicated by dashed lines represent the three states observed by Herzberg et al. (1969). These curves were drawn on the basis of the data provided by them.

The correct value of the dissociation energy of C_2 has remained uncertain for many years. An accurate knowledge of this energy is required to predict the thermodynamic properties and C_2 concentrations of gas mixtures in which C_2 is a major constituent. It is thus needed for the thermochemical calculations which lead to the number densities of C_2 in our shock-heated source. Herzberg (1946) suggested a dissociation energy value of 3.6 ev. He argued that the high pressure Swan bands which arise only from the $v = 6$ level of the upper state of the Swan transition were due to an inverse predissociation and that this level must be at the same energy as the separated carbon atoms. This reasoning is now known to be incorrect (Ballik and Ramsay, 1963).

Brewer, Gilles, and Jenkins (1948) reported a value of 4.7 ± 0.3 ev for the dissociation energy. This value was deduced from measured values of the emission of the Swan system at various temperatures using a King furnace as a source. Another study by Brewer, Hicks, and Krikorian (1962) using this same technique as well as mass spectrometer measurements yielded an average value of 6.25 ± 0.2 ev. Diowart, Burns, DeMaria, and Ingham (1959) performed a mass spectrometric study of the gas effusing from a Knudsen cell and listed a value of 6.21 ± 0.07 ev. Messerle and Krauss (1967) have made Birge-Spooner extrapolations of

the vibrational levels of the $d\ ^3\pi_g$ and $e\ ^3\pi_g$ states to limits of 6.07 and 6.09 ev, respectively. The extrapolation of the $E\ ^1\Sigma_g^+$ level to its limit by Gaydon (1968) indicates a value of 6.4 ± 0.3 ev.

From these results, it appears that Brewer et al.'s value of 6.25 ev is reasonable and since Gaydon (1968) also recommends this value (6.25 ± 0.20 ev), it will be used for the dissociation energy of C_2 in this work. A value of 6.25 ev is shown on figure 2.1 as the dissociation energy and therefore represents a slight modification of the curves as given by Ballik and Ramsay.

Theoretical calculations of the electronic structure of C_2 have been performed by Mulliken (1939), Clementi and Pitzer (1960), and Fougere and Nesbet (1966). The most comprehensive and sophisticated of these is the work by Fougere and Nesbet. They have calculated the C_2 electronic structure over a wide range of internuclear separations using three different Slater-type orbital basis sets and two different levels of configuration interaction. The calculated values of potential curves and spectroscopic constants of 27 electronic states are reported. A comparison of these calculations with the experimentally determined values given in table 2.1 indicates only a reasonable agreement between the two. However, one of the important features of their work is the prediction of electronic spectra which contain transitions between pairs of states in which only one of the states has been experimentally observed. These predictions should be of considerable value in future attempts to locate new C_2 spectra.

2.3 Electronic Transitions and Spectra

All of the known electronic transitions of the C_2 molecule are listed on table 2.2. The old transition notation when available is given in parentheses for reference. Figure 2.2 is a partial energy level diagram showing the eight electronic transitions which are of interest in this work. The singlet and triplet transitions have been separated for clarity.

Table 2.2 also contains the approximate observed spectral extent of each system. Moderate reciprocal dispersion survey spectra showing portions of the Phillips, Swan, Deslandres-d'Azambuja, Fox-Herzberg, Mulliken, and Freymark band systems are given in section 4.4.

2.4 Previous Work on C_2 Electronic Transition Moments

This section summarizes the results of the previous work on C_2 electronic transition moments. Both experimental measurements and theoretical predictions are included. A comparison of these results with those of the present effort may be found in section 6.1. The results are represented in terms of the sum of the squares of the electronic transition moments, $\Sigma|R_e/ea_o|^2$, which is often referred to as the electron transition moments squared.

Other than the present work, the only systematic study of the absolute strengths of the C_2 band systems was attempted by Wentink et al. (1967) using the laser excitation technique. They encountered and discussed several difficult and complex problems (see section 6.1) which led them to question the validity of their results. They have concluded that their results usually give only a lower bound to the

Table 2.2 Band System Designations of All Known Electronic Transitions of the C_2 Molecule.

Band system	Electronic transition, Upper state - Lower state	Approximate spectral region, Å
Swan	$d\ ^3\pi_g - a\ ^3\pi_u$ ($A\ ^3\pi_g - X'\ ^3\pi_u$)	4200 - 7000
Deslandres-d'Azambuja	$C\ ^1\pi_g - A\ ^1\pi_u$ ($c\ ^1\pi_g - b\ ^1\pi_u$)	3300 - 4100
Fox-Herzberg	$e\ ^3\pi_g - a\ ^3\pi_u$ ($B\ ^3\pi_g - X'\ ^3\pi_u$)	2300 - 3300
Mulliken	$D\ ^1\Sigma_u^+ - X\ ^1\Sigma_g^+$ ($d\ ^1\Sigma_u^+ - x\ ^1\Sigma_g^+$)	2200 - 2500
Freymark	$E\ ^1\Sigma_g^+ - A\ ^1\pi_u$ ($e\ ^1\Sigma_g^+ - b\ ^1\pi_u$)	2000 - 2400
Phillips	$A\ ^1\pi_u - X\ ^1\Sigma_g^+$ ($b\ ^1\pi_u - x\ ^1\Sigma_g^+$)	7000 - 12100
Ballik-Ramsay	$b\ ^3\Sigma_g^- - a\ ^3\pi_u$ ($A'\ ^3\Sigma_g^- - X'\ ^3\pi_u$)	11600 - 25000
Ultraviolet bands observed by Herzberg et al. (1967)	$f\ ^3\Sigma_g - a\ ^3\pi_u$ $g\ ^3\Delta_g - a\ ^3\pi_u$ $F\ ^1\pi_u - X\ ^1\Sigma_g^+$	1300 - 1450
Messerle-Krauss	$C'\ ^1\pi_g - A\ ^1\pi_u$	3100 - 3400

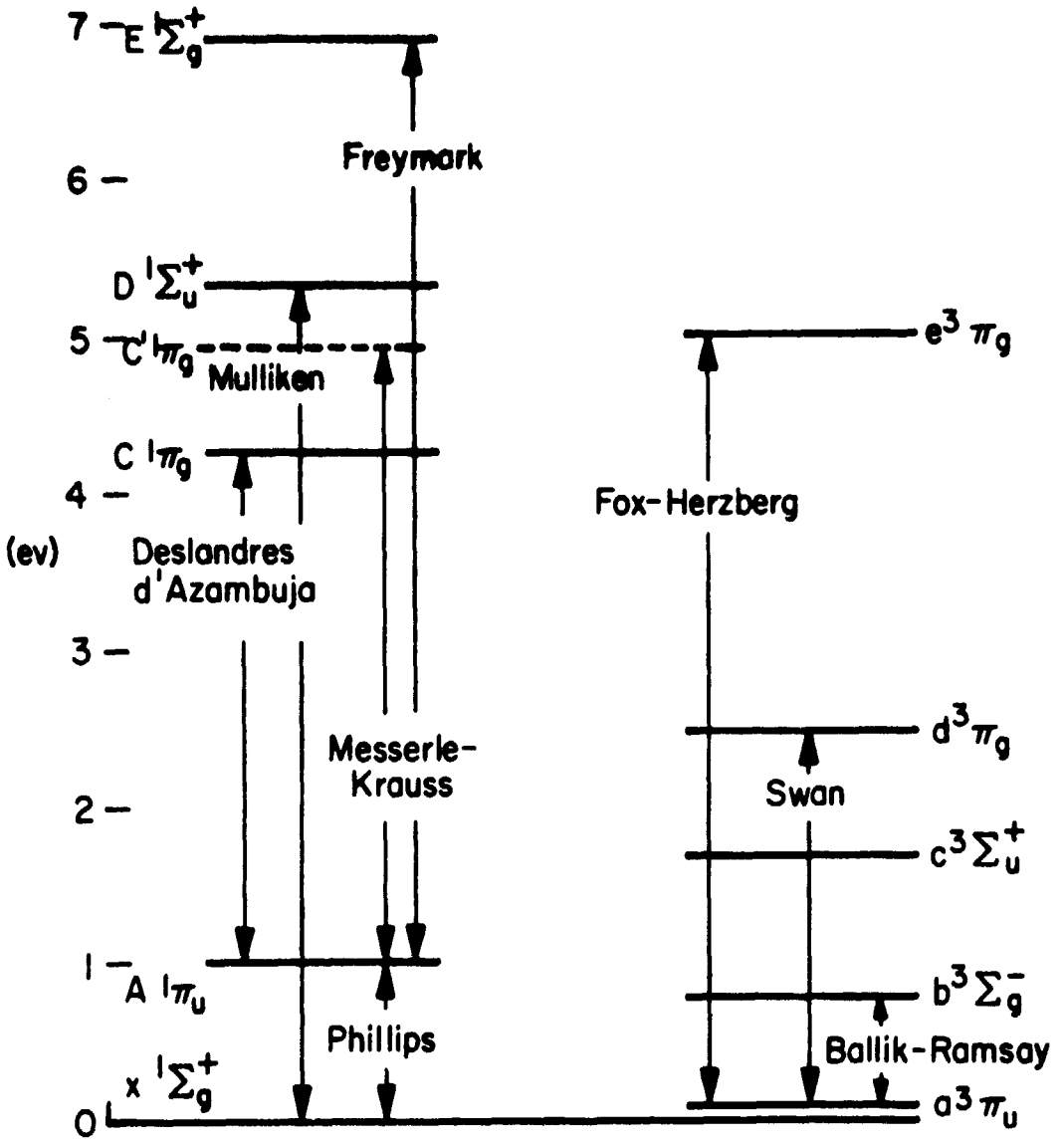

Figure 2.2.- Energy levels diagram for C_2 showing the important electronic transitions. The singlet and triplet transitions have been separated and some of the electronic states omitted for clarity.

electronic transition moments squared value. Consequently on the following pages, their results will be given as lower bounds.

Since the Swan system is the strongest radiating system of the C_2 molecule, it has been studied extensively. Table 2.3 is a comparison of the experimental values of the $\Sigma|R_e/ea_o|^2$ value of the Swan system found in the literature. Only measurements of the $\Delta v = 0$ sequence (5165 Å) are included.

The shock-tube results of Arnold (1968) and Fairbairn (1966) obtained behind the incident shock agree well with each other and reasonably well with the results of Harrington et al. (1966), Sviridov et al. (1965), and Sviridov et al. (1966) using a shock tube in the reflected shock mode. With the exception of the measurements by Hicks (1957) in a King furnace, the data obtained in furnaces appear too small. The lifetime measurements of Jeunehomme and Schwenker (1965) and Fink and Welge (1967) differ by a factor of 4 with the latter measurement in fair agreement with the shock-tube data. The results of Wentink et al. (1967) which are also lifetime measurements represent a lower bound. Consequently, the measurements of the absolute strength of the Swan system differ by a factor of about 6. However, it is generally accepted (Arnold, 1968) that the true $\Sigma|R_e/ea_o|^2$ value is probably bounded by the shock-tube measurements listed in table 2.3.

A recent measurement of the variation of the Swan system with internuclear separation was reported by Danylewych (1971) and Danylewych and Nicholls (1974). This work contains an excellent summary and comparison of all of the past measurements of the variations of spectral intensity of the Swan system.

Table 2.3 Measurements of the Values of the Electronic Transition Moments Squared of the $\Delta v = 0$ Sequence (5165 Å) of the C_2 Swan System.

Experimenter	Method	$\Sigma\|R_e/ea_o\|^2$, atomic units
Arnold (1968)	Shock tube	3.56 ± 0.50
Fairbairn (1966)	Shock tube	3.36 ± 1.20
Harrington et al. (1966)	Shock tube	2.95 ± 0.92
Sviridov et al. (1965)	Shock tube	2.24 ± 0.81
Sviridov et al. (1966)	Shock tube	2.85 ± 0.20
Hicks (1957)	King furnace	2.64
Hagen (1963)	King furnace	0.71 ± 0.40
Jeunehomme & Schwenker (1965)	Laser excitation	0.60 ± 0.02
Fink & Welge (1967)	Phase shift	2.24 ± 0.70
Wentink et al. (1967)	Laser excitation	1.35

The results of various theoretical efforts to predict the absolute strength of the Swan system are listed in table 2.4. These results show a discordance similar to that of the experimental measurements. The early predictions of Shull (1951) and Stephenson (1951) show surprisingly good agreement with the higher values reported from shock-tube tests.

The experimental and theoretical results of the absolute strengths of the other C_2 band systems of interest are summarized in table 2.5. It is readily apparent that very little experimental or theoretical work has focused on these weaker band systems. Of these six systems, the only one whose strength has been measured absolutely is the Mulliken system (Smith, 1969). The measurement of the Phillips system by Hicks (1957) was made relative to the (1,0) band of the Swan system and has an uncertainty of a factor of 3. The measurement of the Fox-Herzberg system by Sviridov et al. (1969) is an upper limit. As discussed earlier, the measurements of Wentink et al. (1967) represent lower bounds.

Clementi (1960) using the dipole-moment operator method calculated the absolute strength of five of these band systems. His results are presented in the form of oscillator strengths or f numbers. It should be noted that Clementi apparently omitted the statistical weight of the upper state from the definition of the f number. Consequently, the values given in table 2.5 have been modified to account for this factor. With the exception of the work on the Deslandres-d'Azambuja system by Shull (1951) and Stephenson (1951), no other theoretical calculations of the strength of these systems are known to the author.

Most of the results summarized in tables 2.3 to 2.5 are reported in terms of oscillator strengths or f numbers. The astute student of

Table 2.4 Theoretical Predictions of the Absolute Strength of the C_2 Swan System.

Reference	$\Sigma\|R_e/ea_o\|^2$, A.U.	Remarks
Clementi (1960)	1.14	$\Sigma\|R_e/ea_o\|^2$ value modified to account for the statistical weight of the upper level omitted from defining equation
Shull (1951)	4.24	Same as above
Stephenson (1951)	4.06	
Lyddane, Rogers & Roach (1941)	3.39	
Spindler (1965)	5.04	Based on Jeunehomme's lifetime measurement on the d $^3\pi_g$ state
Coulson & Lester (1955)	33.92	

Table 2.5 Experimental and Theoretical Results of the Absolute Strength of the Band Systems (Excluding the Swan System) of the C_2 Molecule.

Band system	Results in literature $\Sigma\|R_e/ea_o\|^2$, A.U.	
	Experimental	Theoretical
Ballik-Ramsay		1.21 - Clementi (1960)*
Phillips	0.68 - Hicks (1957)	0.13 - Clementi (1960)*
Deslandres-d'Azambuja	> 0.18 - Wentink et al. (1967)	1.12 - Clementi (1960)* 3.97 - Shull (1951)* 1.35 - Stephenson (1951)
Fox-Herzberg	< 0.55 - Sviridov et al. (1965) > 0.45 - Wentink et al. (1967)	57.80 - Clementi (1960)*
Mulliken	0.42 - Smith (1969)	0.78 - Clementi (1960)*
Freymark		

*These values are modified to account for the statistical weight of the upper level omitted from the defining equation.

spectroscopy realizes that this nomenclature is ambiguous and that caution must be exercised when using results described by this terminology. Consequently the author has investigated the original references listed on these tables to determine the manner in which the reported f number was defined. Therefore the results originally reported as f numbers have been converted to $\Sigma|R_e/ea_o|^2$ values by using a consistent set of defining equations. These relations were taken from Schadee (1967) and are given in Appendix A.

2.5 Goals of the Present Work

It is rather obvious from examining table 2.5 that there is a real need for a systematic determination of the absolute strength of the band systems of the C_2 molecule. Thus the present effort was motivated by the gross uncertainties that exist in the absolute strengths of the band systems of C_2. The previous section clearly demonstrated this uncertainty.

The goal of this work is to obtain measurements of the absolute strength of the band systems of the C_2 molecule. These results which are reported in terms of electronic transition moments squared values are deduced from absolute measurements of the radiation by the synthetic spectrum analysis technique. The interest and usefulness of these results was previously set forth in section 1.1.

Chapter 3

Theoretical Bases of Experiments

This chapter is a review of the theory which is necessary for the understanding and interpretation of the experimental measurements. The most important parameter in this work is the integrated intensity, E_{ℓ}^{u}, from spontaneous emission in a rotational line emanating from a light source in local thermodynamic equilibrium. The general equation for this intensity is (Nicholls, 1969):

$$E_{\ell}^{u} = \frac{16 \times 10^{-7}\, \pi^{3} \bar{\nu}_{u\ell}^{4} c}{3(2 - \delta_{o,\Lambda'})(2S' + 1)(2J' + 1)} N_{uv'\Lambda'J'} \cdot \Sigma |R_e(\bar{r}_{v'v''})|^2 \cdot q_{v'v''} \cdot S^{J'\Lambda'}_{j''\Lambda''} \qquad (3.1)$$

The principal goal of this work is to determine the quantity $\Sigma |R_e(\bar{r}_{v'v''})|^2$ which is the square of the electronic transition moment of the band system. This is accomplished as follows: Firstly, the absolute value of the intensities E_{ℓ}^{u} of several band lines are measured using calibrated radiometers; secondly, the quantity, $N_{uv'\Lambda'J'}$, which is the number of excited emitters involved in the radiative transition is obtained from the thermodynamic properties of the source (in this work, the shock-heated gas behind an incident shock wave); thirdly, the necessary Franck-Condon factors, $q_{v'v''}$, and Hönl-London, $S^{J'\Lambda'}_{J''\Lambda''}$, factors are calculated from the theory of molecular spectroscopy. The remaining parameters in equation (3.1) can be obtained from the known molecular constants of C_2. Thus the quantity $\Sigma |R_e(\bar{r}_{v'v''})|^2$ can then be determined directly from equation (3.1) after summing it over all of the lines which contribute to the measured radiation.

The structure of this multicomponent chapter is as follows: Equation (3.1) is derived from equilibrium radiation theory in section 3.1. The calculation of the Franck-Condon and Hönl-London factors is discussed in section 3.2; and section 3.3 reviews the theory of radiative transfer. The application of the general equation (3.1) to the specific transitions and band systems of C_2 is reviewed in section 3.4. Section 3.5 reviews the parts of shock tube and thermochemistry theory necessary to provide the equilibrium concentrations $N_{uv'\Lambda'J'}$ as well as the equilibrium temperature of the source. The final section (3.6) of this chapter reviews the synthetic spectrum data analysis technique and relates the theory of the preceding five sections to the analysis of the experimental data.

3.1 Equilibrium Radiation Theory

The principles of equilibrium radiation theory that pertain to diatomic molecules are reviewed here. Full discussions of the quantum mechanical model of radiative transitions in a diatomic molecule have been made by Pauling and Wilson (1935), Herzberg (1950), and Nicholls (1969).

3.1.1 The Molecular Wave Equation

The theoretical study of radiative transitions in diatomic molecules involves the formulation and solution of the molecular wave equation. Schrödinger's time independent equation for a system of particles representing a diatomic molecule is

$$H\Psi = E\Psi \tag{3.2}$$

where H is the Hamiltonian operator, Ψ is the total wave function, and E is the eigenvalue which represents the total energy of the

system. The solution of equation (3.2) yields a series of Ψ's and E's from which the quantities $\Sigma|R_e(\bar{r}_{v'v''})|^2$, $q_{v'v''}$, $\bar{\nu}_{u\ell}$, and $S^{J'\Lambda'}_{J''\Lambda''}$ in equation (3.1) can be calculated. The Hamiltonian is the total energy of the system and is usually approximated by the sum of the kinetic and potential energies of the nuclei and electrons, that is,

$$\begin{aligned} H &= (K.E.)_n + (K.E.)_e + V_{ee} + V_{nn} + V_{ne} \\ &= -\frac{\hbar^2}{2}\left(\sum_n^2 \frac{\nabla_n^2}{M_n} + \sum_e \frac{\nabla_e^2}{m_e}\right) + \sum_e \frac{e^2}{r_{ii'}} \\ &\quad + \sum_n \frac{Z_j Z_{j'} e^2}{r_{jj'}} - \sum_{n,e} \frac{Z_j e^2}{r_{ij}} \end{aligned} \tag{3.3}$$

The potential energy terms represent the electron-electron (V_{ee}), nucleus-nucleus (V_{nn}), and electron-nucleus (V_{ne}) Coulombic interactions. In equation (3.3), the mass of the nuclei and electrons are represented by M_n and m_e, respectively, while the quantities $r_{ii'}$, $r_{jj'}$, and r_{ij} are the distances between the pairs of interacting particles. The Schrödinger wave equation for this multiparticle system now becomes

$$\sum_n^2 \frac{\nabla_n^2}{M_n}\Psi + \sum_e \frac{\nabla_e^2}{m_e}\Psi - \frac{2}{\hbar^2}(V_{ee} + V_{nn} + V_{ne})\Psi = E\Psi \tag{3.4}$$

The Born-Oppenheimer approximation which asserts that the true molecular wave function may be represented by the product of two different wave functions - one for the electronic motion and the other for the nuclear motion, that is,

$$\Psi_{total}(r, \xi) = \psi_e(r, \xi)\psi_n(r) \tag{3.5}$$

is used to obtain solutions to equation (3.4). The symbol ξ represents the electron coordinates and r is the internuclear separation. Also

inherent in the Born-Oppenheimer approximation is the assumption that the total energy can be separated into two distinct parts, that is,

$$E_{total} = E_e + E_n. \tag{3.6}$$

Substituting these approximations into equation (3.4), expanding the Laplace operators, dividing by the total wave function, and neglecting terms of the order of m/M gives an equation whose terms can be separated into two wave equations. One equation describes the electron motion,

$$\sum_e \nabla_e^2 \psi_e(r, \xi) + \frac{8\pi^2}{h^2} m_e[E_e(r) - V_{ee}(r, \xi) - V_{ne}(r, \xi)]\psi_e(r, \xi) = 0, \tag{3.7}$$

and the other describes the nuclear motion,

$$\sum_n \frac{\nabla_n^2 \psi_n(r)}{M_n} + \frac{8\pi^2}{h^2} [E_n(r) - V_{nn}(r)]\psi_n(r) = 0. \tag{3.8}$$

The quantities in brackets in equations (3.7) and (3.8) are usually rewritten in terms of the molecular potential $U(r)$ which is the sum of the electronic eigenvalue $E_e(r)$ and the nuclear potential $V_{nn}(r)$. The separated wave equations are now given by

$$\sum_e \nabla_e^2 \psi_e(r, \xi) + \frac{8\pi^2}{h^2} m_e[U(r) - V(r)]\psi_e(r, \xi) = 0, \tag{3.9}$$

and

$$\sum_n \frac{\nabla_n^2 \psi_n(r)}{M_n} + \frac{8\pi^2}{h^2} [E - U(r)]\psi_n(r) = 0, \tag{3.10}$$

for the electron and nuclear motions, respectively, where $V(r)$ is the sum of the potential energy terms.

The solution of equation (3.9) is a very difficult problem. Equation (3.10) is somewhat easier to solve although it involves a knowledge of the molecular potential function $U(r)$ which is obtained theoretically from the solution of equation (3.9). However, at the present time,

theoretical calculations of $U(r)$ exist for only the simplest molecules. Therefore, the normal procedure is to adopt an approximate form for $U(r)$ which contains parameters that are determined by a comparison of observed and calculated energy levels and use this analytical form to assist in the solution of equation (3.10).

With the assumed form of the electronic energy, equation (3.10) is solved using various methods and models of varying sophistication to obtain the vibrational and rotational energy levels. In this study, we shall use the energy eigenvalues of the vibrating-rotator model. The vibrational and rotational energy values given by Herzberg (1950) are, respectively,

$$E_v = hc\left[\omega_e\left(v + \frac{1}{2}\right) - \omega_e x_e\left(v + \frac{1}{2}\right)^2 + \omega_e y_e\left(v + \frac{1}{2}\right)^3 + \omega_e z_e\left(v + \frac{1}{2}\right)^4\right]$$
$$= hcG(v) , \tag{3.11}$$

$$E_R = hc[B_v(J + 1) - D_v J^2(J + 1)^2 + (A - B_v)\Lambda^2]$$
$$= hcF(J), \tag{3.12}$$

where

$$B_v = B_e - \alpha_e\left(v + \frac{1}{2}\right)$$
$$B_e = \frac{h}{8\pi^2 c I_e}$$

and

$$D_v = D_e + B_e\left(v + \frac{1}{2}\right)$$
$$D_e = \frac{4B_e^2}{\omega_e^2}$$

In the above equation, ω_e, $\omega_e x_e$, $\omega_e y_e$, and $\omega_e z_e$ are vibrational constants, B, D, and α_e are rotational constants, and the subscript e refers to the equilibrium position.

The total energy of the molecule can therefore be written as

$$E_{total} = hc[T_e + G(v) + F(J)] \qquad (3.13)$$

where T_e is the energy of the minimum of the electronic potential well of the electronic state of interest. This equation is used in the following section to calculate the central wavelength of the rotational line whose total emissive intensity is given by equation (3.1).

3.1.2 Electronic Transition Wavelengths

When a transition from a upper electronic state to a lower electronic state whose energies are given by E' and E'' takes place, a photon of energy $h\nu$ is emitted (Bohr's frequency condition), that is,

$$E' - E'' = h\nu = hc/\lambda \qquad (3.14)$$

In this equation, ν and λ are the frequency and wavelength of the emitted radiation. From this relationship and the molecular energies of the previous section, the central wavenumber of a spectral line resulting from a transition between two electronic states is

$$\bar{\nu}(cm^{-1}) = \frac{\nu}{c} = (T_e' - T_e'') + [G'(v') - G''(v'')] + [F'(J') - F''(J'')]. \qquad (3.15)$$

This quantity is one of the input parameters required for the successful evaluation of equation (3.1).

Equation (3.15) is often written as

$$\bar{\nu}(cm^{-1}) = \bar{\nu}_o(v', v'') + [F'(J') - F''(J'')] = \frac{10^8}{\lambda(\text{Å})} \qquad (3.16)$$

where $\bar{\nu}_o(v', v'')$ is called the band origin of the (v', v'') transition. Calculated band origins (in vacuo) for the (v', v'') transitions of the C_2 molecular systems of interest in this study are listed in appendix B.

In order to calculate the central wavenumber of a rotational line (equation (3.15) or (3.16)), an accurate expression for F(J) must be used. The rotational term energies, F(J), depend on the manner in which the various angular momenta couple together and are discussed in the next section.

3.1.3 Hund's Coupling Cases

The interactions of the various angular momenta are classified on the basis of the strength of the coupling to the internuclear axis and are referred to as Hund's coupling cases (a), (b), (c), (d), and (e). Since the C_2 transitions of interest in this work are represented by either Hund's case (a) or (b), only these two cases will be discussed. Herzberg (1950) gives a more detailed discussion of all of Hund's cases. The vector notation of Herzberg (1950) is used in the following discussion.

Hund's Case (a)

In this case, it is assumed that the coupling of the nuclear rotation with the electronic motion is weak compared to the coupling of the electronic motion to the internuclear axis. Figure 3.1 is a vector diagram for Hund's case (a). As shown in this figure, the rapid precession of the orbital angular momentum $\vec{L}$ and the spin angular momentum $\vec{S}$ about the internuclear axis result in the axial components $\vec{\Lambda}$ and $\vec{\Sigma}$. The total electronic angular momentum along the internuclear axis is therefore $\vec{\Omega} = \vec{\Lambda} + \vec{\Sigma}$ whose values vary from $\Lambda - \Sigma$ to $\Lambda + \Sigma$. The total angular momentum $\vec{J}$ results from the coupling of $\vec{\Omega}$ with the nuclear rotation vector $\vec{N}$. The latter two vectors nutate about $\vec{J}$ as indicated in the figure. The total angular momentum is constant in magnitude and direction and always exceeds its component $\vec{\Omega}$. This

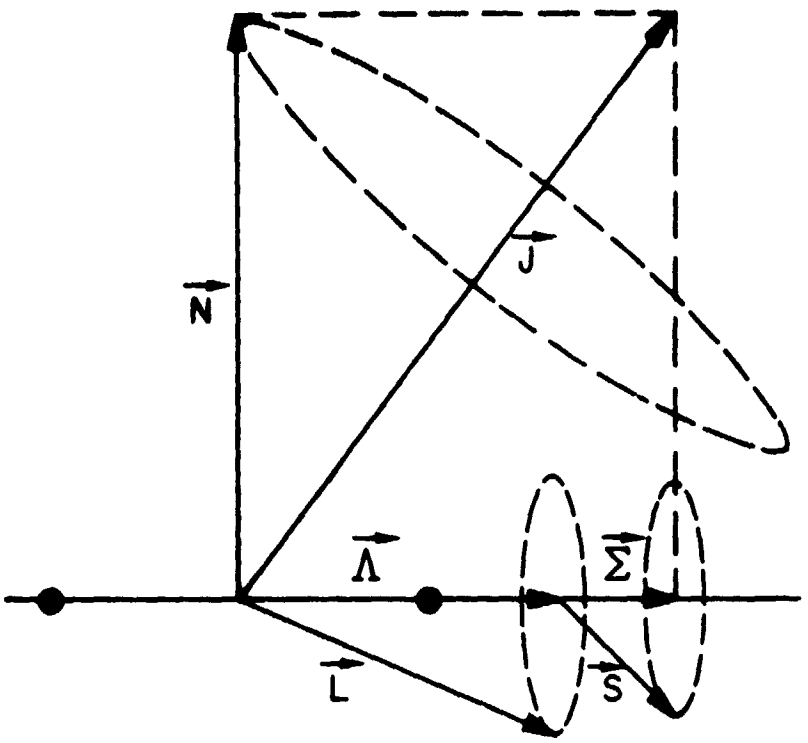

Figure 3.1.- Hund's case (a).

accounts for the fact that energy levels with $J < \Omega$ are not observed. The rotational energy eigenvalues for this case now become

$$E_R = hc[B_v J(J + 1) - D_v J^2(J + 1)^2 - (A - B_v)\Omega^2] \qquad (3.17)$$

where

$$J = \Omega, \Omega + 1, \Omega + 2, \ldots .$$

Hund's Case (b)

Hund's case (b) is characterized by a very weak or zero coupling of the spin angular momentum to the internuclear axis. Therefore only $\vec{L}$ couples to the internuclear axis to produce its component $\vec{\Lambda}$ along the internuclear axis. This vector, $\vec{\Lambda}$, and $\vec{N}$ couple to form an intermediate resultant $\vec{K}$ which is called the total angular momentum apart from spin. The spin angular momentum, $\vec{S}$, now couples to $\vec{K}$ to form the total

angular momentum vector, $\vec{J}$. A vector diagram of this coupling case illustrating the vector motions is shown in figure 3.2. As a result of the coupling between $\vec{S}$ and $\vec{K}$, a splitting of the energy levels with different J but equal K occurs. This phenomenon is observed in the rotational levels of the Swan, Fox-Herzberg, and Ballik-Ramsay systems. Consequently the rotational energy eigenvalues take different forms for the various transitions and will be discussed later when the theory is applied to the specific C_2 transitions.

It should also be noted that Hund's coupling cases are limiting cases and quite often as the rotation increases, a transition from one coupling case to another takes place. This is because the increased rotation rate tends to uncouple the angular momentum vectors from the internuclear axis.

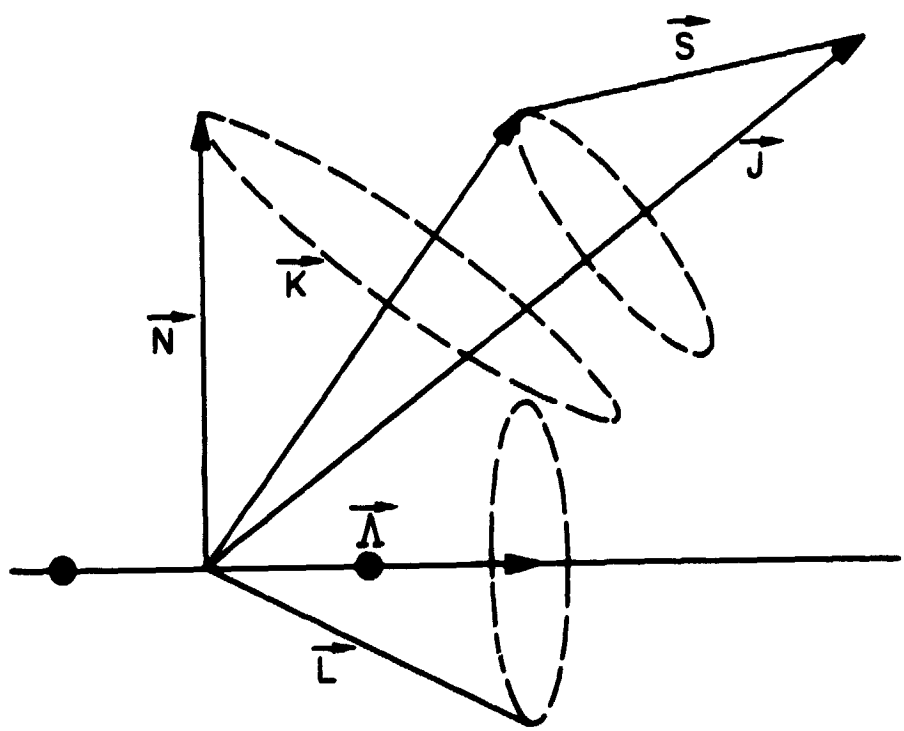

Figure 3.2.- Hund's case (b).

3.1.4 Electronic Transition Intensities

The wavelength of an emitted spectral line resulting from a transition between electronic states was obtained in the previous sections. The probability that this transition will take place, which leads to the derivation of equation (3.1), is discussed below.

The Einstein transition probability of spontaneous emission, $A_{u\ell}$, which is the total probability per second per particle that a spontaneous transition from an upper state u to a lower state ℓ will occur accompanied by emitted radiation of frequency $\nu_{u\ell} = [(E_u - E_\ell)/h]$ is given by (Herzberg, 1950),

$$A_{u\ell} = \frac{64\pi^4 \nu_{u\ell}^3}{3h} |\vec{R}^{u\ell}|^2. \tag{3.18}$$

If one considers only electric dipole transitions, then the matrix element $R^{u\ell}$ which is known as the transition moment is defined as

$$\vec{R}^{u\ell} = \int \psi^{u*} \vec{M} \psi^{\ell} \, d\tau \tag{3.19}$$

where ψ^u and ψ^ℓ are the total eigenfunctions of the states involved in the transition and $\vec{M}$ is the electric dipole moment given by

$$\vec{M} = \sum_i e\vec{r}_i. \tag{3.20}$$

By writing the total eigenfunctions as the product of electronic, vibrational, and rotational components and transforming from electron coordinates to molecular fixed coordinates, Nicholls and Stewart (1962) showed that the transition moment for a molecular line could be written as

$$\left|R^{uv'J'\Lambda'm'}_{\ell v''J''\Lambda''m''}\right| = \int \psi_{v'} \left(\int \psi_u^* \left| \sum_i e r_i \right| \psi_\ell \right) \psi_{v''} \, dr$$

$$\times \int \psi_{J'\Lambda'm'} |\vec{D}| \psi_{J''\Lambda''m''} \sin\theta \, d\theta \, d\phi. \tag{3.21}$$

Squaring this equation and summing over the appropriate states m' and m'' one has

$$\left|R^{uv'J'\Lambda'}_{\ell v''J''\Lambda''}\right|^2 = \left|\int \psi_{v'} R_e \psi_{v''}\, dr\right|^2 \cdot S^{J'\Lambda''}_{J''\Lambda''} \qquad (3.22)$$

If R_e is independent of r, it can be removed from the integral and equation (3.22) becomes:

$$\left|R^{uv'J'\Lambda'}_{\ell v''J''\Lambda''}\right|^2 = |R_e|^2 \cdot \left|\int \psi_{v'} \psi_{v''}\, dr\right|^2 \cdot S^{J'\Lambda'}_{J''\Lambda''} . \qquad (3.23)$$

However, R_e is usually dependent on r. Since this dependence can often be represented by a power series in r, Fraser (1954) defined a characteristic internuclear separation, $\bar{r}_{v'v''}$ known as the r centroid by

$$\bar{r}_{v'v''} = \frac{\int \psi_{v'} \psi_{v''} r\, dr}{\int \psi_{v'} \psi_{v''}\, dr} . \qquad (3.24)$$

Using this approximation, equation (3.22) becomes

$$\left|R^{uv'J'\Lambda'}_{\ell v''J''\Lambda''}\right|^2 = |R_e(\bar{r}_{v'v''})|^2 \cdot \left|\int \psi_{v'} \psi_{v''}\, dr\right|^2 \cdot S^{J'\Lambda'}_{J''\Lambda''}$$

$$= |R_e(\bar{r}_{v'v''})|^2 \cdot q_{v'v''} \cdot S^{J'\Lambda'}_{J''\Lambda''} , \qquad (3.25)$$

where, $|R_e(\bar{r}_{v'v''})|^2$ is the electronic transition moment squared, $\bar{r}$ is the r centroid, $q_{v'v''}$ is the Franck-Condon factor, and $S^{J'\Lambda'}_{J''\Lambda''}$ is the Hönl-London factor. Each of these quantities will be discussed in detail in subsequent sections. The product of $|R_e(\bar{r}_{v'v''})|^2 \cdot q_{v'v''}$ is often referred to as the band strength. Equation (3.18) for $A_{u\ell}$ can be written as

$$A_{u\ell} = \frac{64\pi^4 \nu^3_{u\ell}}{3h\, du} \Sigma |R_e(\bar{r}_{v'v''})|^2 \cdot q_{v'v''} \cdot S^{J'\Lambda'}_{J''\Lambda''} , \qquad (3.26)$$

where $|R_e(\bar{r}_{v'v''})|^2 = \Sigma |R_e(\bar{r}_{v'v''})|^2/du$.

The total energy emitted during a spontaneous emission transition from a upper state u to a lower state ℓ is given by

$$E_\ell^u = \frac{10^{-7}}{4\pi} h\nu_{u\ell} N_u A_{u\ell}, \text{ watts/cm}^3\cdot\text{sr} \qquad (3.27)$$

where N_u is the number density of emitters in the upper state. Equations (3.26) and (3.27) allow the equation for the emitted energy in a single line to be written as

$$E_\ell^u = \frac{16 \times 10^{-7}\pi^3\bar{\nu}_{u\ell}^4 c}{3(2 - \delta_{o,\Lambda'})(2S' + 1)(2J' + 1)} N_{uv'\Lambda'J'} \Sigma|R_e(\bar{r}_{v'v''})|^2 q_{v'v''} S_{J''\Lambda''}^{J'\Lambda'} . \qquad (3.28)$$

which is identical to equation (3.1). In this equation, the total statistical weight is the product of the rotational statistical weight $(2J' + 1)$ and the electronic statistical weight $(2 - \delta_{o,\Lambda'})(2S' + 1)$. The Kronecker delta symbol, $\delta_{i,j}$, suggested by Schadee (1964) is adopted and is zero when $i \neq j$ and unity when $i = j$. The vibrational statistical weight is 1.

Since the bandpass of the experimental measurements contained several rotational lines, equation (3.28) must be summed to include all lines which contribute in the spectral region of the bandpass. Similarly by summing over all states involved in an electronic transition, the total emitted energy in that transition due to spontaneous emission is given by

$$E_\ell^u = \left(\frac{16 \times 10^{-7}}{3}\right)(\pi c\bar{\nu}_{u\ell}^4)\left[\sum_{p'p''}\sum_{\Lambda'\Lambda''} \frac{|R_e(\bar{r}_{v'v''})|^2 \cdot q_{v'v''}}{(2 - \delta_{o,\Lambda'})(2S' + 1)}\right] \times \left[\frac{S_{J''\Lambda''}^{J'\Lambda'}}{2J' + 1}\right][N_{uv'J'\Lambda'}] . \qquad (3.29)$$

The $\sum_{p'p''}$ accounts for the parity of the states. It should be noted that the Hönl-London factors $S^{J'\Lambda'}_{J''\Lambda''}$ in equation (3.29) are normalized in the manner suggested by Schadee (1967):

$$\sum_{\Lambda'\Lambda''} \sum_{J''} S^{J'\Lambda'}_{J''\Lambda''} = (2S' + 1)(2J' + 1). \tag{3.30}$$

3.2 Franck-Condon and Hönl-London Factors

In equation (3.25), it was asserted that the band strength could be separated into two factors through the r centroid approximation of Fraser (1954). That is

$$\left| \int \psi_{v'} R_e(\bar{r}_{v'v''}) \psi_{v''} \, dr \right|^2 = |R_e(\bar{r}_{v'v''})|^2 \cdot q_{v'v''} \tag{3.31}$$

where $\bar{r}$ was defined as

$$\bar{r}_{v'v''} = \frac{\int \psi_{v'} \psi_{v''} r \, dr}{\int \psi_{v'} \psi_{v''} \, dr} \tag{3.32}$$

and the ψ's are the vibrational wave functions and r is the internuclear separation. Despite some criticisms of applicability to individual cases (James, 1966 and Klemsdal, 1973) this approximation has been shown to be adequate for bands of most systems (McCallum, Jarmain, and Nicholls, 1970 and Nicholls, 1974).

The Franck-Condon factor

$$q_{v'v''} = \left| \int \psi_{v'} \psi_{v''} \, dr \right|^2 \tag{3.33}$$

is the square of the overlap integral of the vibrational wavefunctions and its magnitude is controlled by the relative position of the potentials and the relative phase of the wavefunctions. It exerts a very strong influence on the relative band intensities within a system. In the present work, the Franck-Condon factors of McCallum, Jarmain, and

Nicholls (1970) are used. These Franck-Condon factors are based on realistic Klein-Dunham potentials derived from measured molecular constants. A complete list of the Franck-Condon factors used in this work is given in appendix C.

The Hönl-London factors were defined as

$$S^{J'\Lambda'}_{J''\Lambda''} = \left| \int \psi_{J'\Lambda'} |D| \psi_{J''\Lambda''} d\Gamma \right|^2 \tag{3.34}$$

where $\psi_{J'\Lambda'}$ and $\psi_{J''\Lambda''}$ are the electronic-rotational wave functions for the upper and lower levels, and D is the dyadic of coordinate transformation. These factors are well known for most common types of transitions. The Hönl-London factors used in this work were taken from Schadee (1964) whose calculations have been verified by Kovacs (1969) and Whiting (1973).

The electronic transition moment $\Sigma|R_e(\bar{r}_{v'v''})|^2$ is often nondimensionalized by dividing by the product of the electron charge, e, and the Bohr radius, a_o. The band strength is then written as

$$S_{v'v''} = \Sigma|R_e(\bar{r}_{v'v''})/ea_o|^2 \cdot q_{v'v''} = \Sigma|R_e/ea_o|^2 \cdot q_{v'v''}, \text{ A.U.} \tag{3.35}$$

The total line strength can be defined as

$$S^{uv'J'}_{\ell v''J''} = \Sigma|R_e/ea_o|^2 \cdot q_{v'v''} \cdot S^{J'\Lambda'}_{J''\Lambda''}, \text{ A.U.}, \tag{3.36}$$

where roughly speaking the electronic transition moment, $\Sigma|R_e/ea_o|^2$, determines the absolute strength of the whole band system, the Franck-Condon factors, $q_{v'v''}$, control the relative strength of the bands within a system, and the Hönl-London factors, $S^{J'\Lambda'}_{J''\Lambda''}$, determine the relative intensities of the lines within a band.

3.3 Radiative Transport Theory

The data reduction technique used in this study requires the theoretical computation of spectral intensities. In order to compute these intensities accurately, it is necessary to consider the interaction of the radiation (given by equation (3.1) or (3.28)) with the heated gas particles. This interaction is well described by the equation of radiative transfer and is discussed in detail by Vincenti and Kruger (1965).

The one-dimensional radiative transfer equation which applies well to the case of shock-heated gas is (Vincenti and Kruger, 1965):

$$\frac{dI_\lambda}{dx} = \alpha_\lambda\left[1 - \exp\left(-\frac{hc}{\lambda kT}\right)\right]B_\lambda(T) + \alpha_\lambda I_\lambda \exp\left(-\frac{hc}{\lambda kT}\right) - \alpha_\lambda I_\lambda \,, \qquad (3.37)$$

where I_λ is the specific intensity along a given path x, B_λ is the Planck black-body function, and α_λ is the absorption coefficient. This equation is based on the assumption that the gas is in local thermodynamic equilibrium and that the various atomic and molecular states are populated predominately by particle collisions rather than through radiative emission or absorption. The three terms on the right-hand side of equation (3.37) are due to spontaneous emission, induced emission, and absorption, respectively. Integrating equation (3.37) over x and substituting $\alpha_\lambda' = \alpha_\lambda[1 - \exp(-hc/\lambda kT)]$, which is the absorption coefficient corrected for stimulated emission, one gets

$$I_\lambda = B_\lambda(T)[1 - \exp(-\alpha_\lambda'\ell)] + I_\lambda(\ell_s)\exp(-\alpha_\lambda'\ell), \qquad (3.38)$$

where ℓ is the optical path length, ℓ_s represents the gas boundary, and $I_\lambda(\ell_s)$ is the specific intensity incident on the gas boundary.

If one also assumes, as is true in the present tests, that the spontaneous emission processes dominate the absorption and induced

emission processes, equation (3.38) becomes

$$I_\lambda = B_\lambda(T)[1 - \exp(-\alpha_\lambda'\ell)]. \tag{3.39}$$

In the present tests the gas is also optically thin, that is, $\alpha_\lambda' << 1$, and the exponential in equation (3.39) can be expanded to give

$$I_\lambda = \alpha_\lambda'\ell B_\lambda(T). \tag{3.40}$$

Using Kirchoff's law, $\alpha_\lambda' = E_\lambda/B_\lambda(T)$, this becomes

$$I_\lambda = E_\lambda\ell. \tag{3.41}$$

The spontaneous emission intensities (equation (3.1) or (3.28)) described in section 3.1 can now be used to compute the specific intensity directly. With this information, a synthetic spectrum (section 3.6) can be calculated and consequently the data reduction procedure can be completed.

3.4 Application of Theory to C_2 Transitions

The theory of molecular spectroscopy reviewed above is here applied to the specific transitions of C_2. However, before this application is made, the selection rules which limit the transitions between energy levels must be recalled.

3.4.1 Electric Dipole Transition Selection Rules

Selection rules govern both the quantum numbers and the symmetry properties of the states involved in a transition. In the following review, the selection rules are valid for both Hund's case (a) and case (b), except where noted.

The symmetry selection rules depend on the symmetry properties of the eigenfunctions of the state under consideration. A rotational level is designated positive or negative depending on whether or not the total eigenfunction changes sign when it undergoes a reflection at the origin.

This property is known as parity. A rotational level of a homonuclear molecule is also designated symmetric (s) or antisymmetric (a) if when the nuclei are interchanged the total eigenfunction remains unchanged or only changes its sign. The symmetry selection rules of the rotational levels for a dipole transition in a homonuclear molecule are:

(1) Positive levels combine only with negative levels and vice versa, that is,

$$+ \leftrightarrow -, \quad + \not\leftrightarrow +, \quad - \not\leftrightarrow -.$$

(2) Symmetric states combine only with symmetric states and antisymmetric states combine only with antisymmetric states, that is,

$$\text{sym} \dashrightarrow \text{sym}, \quad \text{sym} \not\dashrightarrow \text{antisym}, \quad \text{antisym} \dashrightarrow \text{antisym}.$$

Since the C_2 molecule has zero nuclear spin, the latter selection rule is true for all transitions.

In addition to the symmetry properties of the total eigenfunction, the symmetry properties of the electronic eigenfunction are also important in determining the selection rules of electronic transitions. These properties depend on the symmetry properties of the field in which the electrons move. A nondegenerate state (Σ state) is called positive (Σ^+) or negative (Σ^-) if its electronic eigenfunction remains unchanged or changes sign when reflected at any plane passing through both nuclei. For degenerate states, linear combinations of the eigenfunctions can be obtained in order that the electronic eigenfunctions sign either changes or remains the same. Consequently this nomenclature (+ or -) is usually omitted for degenerate states. If an electronic eigenfunction remains unchanged when reflected at the center of symmetry (midpoint of the internuclear axis for a homonuclear molecule), then the state to which

it belongs is called an even or "gerade" state and is indicated by the subscript g. If the eigenfunction changes signs when reflected at the center of symmetry, its state is called an odd or "ungerade" state and is indicated by the subscript u. The selection rules resulting from the electronic eigenfunction properties are:

(1) Positive states combine only with positive states and negative states only with negative states, that is,

$$\Sigma^+ \leftrightarrow \Sigma^+, \ \Sigma^- \leftrightarrow \Sigma^-, \ \Sigma^+ \not\leftrightarrow \Sigma^-.$$

(2) Even electronic states can only combine with odd states or vice versa, that is,

$$g \leftrightarrow u, \ g \not\leftrightarrow g, \ u \not\leftrightarrow u.$$

The selection rule for the total angular momentum number, J, is

$$\Delta J = 0, \pm 1$$

where $J = 0 \not\rightarrow J = 0$ is prohibited. The selection rule for the quantum number Λ which represents the component of the electronic orbital angular momentum along the internuclear axis is

$$\Delta \Lambda = 0, \pm 1.$$

An additional selection rule imposed on the resultant spin, S, is

$$\Delta S = 0.$$

This rule implies that only states of the same multiplicity can combine with one another.

As mentioned above, the previous selection rules apply generally to both Hund's case (a) and case (b). The following selection rules apply only if both of the electronic states involved in the transition belong to the same coupling case. For Hund's case (a), the following selection rules are valid:

(1) $\Delta\Sigma = 0$

(2) $\Delta\Omega = 0, \pm 1$

where Σ and Ω are the quantum numbers which represent the component of spin along the internuclear axis and the component of the total electronic angular momentum about the internuclear axis, respectively. If the quantum number Ω is zero for both electronic states, then an additional restriction is placed on the quantum number J - only $\Delta J = \pm 1$ transitions can occur.

In Hund's case (b), the following selection rule is placed on the quantum number K, the total angular momentum apart from spin,

$$\Delta K = 0, \pm 1$$

where $\Delta K = 0$ is forbidden for Σ-Σ transitions.

All of these selection rules are summarized in table 3.1.

The structure of each of the C_2 band systems studied experimentally will now be discussed.

3.4.2 The C_2 Swan System Transition, d $^3\pi_g$ - a $^3\pi_u$

The C_2 Swan system (Swan, 1857) results from transitions between the d $^3\pi_g$ and a $^3\pi_u$ electronic states (see figure 2.1). Term energies corresponding to these states are given in table 2.1. The vibrational term energies are calculated using equation (3.11) and the vibrational constants which are also listed in table 2.1. A tabulation of the band origins, λ_o, of this system in appendix B shows that the approximate spectral range is between 3600 and 8600 Å.

Franck-Condon factors (appendix C) which control the relative intensity distribution of the bands within a system can be used to

Table 3.1 Electric Dipole Transition Selection Rules.

Molecule	Selection rules	
	Rotational	Electronic
	General selection rules for Hund's cases (a) and (b):	
	$+ \leftrightarrow -$	$+ \leftrightarrow +$
	$+ \not\leftrightarrow +$	$- \leftrightarrow -$
	$- \not\leftrightarrow -$	$+ \not\leftrightarrow -$
	$s \leftrightarrow s$	$g \leftrightarrow u$
	$a \leftrightarrow a$	$g \not\leftrightarrow g$
	$s \not\leftrightarrow a$	$u \not\leftrightarrow u$
Any diatomic molecule with identical nuclei, e.g., C_2^{12}	$\Delta J = 0, \pm 1$ where $J = 0 \not\rightarrow J = 0$ is forbidden	$\Delta \Lambda = 0, \pm 1$ $\Delta S = 0$
	Selection rules if both electronic states in a transition belong to:	
	Hund's case (a)	
	$\Delta J = 0$ is forbidden for $\Sigma \leftrightarrow \Sigma$ transitions	$\Delta \Sigma = 0$ $\Delta \Omega = 0, \pm 1$
	Hund's case (b)	
	$\Delta K = 0, \pm 1$ where $\Delta K = 0$ is forbidden for $\Sigma \leftrightarrow \Sigma$ transitions	

determine the most intense bands. Figure 3.3 is a Deslandres diagram of Franck-Condon factors normalized to the maximum value. Only those normalized values exceeding 0.1 are included. As observed on the figure, the most intense bands form a parabolic curve whose axis is the principal diagonal of the diagram. This curve is known as the Condon parabola or Condon locus. The width of this parabola increases with increasing difference (Δr_e) of the equilibrium internuclear distances (minima of the potential curves) of the upper and lower states. Since Δr_e is small for this system, the narrow width of the Condon parabola for the Swan system is expected. Figure 3.3 can be used a priori to determine rapidly the prominent features of the excited Swan system.

The Swan system is an example of a transition in which both states are well represented by Hund's case (a) at low values of J and Hund's case (b) at large values of J. Figure 3.4 is an energy level diagram of the rotational structure of the Swan system. Both electronic states are assumed to comply with Hund's case (b) conditions. The rotational energy levels, where F_1, F_2, and F_3 refer to the levels with $J = K + 1$, K, $K - 1$, respectively, are given by

$$\left.\begin{aligned} F_1 &= B_v K(K+1) + D_v K^2(K+1)^2 + \frac{A}{K+1} + K\left(\gamma - \frac{2G}{2K+3}\right) + \phi_{\pm}(K) , \\ F_2 &= B_v K(K+1) + D_v K^2(K+1)^2 - \frac{A}{K(K+1)} - \gamma + 2\varepsilon + \phi_{\pm}(K) , \\ F_3 &= B_v K(K+1) + D_v K^2(K+1)^2 - \frac{A}{K} - (K+1)\left(\gamma + \frac{2\varepsilon}{2K-1}\right) + \phi_{\pm}(K) , \end{aligned}\right\} \quad (3.42)$$

where $\phi_{\pm}(K)$ is the Λ doubling function and is different for the two ($\pm$) components. In the above equations, A is the coupling constant and γ and ε are splitting constants. There are three possible values of J

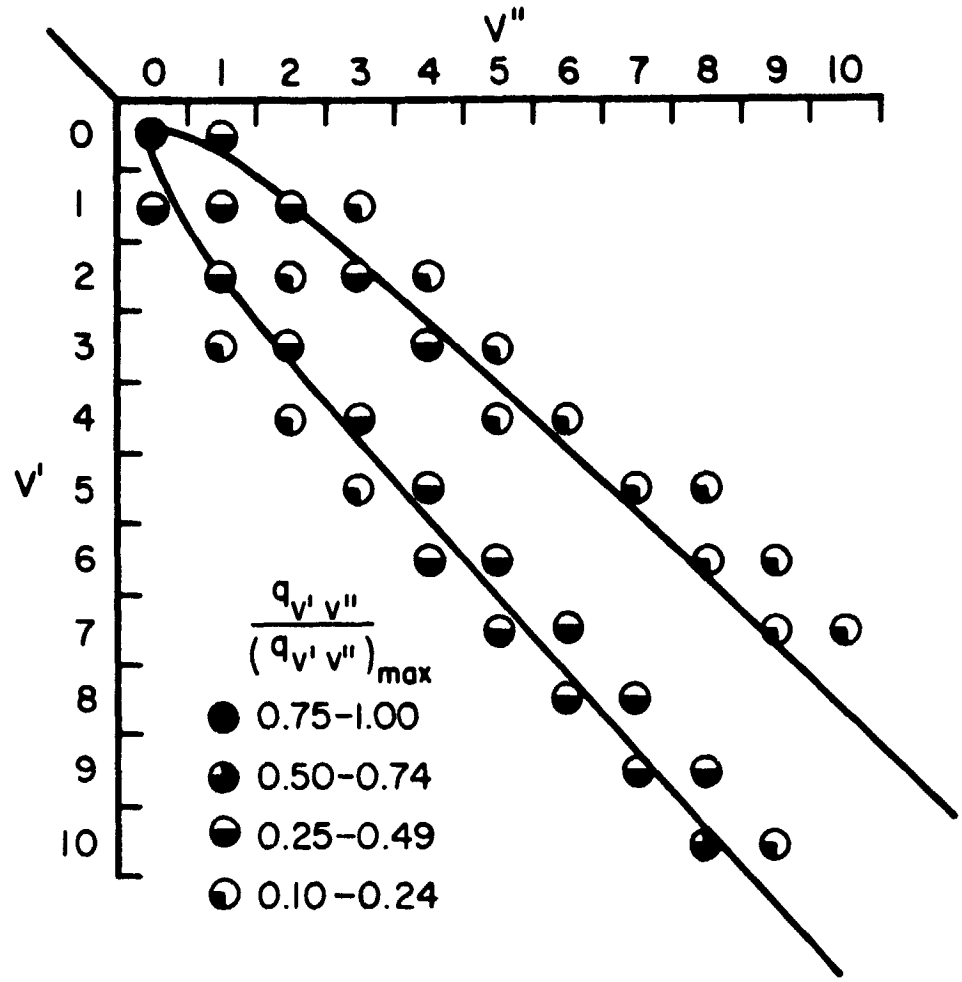

Figure 3.3.- Deslandres diagram of normalized Franck-Condon factors for the Swan system. Only normalized values exceeding 0.1 are included.

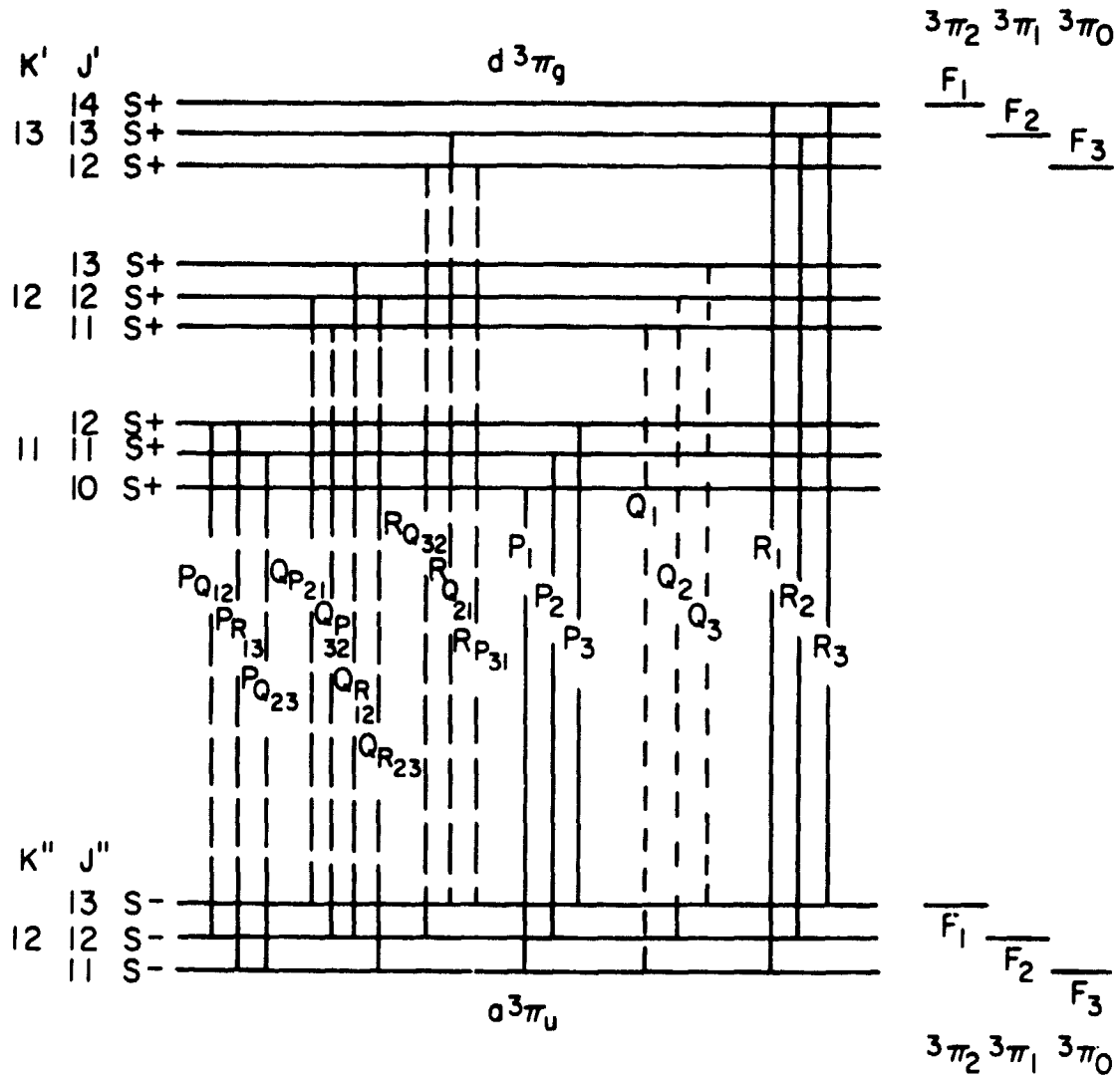

Figure 3.4.- Energy level diagram for the rotational structure of the Swan (d $^3\pi_g$ - a $^3\pi_u$) transition K" = 12. Both electronic states are inverted and assumed to belong to Hund's case (b). The antisymmetric levels do not occur. The transitions indicated by the dashed lines are very weak for large J.

for each K value because

$$J = K + S,\ K + S - 1,\ \ldots,\ |K - S|.$$

Since the coupling constant (A) is negative for both electronic states involved in the Swan transition, the triplet terms are inverted - that is, terms of the triplet components lie in the inverse order of their quantum number, Ω, which represents the resultant of the electronic angular momentum about the internuclear axis. In a homonuclear molecule such as C_2 which has zero nuclear spin, the antisymmetric levels do not occur and consequently one component of the Λ-type doubling does not appear in each electronic state. These are the negative levels of the $^3\pi_g$ state and the positive levels of the $^3\pi_u$ state.

From the selection rules given in table 3.1, P($\Delta J = -1$), Q($\Delta J = 0$), and R($\Delta J = +1$) branches as well as P-form, Q-form, and R-form branches are all theoretically possible. Sample transitions corresponding to these branches for the $K'' = 12$ level are displayed in figure 3.4. This energy level diagram is not drawn to scale and the multiplet splitting is greatly exaggerated. By examining the Hönl-London factors which are given in table 3.2, one can see that the P-, Q-, and R-form branches and the Q branch are extremely weak for large values of J. Therefore the transitions corresponding to these branches are given by dashed lines in figure 3.4. A close examination of the spectra resulting from the transitions on figure 3.4 would reveal that the lines from even-numbered K values are displayed to one side of a mean position and odd-numbered K values to the other side. This effect in the branches is called staggering.

Table 3.2 Hönl-London Factors for the Swan (d $^3\pi_g$ - a $^3\pi_u$) and Fox-Herzberg (e $^3\pi_g$ - a $^3\pi_u$) Transitions (Schadee, 1964). These Hönl-London Factors are Normalized to $(2S' + 1)(2J' + 1)$.

Branch	$S^{J'\Lambda'}_{J''\Lambda''}$	Branch	$S^{J'\Lambda'}_{J''\Lambda''}$
$P_1(J)$	$\frac{J(J-2)(2J+1)}{(J-1)(2J-1)}$	$R_2(J)$	$\frac{J^2(J+2)^2}{(J+1)^3}$
$Q_1(J)$	$\frac{(J+1)(2J+1)}{J^3}$	$QP_{32}(J)$	$\frac{2J-1}{J^3(J+1)}$
$R_1(J)$	$\frac{(J+1)(J-1)(2J+3)}{J(2J+1)}$	$RQ_{32}(J)$	$\frac{J(J+2)}{(J+1)^3}$
$QP_{21}(J)$	$\frac{2J+1}{J^3(J-1)}$	$PR_{13}(J)$	$\frac{J(J+2)}{(J+1)^3(2J+3)(2J+1)}$
$RQ_{21}(J)$	$\frac{(J+1)(J-1)}{J^3}$	$PQ_{23}(J)$	$\frac{J(J+2)}{(J+1)^3}$
$RP_{31}(J)$	$\frac{(J+1)(J-1)}{J^3(2J+1)(2J-1)}$	$QR_{23}(J)$	$\frac{2J+1}{(J+2)(J+\ ^3}$
$PQ_{12}(J)$	$\frac{(J+1)(J-1)}{J^3}$	$P_3(J)$	$\frac{J(J+2)(2J-1)}{(J+1)(2J+1)}$
$QR_{12}(J)$	$\frac{2J+3}{J(J+1)^3}$	$Q_3(J)$	$\frac{J(2J+1)}{(J+1)^3}$
$P_2(J)$	$\frac{(J+1)^2(J-1)^2}{J^3}$	$R_3(J)$	$\frac{(J+3)(J+1)(2J+1)}{(J+2)(2J+3)}$
$Q_2(J)$	$\frac{(2J+1)(J^2+J-1)^2}{J^3(J+1)^3}$		

3.4.3 The Fox-Herzberg System Transition, e $^3\pi_g$ - a $^3\pi_u$

The Fox-Herzberg system (Fox and Herzberg, 1937) results from transitions between the e $^3\pi_g$ and a $^3\pi_u$ electronic states. The electronic term energies and vibrational constants required to calculate the vibrational energies (equation (3.11)) are given in table 2.1. This system occurs in the spectral region between approximately 2300 and 3500 Å.

Figure 3.5 is a Deslandres diagram of Franck-Condon factors of this system normalized to the maximum value. The primary Condon locus for this system has broadened and its apex has moved diagonally away from the (0,0) transition. This feature is typical of band systems in which the difference between the equilibrium internuclear distance (Δr_e) of the electronic states is large (see table 2.1). A number of subsidary loci can also be seen in figure 3.5.

The rotational structure of the Fox-Herzberg system is almost identical in character to that of the Swan system. Both systems make a rapid transition from Hund's case (a) to case (b) as J increases. The primary difference between these two systems apart from wavelength, however, is that the coupling constant, A, is very small and positive for the upper electronic state of the Fox-Herzberg system. As a result of this, the triplet term components of the upper state lie in a normal order, that is, terms of the triplet components lie in the order of increasing quantum number, Ω, as shown in figure 3.6. The energy level equations, selection rules, and Hönl-London factors are the same as those given previously for the Swan system. Once again the very weak Q branch and P-, Q-, and R-form branches are represented by dashed lines.

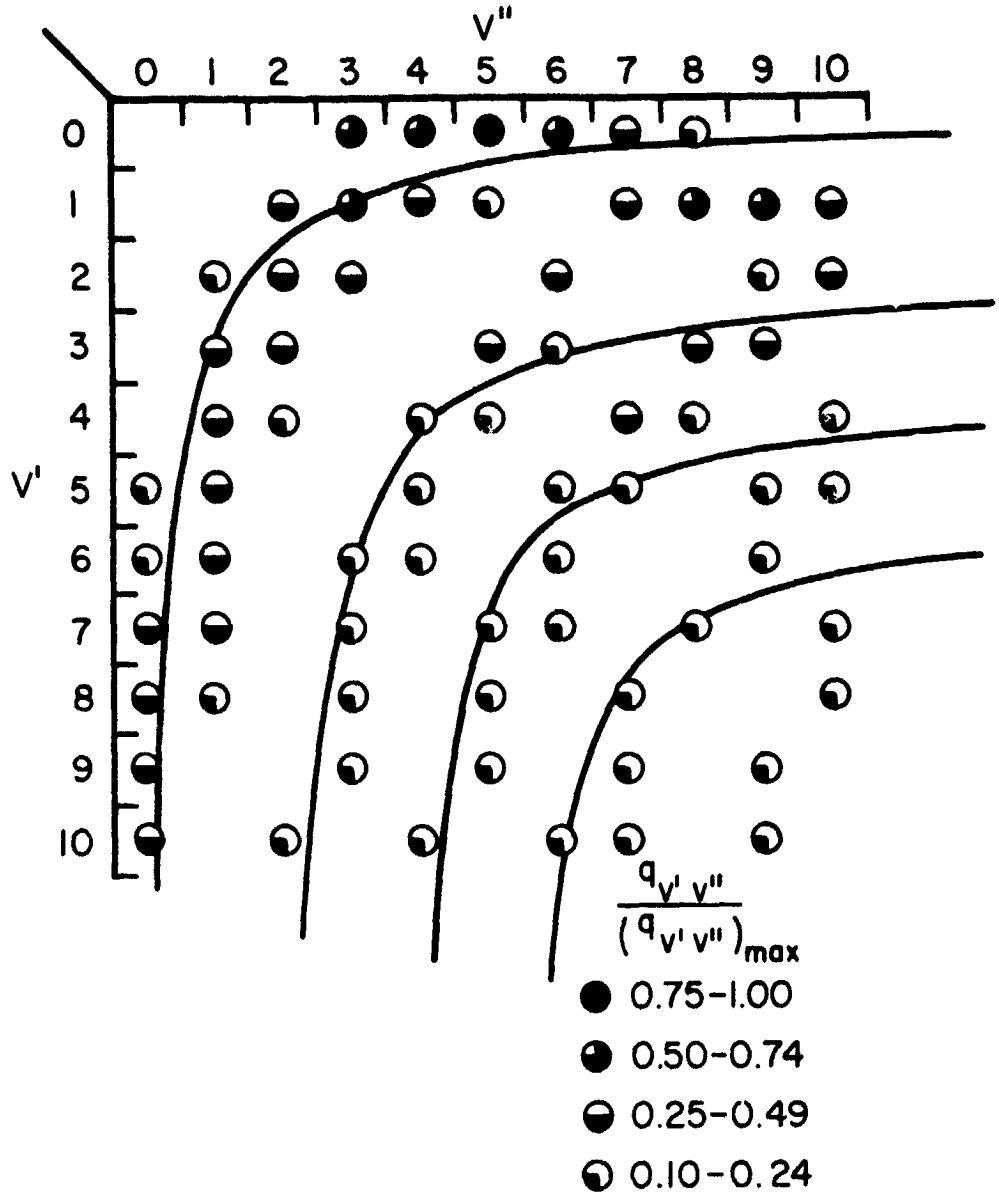

Figure 3.5.- Deslandres diagram of normalized Franck-Condon factors for the Fox-Herzberg system. Only normalized values exceeding 0.1 are included.

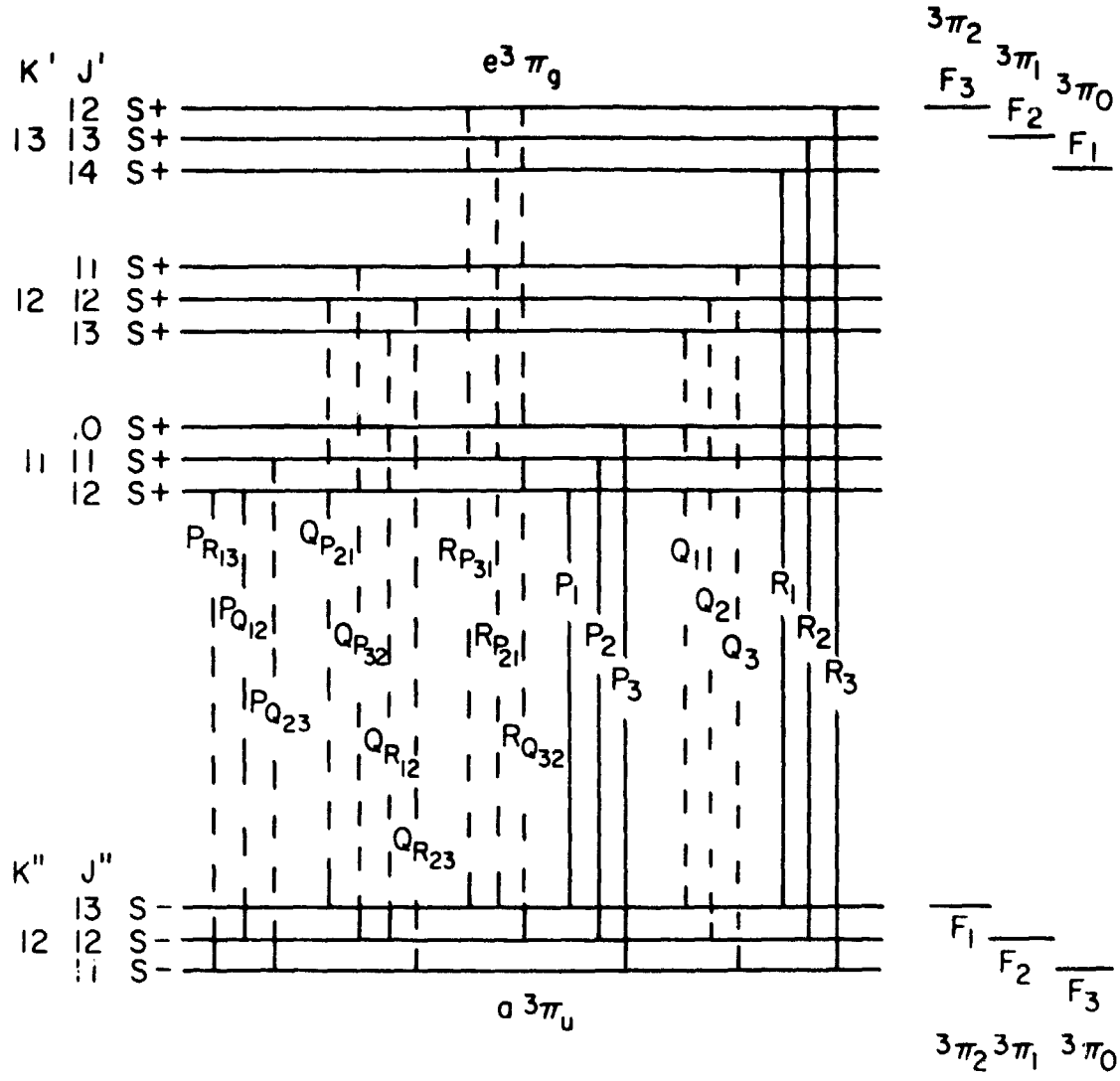

Figure 3.6.- Energy level diagram for the rotational structure of the Fox-Herzberg (e $^3\pi_g$ - a $^3\pi_u$) transition, K" = 12. Both electronic states belong to Hund's case (b) and the lower state (a $^3\pi_u$) is inverted. The transitions indicated by dashed lines are very weak for large J.

The staggering effect in the branches can also be observed in the spectrum of this system.

3.4.4 The Ballik-Ramsay System Transition, b $^3\Sigma_g^-$ - a $^3\pi_u$

The final triplet system of interest in this work is the Ballik-Ramsay system (Ballik and Ramsay, 1959). It occurs when transitions take place between the b $^3\Sigma_g^-$ and a $^3\pi_u$ electronic states. Electronic and vibrational term energies are given in table 2.1 and equation (3.11), respectively. The approximate spectral range (appendix B) is from 7100 to 25,000 Å.

Figure 3.7 is a Deslandres diagram of normalized Franck-Condon factors for this system. The Condon parabola is narrow as one would expect since Δr_e for this system is small.

The lower electronic state is the same as that of the Swan and Fox-Herzberg systems and therefore the rotational energy levels are given by equations (3.42). For the upper state, b $^3\Sigma_g^-$, the rotational levels are given by

$$\left.\begin{aligned} F_1 &= B_v K(K+1) + (2K+3)B_v - \lambda - \sqrt{(2K+3)^2 B_v^2 + \lambda^2 - 2\lambda B_v} + \gamma(K+1), \\ F_2 &= B_v K(K+1), \\ F_3 &= B_v K(K+1) - (2K-1)B_v - \lambda + \sqrt{(2K+1)^2 B_v^2 + \lambda^2 - 2\lambda B_v} - \gamma K, \end{aligned}\right\} \tag{3.43}$$

where F_1, F_2, and F_3 refer to the levels with $J = K + 1$, K, and $K - 1$, respectively, and λ and γ are splitting constants. Again the $^3\pi$ lower state is assumed to conform to Hund's case (b) conditions. The branches of the $^3\Sigma_g^-$ - $^3\pi_u$ electronic transitions are shown on figure 3.8. The dashed transitions are extremely weak as one can readily verify by consulting the Hönl-London factors in table 3.3.

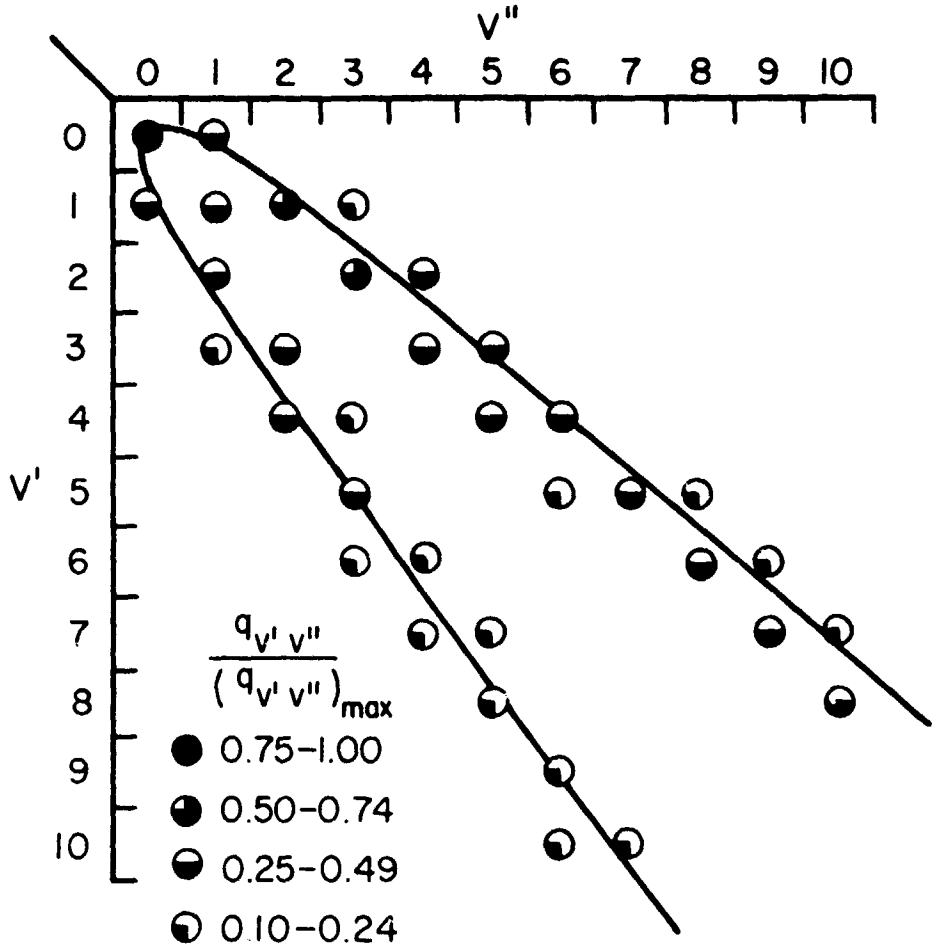

Figure 3.7.- Deslandres diagram of normalized Franck-Condon factors for the Ballik-Ramsay system. Only normalized values exceeding 0.1 are included.

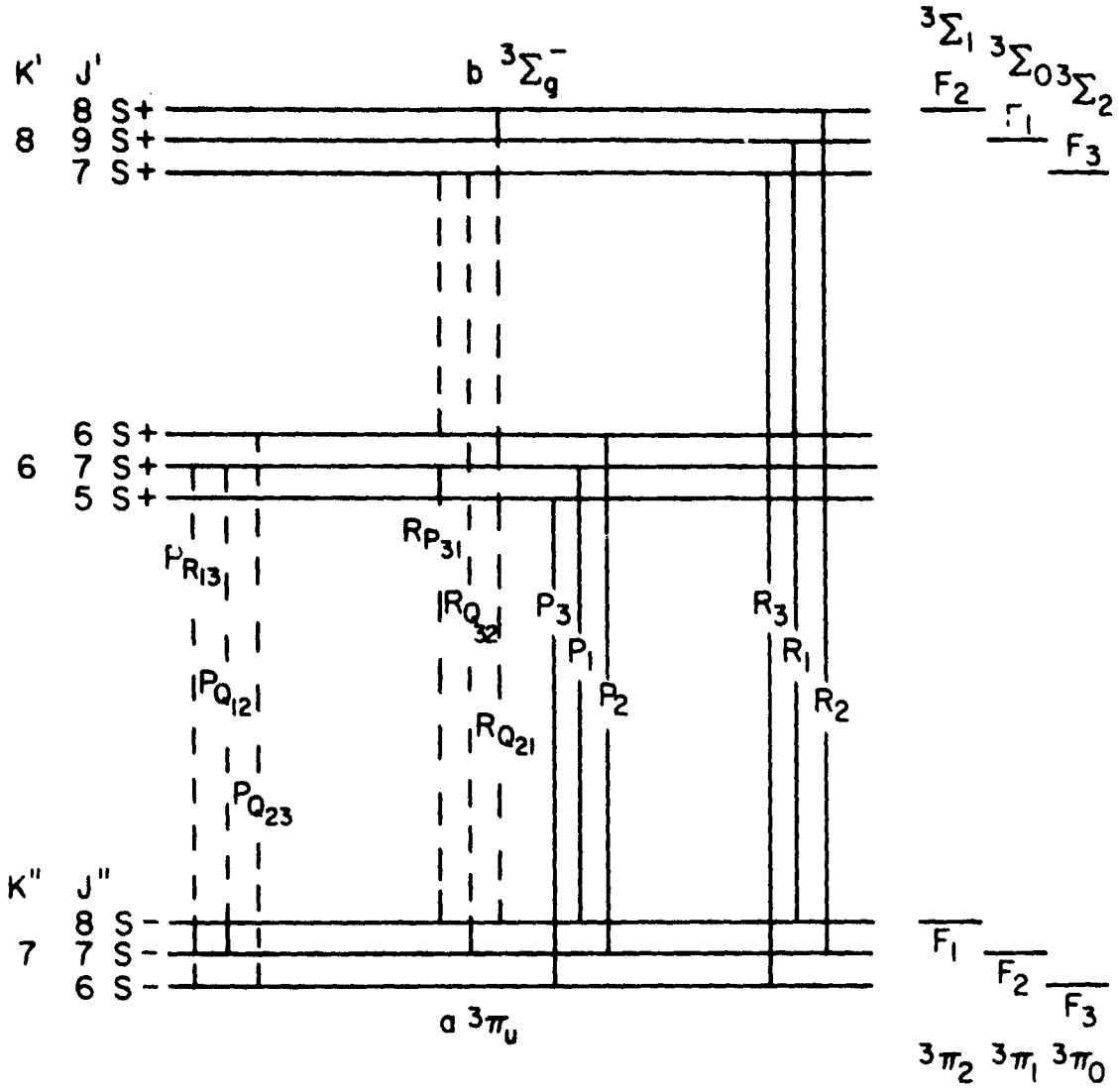

Figure 3.8.- Energy level diagram for the rotational structure of the Ballik-Ramsay (b $^3\Sigma_g^-$ - a $^3\pi_u$) transition, K" = 7. The lower electronic state obeys Hund's case (b) conditions and is inverted. The P form and R form branches (represented by dashed lines) are very weak.

Table 3.3 Hönl-London Factors for the Ballik-Ramsay ($b\ ^3\Sigma_g^- - a\ ^3\pi_u$) Transition (Schadee, 1964). These Factors are Normalized to $(2S' + 1)(2J' + 1)$.

Branch	$S^{J'\Lambda'}_{J''\Lambda''}$	Branch	$S^{J'\Lambda'}_{J''\Lambda''}$
$P_1(J)$	$\frac{J(2J + 1)}{2(2J - 1)}$	$R_2(J)$	$\frac{J^2(J + 2)}{2(J + 1)^2}$
$Q_1(J)$	$\frac{(2J + 1)(J + 1)(J - 1)}{2J^2}$	$QP_{32}(J)$	$\frac{2J - 1}{2J^2}$
$R_1(J)$	$\frac{(J - 1)(2J + 3)}{2(2J + 1)}$	$RQ_{32}(J)$	$\frac{J}{2(J + 1)^2}$
$QP_{21}(J)$	$\frac{2J + 1}{2J^2}$	$PR_{13}(J)$	$\frac{J + 2}{2(J + 1)^2(2J + 3)(2J + 1)}$
$RQ_{21}(J)$	$\frac{J - 1}{2J^2}$	$PQ_{23}(J)$	$\frac{J + 2}{2(J + 1)^2}$
$RP_{31}(J)$	$\frac{J - 1}{2J^2(2J + 1)(2J - 1)}$	$QR_{23}(J)$	$\frac{2J + 1}{2(J + 1)^2}$
$PQ_{12}(J)$	$\frac{J + 1}{2J^2}$	$P_3(J)$	$\frac{(J + 2)(2J - 1)}{2(2J + 1)}$
$QR_{12}(J)$	$\frac{2J + 3}{2(J + 1)^2}$	$Q_3(J)$	$\frac{J(J + 2)(2J + 1)}{2(J + 1)^2}$
$P_2(J)$	$\frac{(J - 1)(J + 1)^2}{2J^2}$	$R_3(J)$	$\frac{(J + 1)(2J + 1)}{2(2J + 3)}$
$Q_2(J)$	$\frac{(2J + 1)(J^2 + J - 1)^2}{2J^2(J + 1)^2}$		

3.4.5 The Mulliken System Transition, $D\ ^1\Sigma_u^+ - X\ ^1\Sigma_g^+$

The simplest of the singlet transitions is the $D\ ^1\Sigma_u^+ - X\ ^1\Sigma_g^+$ transition which is the Mulliken (Mulliken, 1930) system. The term energies for the electronic states involved in this transition are given in table 2.1, and the vibrational term energies can be calculated from equation (3.11) using the vibrational constants in table 2.1. This system has an approximate theoretical spectral range of 2100 to 2500 Å. However, the observed spectral range (see the following paragraph) is considerably smaller.

Figure 3.9 is a Deslandres diagram of the normalized Franck-Condon factors for this system. The Condon parabola has degenerated into a straight line lying along the principal diagonal of the diagram. This phenomenon occurs when the equilibrium internuclear distances for the electronic states are nearly the same.

Since the selection rules are identical for Hund's case (a) and case (b) for $^1\Sigma_u^+ - {}^1\Sigma_g^+$ transitions, it is immaterial to which case the states belong. The only allowed transitions are those with $\Delta J = \Delta K = \pm 1$. Consequently, the band structure which is shown in figure 3.10 consists of a single P and a single R branch. The energy levels $J' = 0, 2, 4, 6$ and $J'' = 1, 3, 5$ missing from figure 3.10 correspond to the anti-symmetric levels which as mentioned above do not occur in homonuclear molecules with zero nuclear spin.

The rotational term values are:

$$F(J) = B_v J(J + 1) - D_v J^2(J + 1)^2 + \ldots, \qquad (3.44)$$

and the Hönl-London factors are:

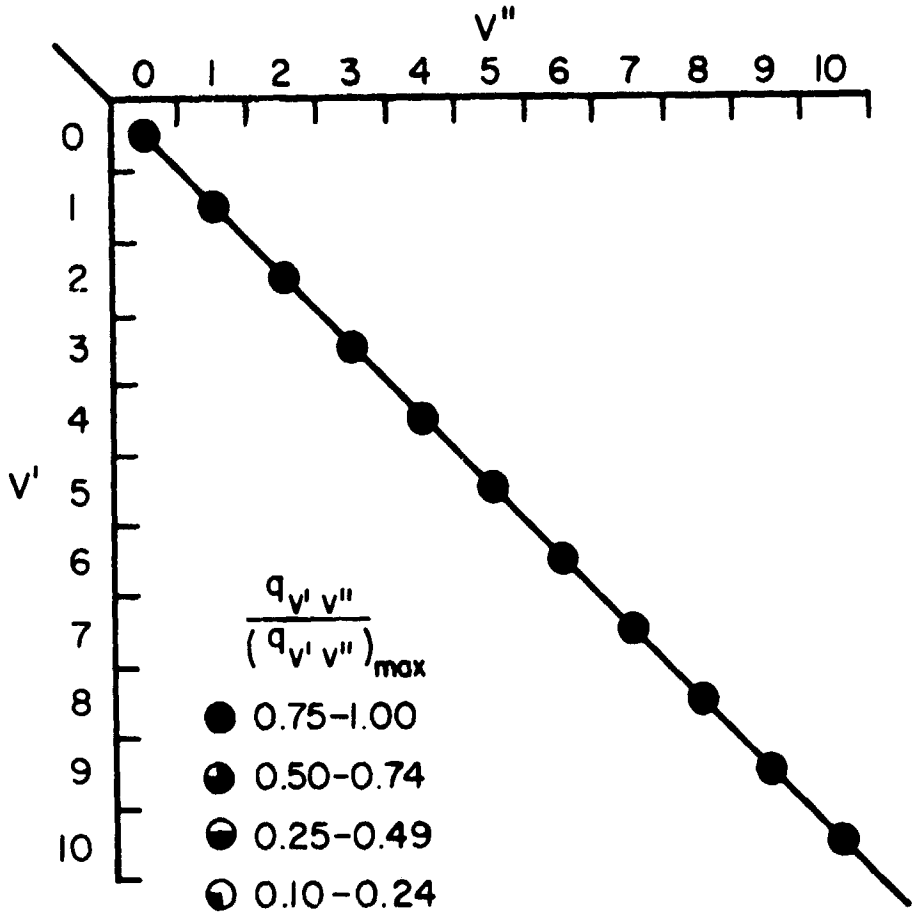

Figure 3.9.- Deslandres diagram of normalized Franck-Condon factors for the Mulliken system. Only normalized values exceeding 0.1 are included.

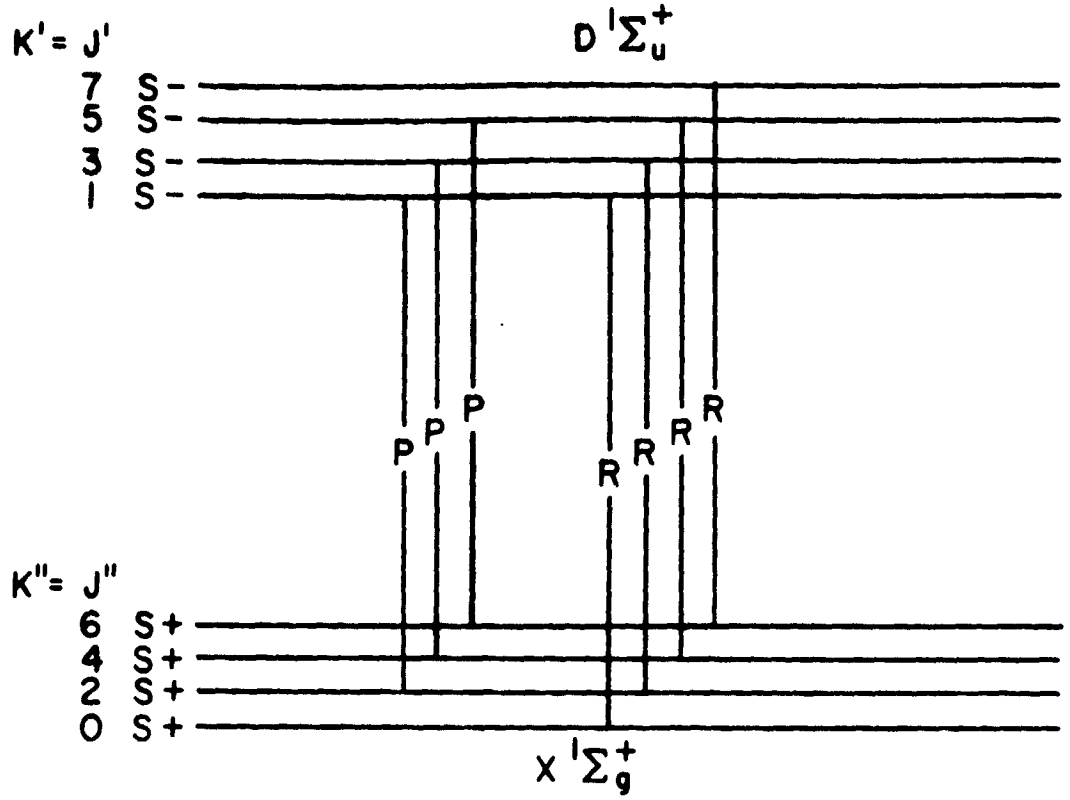

Figure 3.10.- Energy level diagram for the rotational structure of the Mulliken ($D\ ^1\Sigma_u^+ - X\ ^1\Sigma_g^+$) transition. The energy levels $J' = 0, 2, 4, 6, \ldots$ and $J'' = 1, 3, 5$ correspond to antisymmetric levels and therefore do not occur.

Branch	$S^{J'\Lambda'}_{J''\Lambda''}$
P	J
R	J + 1

It is interesting to note that the Mulliken system is "headless" and in this sense is unique among the C_2 systems investigated in this study. The appearance of this headless structure is readily understood by noting the relation between the band origin, $\bar{\nu}_o$, and the band head, $\bar{\nu}_m$, spectral locations,

$$\bar{\nu}_m - \bar{\nu}_o = - \frac{(B_{v'} + B_{v''})^2}{4(B_{v'} - B_{v''})} , \text{ cm}^{-1}. \qquad (3.45)$$

In this equation, $B_{v'}$ and $B_{v''}$ are the rotational constants for a vibrational level v of the upper and lower states, respectively. For the Mulliken system, the quantity $(B_{v'} - B_{v''})$ is very small and consequently the band head lies a great distance from the band origin and corresponds to a large J value. Since the intensity of large J lines is approximately zero, the bandhead in these cases is normally too weak to be observed.

3.4.6 The Deslandres-d'Azambuja System Transition, $C\ ^1\pi_g - A\ ^1\pi_u$

The Deslandres-d'Azambuja system (Deslandres and d'Azambuja, 1905) results from the $C\ ^1\pi_g - A\ ^1\pi_u$ transition. The electronic term energies are given in table 2.1 and the vibrational term energies may be obtained by using equation (3.11). This system radiates in the spectral region between approximately 2950 and 5400 Å (appendix B).

Figure 3.11 is a Deslandres diagram of the normalized Franck-Condon factors for this system. The Condon parabola is narrow which is indicative of a small Δr_e.

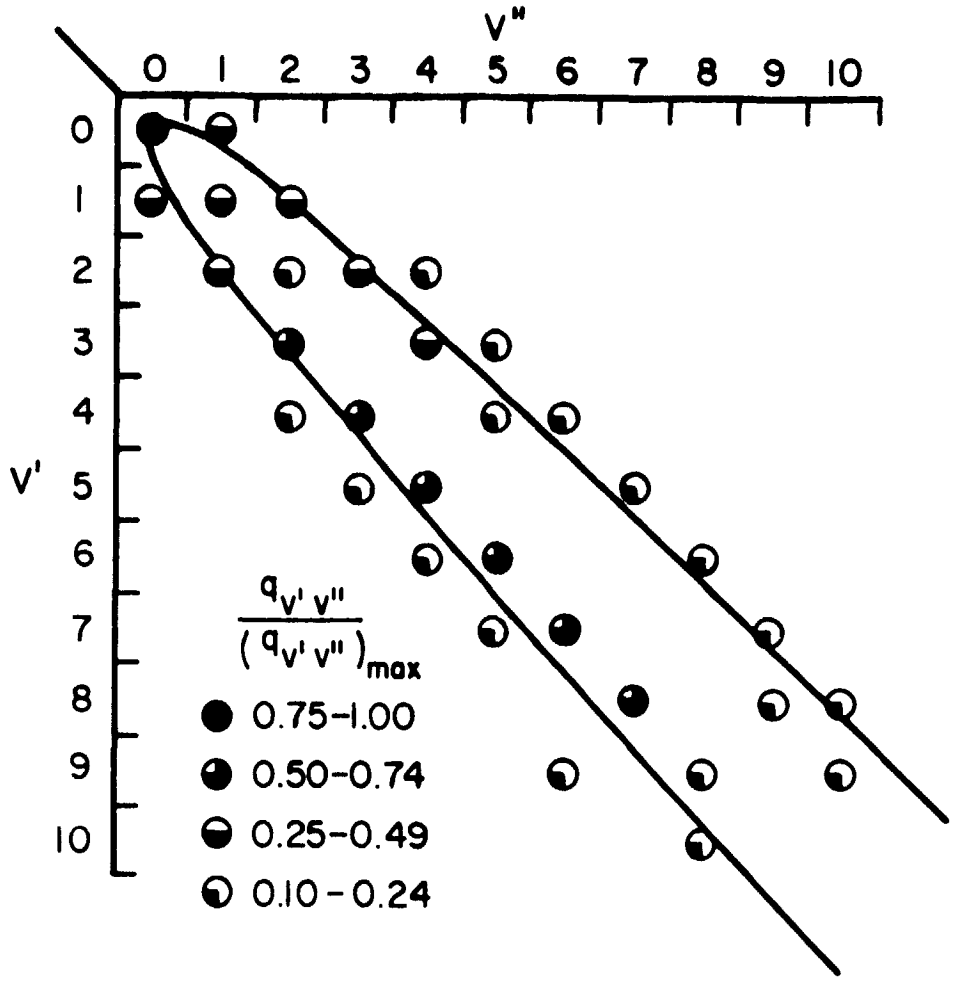

Figure 3.11.- Deslandres diagram of normalized Franck-Condon factors for the Deslandres-d'Azambuja system. Only normalized values exceeding 0.1 are included.

Since both electronic states are singlets, it is not necessary to distinguish between Hund's cases. From the selection rules $\Delta J = 0, \pm 1$, it is clear that P, Q, and R branches can all exist. Sample transitions are shown in figure 3.12. The Λ-type doubling component corresponding to the antisymmetric levels does not appear. In Λ-type doubling as J changes, the symmetric levels are alternately above and below the antisymmetric levels. This feature which is greatly exaggerated in figure 3.12 produces the "staggering" effect in the observed spectrum of this system.

The rotational levels for each state are given by

$$F(J) = B_v J(J+1) - (A - B_v)\Lambda^2 - D_v J^2(J+1)^2 + \ldots + \phi_{\pm}(J) \qquad (3.46)$$

where $\phi_{\pm}(J)$ is a very small correction to account for the Λ-type doubling. Inspection of the Hönl-London factors for this transition reveals that the Q branch is considerably weaker than the P and R branches and its intensity decreases rapidly as J increases.

Branch	$S^{J'\Lambda'}_{J''\Lambda''}$
P	$\frac{J^2 - 1}{J}$
Q	$\frac{2J + 1}{J(J + 1)}$
R	$\frac{J(J + 2)}{J + 1}$

3.4.7 The Phillips System Transition, $A\ ^1\pi_u - X\ ^1\Sigma_g^+$

An $A\ ^1\pi_u - X\ ^1\Sigma_g^+$ transition produces the Phillips system (Phillips, 1948). This system has the same lower electronic state as the Mulliken system and the same upper electronic state as the Deslandres-d'Azambuja system and therefore the electronic, vibrational, and rotational energy

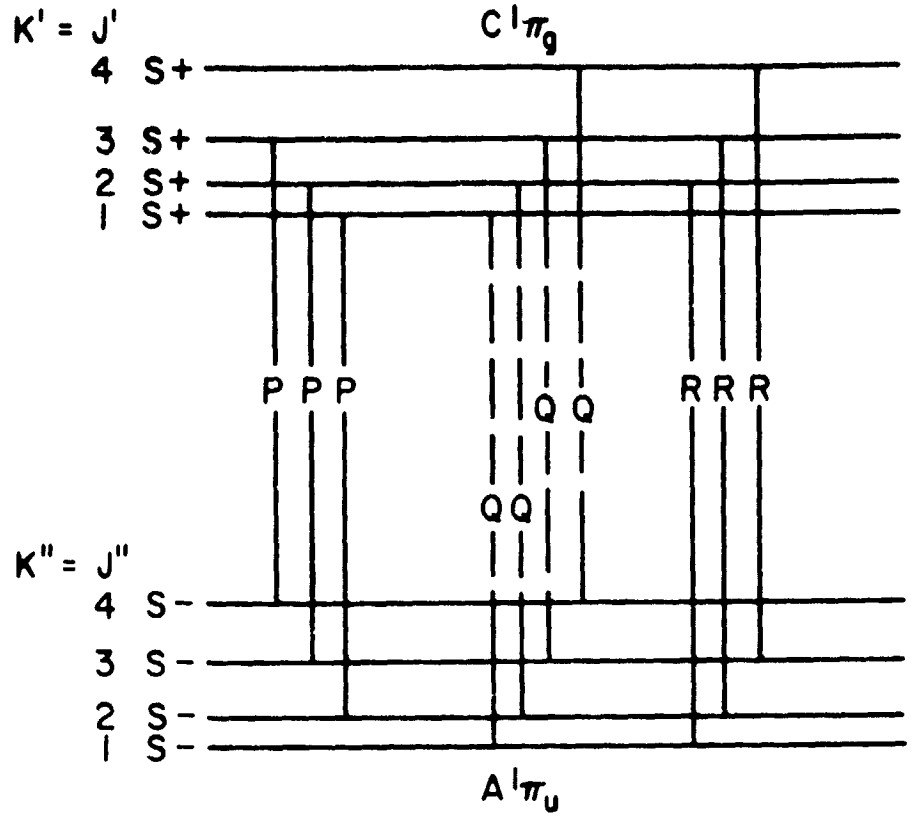

Figure 3.12.- Energy level diagram for the rotational structure of the Deslandres-d'Azambuja ($C\ ^1\pi_g$ - $A\ ^1\pi_u$) transition. The Q branch (dashed line) is considerably weaker than the P and R branches.

levels for the lower and upper states may be obtained from sections 3.4.5 and 3.4.6, respectively. The spectral range of the band origins of this system is 5000 to 23,400 Å (appendix B).

A Deslandres diagram of the normalized Franck-Condon factors for this system is plotted in figure 3.13. The principal Condon parabola is rather broad which is typical of a band system with a medium Δr_e. Note that the apex of the principal parabola is still located at (0,0). A subsidiary parabola also appears in the diagram. Its presence is also typical of medium (and large) Δr_e's.

For this electronic transition, the distinction between Hund's case (a) and case (b) is again needless. The selection rules $\Delta J = 0, \pm 1$ limit the transitions so that only simple P, Q, and R branches occur. These transitions are shown on the energy level diagram in figure 3.14. The odd J" levels are antisymmetric and do not appear.

The Hönl-London factors are:

Branch	$S^{J'\Lambda'}_{J''\Lambda''}$
P	$(1/2)(J - 1)$
Q	$(1/2)(2J + 1)$
R	$(1/2)(J + 2)$

3.4.8 The Freymark System Transition, $E\ ^1\Sigma_g^+ - A\ ^1\pi_u$

The Freymark system (Freymark, 1951) results from transitions between the $E\ ^1\Sigma_g^+$ and $A\ ^1\pi_u$ electronic states. The electronic term energies are given in table 2.1, and the vibrational term energies can be obtained from equation (3.11). The band origins (appendix B) for this system range from 1950 to 2550 Å.

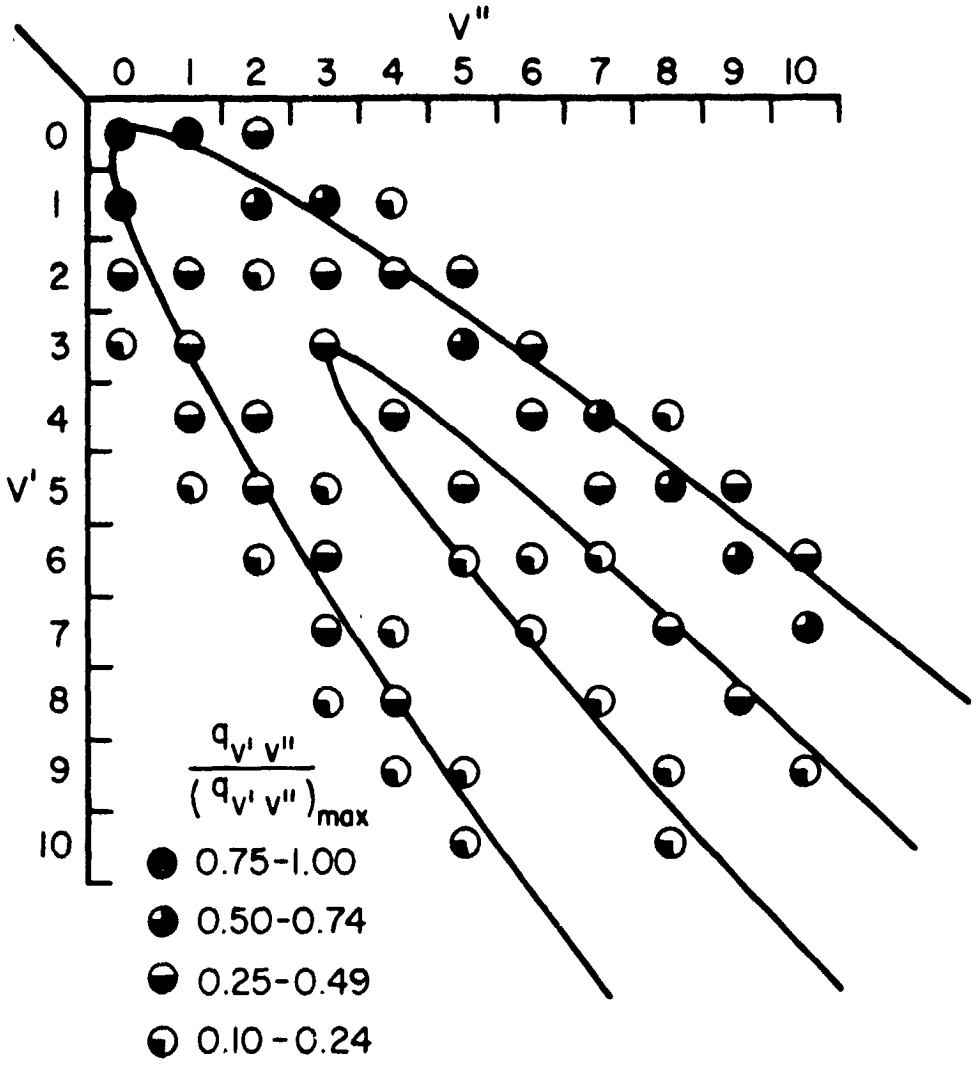

Figure 3.13.- Deslandres diagram of normalized Franck-Condon factors for the Phillips system. Only normalized values exceeding 0.1 are included.

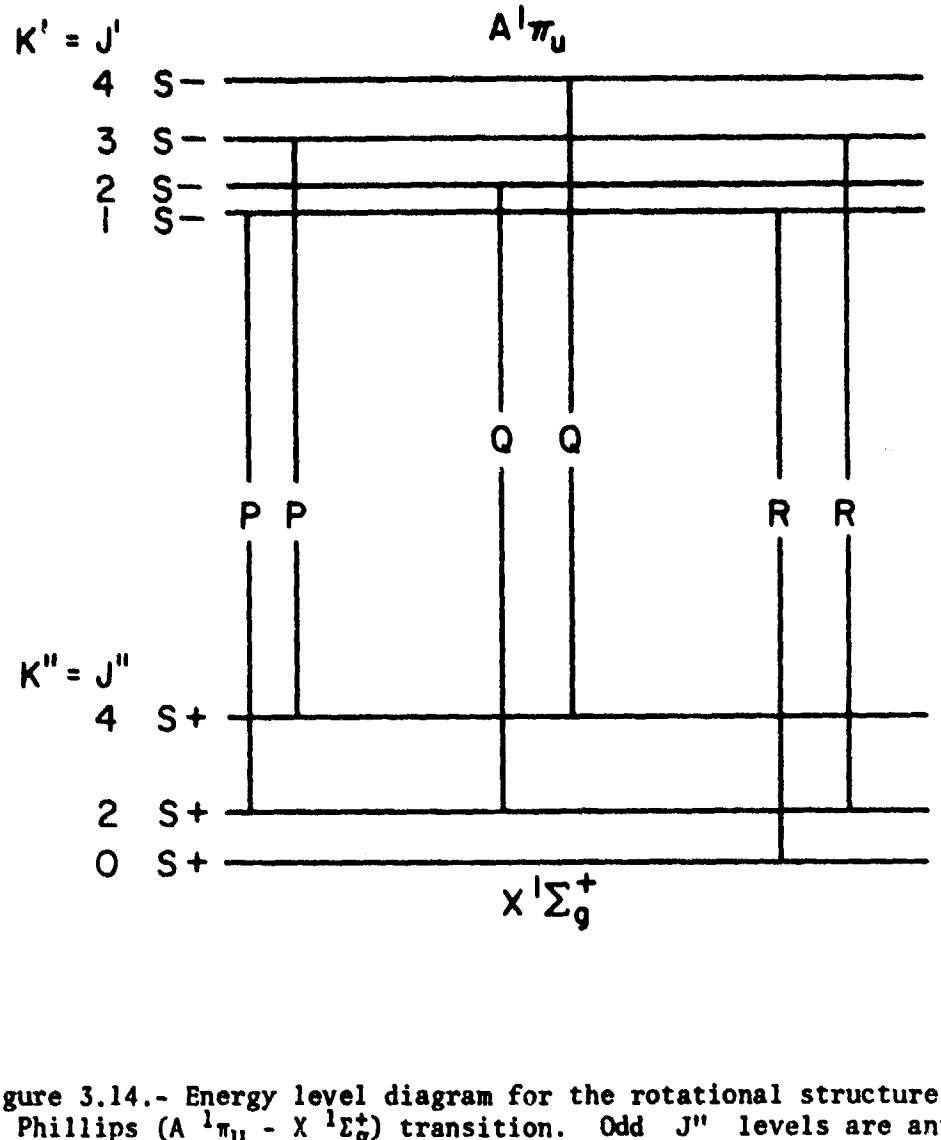

Figure 3.14.- Energy level diagram for the rotational structure of the Phillips ($A\ ^1\pi_u$ - $X\ ^1\Sigma_g^+$) transition. Odd J" levels are antisymmetric levels and do not occur.

Figure 3.15 is a Deslandres diagram of the normalized Franck-Condon factors for this system. The Condon parabola is narrow as expected since the Δr_e for this band system is small.

The rotational energy levels for the upper and lower states can be obtained from equations (3.44) and (3.46), respectively. Sample transitions are shown on the energy level diagram in figure 3.16.

The Hönl-London factors for this system are:

Branch	$S^{J'\Lambda'}_{J''\Lambda''}$
P	$(1/2)(J + 1)$
Q	$(1/2)(2J + 1)$
R	$(1/2)J$

3.5 Shock-Tube and Thermochemistry Theory

This section reviews the parts of shock-tube and thermochemistry theory necessary to calculate the equilibrium concentration, $N_{uv'\Lambda'J'}$. This quantity is an input parameter for equation (3.1) and must be accurately known in order to calculate the rotational line intensities which are used in the data analysis technique.

3.5.1 Thermally Perfect Gases in Equilibrium

The thermodynamic properties of most gases at moderate temperatures and pressures are well approximated by an equation of state of the form:

$$P_i V = N_i kT. \tag{3.47}$$

By definition, a thermally perfect gas is one which obeys this equation of state. The gas mixture in this study is assumed to consist of chemically reacting, thermally perfect species.

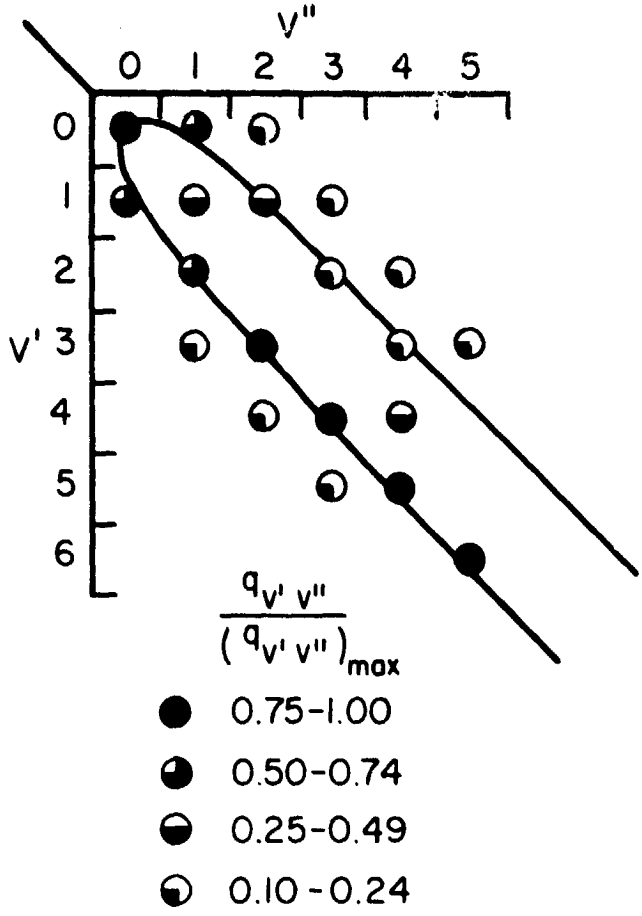

Figure 3.15.- Deslandres diagram of normalized Franck-Condon factors for the Freymark system. Only normalized values exceeding 0.1 are included.

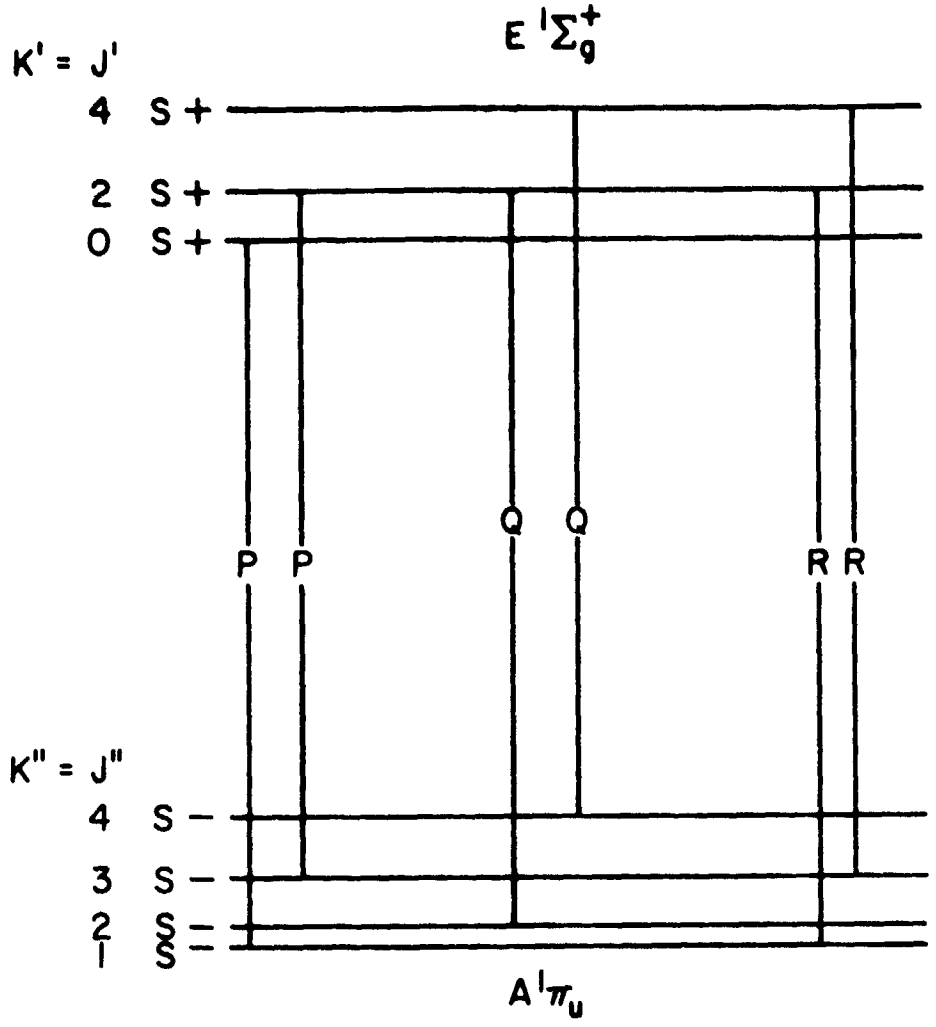

Figure 3.16.- Energy level diagram for the rotational structure of the Freymark ($E\ ^1\Sigma_g^+ - A\ ^1\pi_u$) transition. Odd J' levels are antisymmetric and do not occur.

The basic condition for thermochemical equilibrium is that at a constant temperature and pressure the concentrations of the various reacting species must be such as to minimize the Gibbs free energy of the gas mixture. It should be noted that conservation of mass and charge place certain constraints on this minimization. Gibbs free energy, F, for a single species thermally perfect gas is given by Vincenti and Kruger (1965) as

$$F = NkT(\ell n\ N - \ell n\ Q) \tag{3.48}$$

where N and Q are the particle concentration and partition function, respectively. Therefore the total Gibbs free energy of a gas mixture consisting of j species is

$$F = kT \sum_j N_j [\ell n\ N_j - \ell n(Q)_j]. \tag{3.49}$$

Applying the free-energy minimization principle to this relation while the temperature and pressure are held constant gives

$$dF = kT \sum_j dN_j [\ell n\ N_j - \ell n(Q)_j] + kT \sum_j N_j\, d(\ell n\ N_j) = 0. \tag{3.50}$$

Since $d(\ell n\ N_j) = dN_j/N_j$, the last summation in this equation vanishes and the final condition for equilibrium is:

$$\sum_j dN_j [\ell n\ N_j - \ell n(Q)_j] = 0 \tag{3.51}$$

for all values of dN_j which satisfy the mass and charge conservation constraints. Applying equation (3.51) to the general chemical reaction,

$$\alpha_1 x_1 + \alpha_2 x_2 + \ldots + \alpha_\ell x_\ell \rightleftarrows \alpha_{\ell+1} x_{\ell+1} + \ldots + \alpha_j x_j, \tag{3.52}$$

one obtains

$$K_N \equiv \prod_j (N_j)^{\alpha_j} = \prod_j (Q_j)^{\alpha_j}, \tag{3.53}$$

from which the equilibrium species concentrations can be calculated provided the partition functions are known. In the above equations, the stoichiometric coefficients, α_j, are negative for reactants and positive for products. Following the usual convention, the equilibrium constant K_N is defined by equation (3.53).

The partition function Q is defined by the expression

$$Q = \sum_n g_n e^{-E_n/kT} \tag{3.54}$$

where the n summation extends over all known energy levels. Since molecules (and atoms) possess various modes of energy, the total energy, E, of a molecule can be closely approximated by

$$E = E_{trans} + E_{rot} + E_{vib} + E_{elec} . \tag{3.55}$$

By substituting this expression into equation (3.54), one finds that the total partition function Q is expressible as the product of individual partition functions for each mode of energy, that is,

$$Q = Q_{trans} \cdot Q_{rot} \cdot Q_{vib} \cdot Q_{elec} = Q_{trans} \cdot Q_{int} . \tag{3.56a}$$

In order to calculate the thermochemical properties of a gas mixture, it is necessary that each species be referenced to a common zero of energy. For this requirement, the partition function becomes

$$Q = Q_{trans} \cdot Q_{int} \cdot e^{-h_i^o/kT} \tag{3.56b}$$

where h_i^o is the heat of formation of the species i and represents the energy difference between the lowest quantum state of the species i and the zero of energy.

The translation partition function is given by (Herzberg, 1950)

$$Q_{trans} = V\left(\frac{2\pi mkT}{h^2}\right)^{3/2} \tag{3.57}$$

where m is the mass of the particle and V is the volume of the system under consideration.

The energy E_n of an individual molecular energy level in an electronic state n is given by (section 3.1)

$$E_n = hc[T_e + G(v) + F(J)]_n \tag{3.58}$$

where T_e is the term energy of the electronic state referenced to the lowest level ($v = 0$, $J = 0$) of the ground state; $G(v)$ is the vibrational energy of the vth level above the value T_e; and $F(J)$ is the rotational energy of the Jth level above the value $T_e + G(v)$. With this expression, the internal partition function for diatomic molecules is

$$Q_{int} = \sum_n \sum_v \sum_J \frac{(2 - \delta_{o,\Lambda})(2S + 1)(2J + 1)}{\sigma} \exp\left\{\left(-\frac{hc}{kT}\right)[T_e + G(v) + F(J)]\right\}_n \tag{3.59}$$

where $(2 - \delta_{o,\Lambda})(2S + 1)(2J + 1)$ is the total statistical weight of each level, σ is a symmetry factor which approximates the nuclear spin effects of homonuclear molecules - it is set equal to 2.0 for homonuclear molecules and 1.0 for all others.

For atoms, since vibrational and rotational energy modes are absent, the total partition function becomes

$$Q = Q_{trans} Q_{elec} \tag{3.60}$$

where Q_{trans} is again given by equation (3.57) and $Q_{elec} = Q_{int}$ is given by

$$Q_{int} = \sum_n g_n \exp(-E_n/kT). \tag{3.61}$$

In this equation, g_n is the statistical weight of the level n.

The equilibrium concentrations, $N_{uv'J'\Lambda'}$, can now be calculated using equations (3.53) and (3.57) with equations (3.59) and (3.61) for molecular and atoms, respectively. Before this can be accomplished, however, the thermodynamic state of the gas must be obtained. This procedure is outlined in the following section.

3.5.2 Shock-Tube Theory

The gasdynamics of shock waves is well documented in many sources. Among these are the textbooks by Liepmann and Rosko (1957) and Vincenti and Kruger (1965). The following brief discussion was taken from these references.

For a flow which contains a normal shock wave (see fig. 3.17) the conservation equations of fluid flow written in terms of shock-fixed coordinates are:

Mass: $\rho_1 u_1 = \rho_2 u_2$ (3.62)

Momentum: $P_1 + \rho_1 u_1^2 = P_2 + \rho_2 u_2^2$ (3.63)

Energy: $h_1 + (1/2)u_1^2 = h_2 + (1/2)u_2^2$ (3.64)

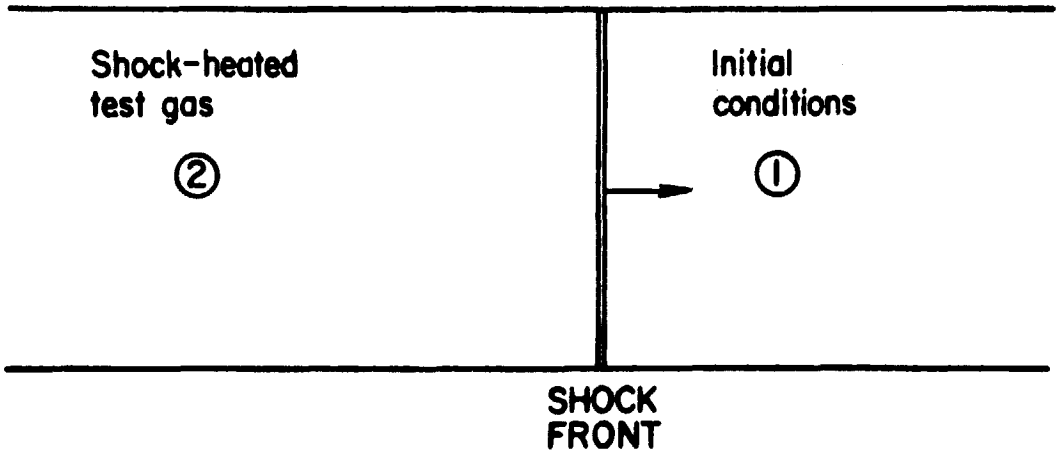

Figure 3.17.- Sketch of normal shock flow in a constant area shock tube.

where the subscripts 1 and 2 denote conditions upstream and downstream of the shock, respectively. Equations (3.62)-(3.64) assume a constant area shock tube. The shock velocity is equal to u_1. These equations are equivalent to the Rankine-Hugoniot equations and give the jump conditions that exist when a shock wave is represented by a discontinuity. If the initial conditions 1 are known, the set of equations (3.62)-(3.64) can be solved by assuming the gas to be in thermodynamic equilibrium on each side of the shock wave. This assumption adds the state equation

$$\rho = \rho(P, h) \tag{3.65}$$

and one then has four equations and four unknowns. Since the relationship in equation (3.65) is normally not given in analytical form, the usual procedure is to solve the set of normal shock relations using an iterative technique described by Vincenti and Kruger. In this technique, equations (3.63) and (3.64) are rewritten in the form:

$$P_2 = P_1 + \rho_1 u_1^2 [1 - (\rho_1/\rho_2)], \tag{3.66}$$

$$h_2 = h_1 + (u_1^2/2)[1 - (\rho_1/\rho_2)^2]. \tag{3.67}$$

Using these equations and an estimated value of (ρ_1/ρ_2), trial values of P_2 and h_2 are obtained. These results are used in the equation of state to obtain a value of ρ_2 and thus a revised value of (ρ_1/ρ_2). This procedure is repeated until the initial and final values of (ρ_1/ρ_2) are identical. With P_2, h_2, and ρ_2 known, all of the other thermodynamic parameters as well as the equilibrium concentrations $N_{uv'\Lambda'J'}$ can be calculated.

The application of the equations, reviewed in this section and the preceding one, to the present study is presented in the next section.

3.5.3 Thermochemistry Calculations

The computer program used to calculate the equilibrium thermochemical properties of the shock-heated gas mixtures was developed by Horton and Menard (1969). In this program, the thermodynamic properties of the shocked gas are determined by an iterative procedure similar to that described in section 3.5.2. A final temperature T_2 is specified and (ρ_1/ρ_2) is varied until the Rankine-Hugoniot equations are satisfied. The solution is assumed to be converged after n iterations if

$$\left|\frac{(\rho_1/\rho_2)_{n+1} - (\rho_1/\rho_2)_n}{(\rho_1/\rho_2)_n}\right| \leq 10^{-3}. \tag{3.68}$$

With the thermodynamic properties completely determined, the equilibrium species concentrations can then be calculated from equation (3.53),

$$K_N = \prod_j (N_j)^{\alpha_j} = \prod_j \left[\left(\frac{2\pi m_j kT}{h^2}\right)^{3/2} (Q_i)_j\right]^{\alpha_j}, \tag{3.69}$$

and the conservation of mass equation,

$$N_j = \sum_i \beta_{ij} N_i \tag{3.70}$$

where β_{ij} is the number of atoms of the jth numbered element in the molecule of the ith numbered species.

In this work, the internal partition function of molecules

$$Q_{int} = \sum_n \sum_v \sum_J \frac{(2 - \delta_{o,\Lambda})(2S + 1)(2J + 1)}{\sigma} \exp\left[\left(-\frac{hc}{kT}\right)[T_e + G(v) + F(J)]\right]_n \tag{3.71}$$

was approximated as described below.

The rotational partition function was approximated (see Herzberg, 1950) by

$$\left.\begin{aligned} Q_{rot} &= \sum_{J} (2J + 1)\exp\left[-\frac{hcF(J)}{kT}\right] \\ &\simeq \int_{o}^{\infty} (2J + 1)\exp\left[-B_v J(J + 1)\frac{hc}{kT}\right]dJ \\ &\simeq \frac{kT}{hcB_v} \end{aligned}\right\} \qquad (3.72)$$

where $B_v = B_e - \alpha_e[v + (1/2)]$.

The vibrational energy within each electronic state was assumed to be given by

$$G(v) = \omega_e[v + (1/2)] - \omega_e x_e[v + (1/2)]^2 + \omega_e y_e[v + (1/2)]^3 + \omega_e z_e[v + (1/2)]^4. \qquad (3.73)$$

Therefore, the internal partition function for diatomic molecules was calculated from

$$Q_{int} = \sum_{n}\left\{\frac{(2 - \delta_{o,\Lambda})(2S + 1)}{\sigma}\exp\left(\frac{-hcT_{en}}{kT}\right)\sum_{v}\frac{kT}{hcB_v}\exp\left[\frac{-hcG(v)}{kT}\right]\right\}_n. \qquad (3.74)$$

The summation is over all electronic levels of importance and over all vibrational levels in each electronic state until

$$\frac{\exp[-hcG(v)/kT]}{\sum_{v}\exp[-hcG(v)/kT]} \leq 10^{-3}. \qquad (3.75)$$

Appendix D contains a list of the species included in the thermochemical calculations of mixtures of argon and acetylene. The energy levels and other significant constants pertinent to the calculations are also included.

3.6 Synthetic Spectrum Data Analysis Technique

In this section, the data analysis technique which incorporates synthetic spectrum calculations based on equation (3.1) is described. The assumptions and approximations to the theory presented earlier on which these calculations are based are discussed. Finally, the details of the reduction of absolute measurements of spectral emission to electronic transition moments, $\Sigma|R_e/ea_o|^2$, are disclosed.

3.6.1 Synthetic Spectrum Calculations

Synthetic spectra were calculated using the computer program described by Arnold, Whiting, and Lyle (1969) and Whiting, Arnold, and Lyle (1969). This program produces a spectrum by accounting for the contribution of each rotational line (equation (3.1)) of interest in an electronic transition.

The integrated spectral intensity due to spontaneous emission for each rotational line was previously shown to be given by

$$E_{\ell}^{u} = \frac{16 \times 10^{-7}\, \pi^3 \bar{\nu}_{u\ell}^4 c}{3(2 - \delta_{o,\Lambda'})(2S' + 1)(2J' + 1)} N_{uv'\Lambda'J'}\, \Sigma|R_e(\bar{r}_{v'v''})|^2 q_{v'v''} S_{J''\Lambda''}^{J'\Lambda'}. \tag{3.76}$$

The input parameters used by the computer program to compute E_{ℓ}^{u} are discussed in the following paragraphs.

The central wavelength of a rotational line is calculated from

$$\bar{\nu} = \nu/c = \bar{\nu}_o(v', v'') + F'(J') - F''(J''), \text{ cm}^{-1} \tag{3.77}$$

where the band origin $\bar{\nu}_o(v', v'')$ is given by

$$\bar{\nu}_o(v', v'') = (T_e' - T_e'') + [G'(v') - G''(v'')]. \tag{3.78}$$

The expressions for $F(J)$ listed in section 3.4 are approximated in the program by

$$F(J) = B_v J(J + 1) - D_v J^2(J + 1)^2. \tag{3.79}$$

This expression is used for all singlet transitions and all triplet transitions in which spin splitting is negligible with the exception of the $\Delta\Lambda = 0$ triplet cases. For these transitions, the central component of the triplet is used as an effective line wavelength and $F(J)$ is approximated by

$$F(J) = B_v[J(J + 1) + 4Z_2] - D_v[J + (1/2)]^4 \tag{3.80}$$

where

$$Z_2 = \frac{\Lambda Y(Y + 1) - (4/9) - 2J(J + 1)}{3[\Lambda^2 Y(Y - 4) + (4/3) + 4J(J + 1)]}, \tag{3.81}$$

and

$$Y = A/B_v. \tag{3.82}$$

The quantity $G(v)$ is approximated by

$$G(v) = \omega_e[v + (1/2)] - \omega_e x_e[v + (1/2)]^2 + \omega_e y_e[v + (1/2)]^3 + \omega_e z_e[v + (1/2)]^4. \tag{3.83}$$

Molecular constants such as T_e, ω_e, $\omega_e x_e$, etc. required as program inputs were taken from Rosen (1970) and Herzberg (1950) and are listed in table 2.1.

The Franck-Condon factors, $q_{v'v''}$, used in the calculations were discussed in section 3.2 and are listed in appendix C.

The expressions for the Hönl-London factors, $S^{J'\Lambda'}_{J''\Lambda''}$, listed in section 3.4, are approximated in the program as follows:

1. Parallel transitions ($\Delta\Lambda = 0$): These transitions (Swan, Fox-Herzberg, Mulliken, and Deslandres-d'Azambuja systems) are characterized by strong P and R branches and very weak Q, P-form, Q-form, and R-form branches. The Hönl-London factors for these transitions are approximated in the program by:

Branch	$S^{J'\Lambda'}_{J''\Lambda''}$
P	J
R	$J + 1$

These strength factors are exact for the $^1\Sigma - {}^1\Sigma$ transitions (section 3.4.5). In this assignment, the weak branches are assumed to have zero intensity. However, the intensity actually possessed by these transitions is incorporated into the P and R branches because the sum of the Hönl-London factors for a given J value is held equal to $2J + 1$.

2. Perpendicular transitions ($\Delta\Lambda = \pm 1$): These transitions (Ballik-Ramsay, Phillips, and Freymark systems) are characterized by strong P, Q, and R branches and very weak P-form, Q-form, and R-form branches. The Hönl-London factors for these transitions used in the program are:

Branch	$S^{J'\Lambda'}_{J''\Lambda''}$
P	$\frac{(J \pm \Lambda)(J - 1 \pm \Lambda)}{2J}$
Q	$\frac{(J \pm \Lambda)(J + 1 \mp \Lambda)(2J + 1)}{2J(J + 1)}$
R	$\frac{(J + 1 \mp \Lambda)(J + 2 \mp \Lambda)}{2(J + 1)}$

where the upper sign is for $\Delta\Lambda = +1$ transitions and the lower sign is for $\Delta\Lambda = -1$ transitions. As discussed above, the intensity of the weak branches is accounted for in the P, Q, and R branch intensities.

In the program, the number of particles in the upper state is calculated from

$$N_{uv'\Lambda'J'} = \frac{N\, du(2J' + 1)}{Q} \exp\left\{\frac{-hc}{k}\left[\frac{T_e' + G'(v') + F'(J')}{T}\right]\right\} \quad (3.84)$$

where du is the electronic multiplicity of the upper state. The partition function, Q (see section 3.5.1), is approximated by

$$Q = \sum_n \left\{ \frac{(2 - \delta_{o,\Lambda})(2S + 1)}{\sigma} \exp\left(\frac{-hcT_{en}}{kT}\right) \sum_v \frac{kT}{hcB_v} \exp\left[\frac{-hcG(v)}{kT}\right] \right\}_n \qquad (3.85)$$

where the summation is carried out over all electronic levels of importance for the temperatures considered and over all vibrational levels within each electronic state until either

$$\frac{\exp[-hcG(v)/kT]}{\sum_v \exp[-hcG(v)/kT]} \leq 10^{-3} \qquad (3.86)$$

or the equation repressing the vibrational energy (equation (3.83)) has reached a fictitious peak, that is, $G(v_{max} + 1) \leq G(v_{max})$.

Once the integrated intensity of each line has been calculated from equation (3.76), this intensity is then distributed in the spectrum by an approximate Voigt profile which is given by

$$E_\lambda = E_{\lambda_{C_L}} \left(\left(1 - \frac{W_L}{W_V} \right) \exp\left[2.772 \left(\frac{\lambda - \lambda_{C_L}}{W_V} \right)^2 \right] + \frac{W_L/W_V}{1 + 4[(\lambda - \lambda_{C_L})/W_V]^2} + 0.016 \left(1 - \frac{W_L}{W_V} \right) \left(\frac{W_L}{W_V} \right) \left\{ \exp\left[-0.4 \left(\frac{\lambda - \lambda_{C_L}}{W_V} \right)^{2.25} \right] - \frac{10}{10 + [(\lambda - \lambda_{C_L})/W_V]^{2.25}} \right\} \right) \qquad (3.87)$$

The spectral intensity at the line center is

$$E_{\lambda_{C_L}} = \frac{E_\ell^u}{W_V[1.065 + 0.447(W_L/W_V) + 0.058(W_L/W_V)^2]}, \qquad (3.88a)$$

where

$$W_V = W_L/2 + \sqrt{(W_L/2)^2 + W_g^2}. \qquad (3.88b)$$

In the above equations, W_V, W_L, and W_g are the Voigt, Lorentzian, and Gaussian profiles at half-height. The Gaussian line profiles at half-height were calculated from:

$$W_g = 7.16 \times 10^{-7} \lambda\sqrt{T/M} \ , \ \text{Å} \tag{3.89a}$$

and are related to the Lorentzian profiles at half-height by

$$W_g = \sqrt{\ell n\ 2}/a \ (W_L) \ . \tag{3.89b}$$

In the above equations, T is the temperature of the radiating gas, M is its molecular weight, λ is the wavelength of the radiation, and a is a parameter which is usually determined from experimental measurements. However, since the measurements were made in the optically thin regime (see Chapter 4), the exact line profile used in the calculations is not critical and therefore the value of a used is not either. As an example, the integrated intensity of the $\Delta v = 0$ sequence of the Swan system was calculated for values of a ranging from 1.0 to 0.001. The maximum difference in integrated intensity was only 2.7 percent.

The contribution from each line is then summed yielding a synthetic spectrum.

3.6.2 Data Reduction Technique

The data reduction technique used the synthetic spectrum calculations discussed in the previous section. A synthetic spectrum was calculated by assigning a value of unity to the $\Sigma|R_e/ea_o|^2$ value. This spectrum is then folded with the measured experimental instrument function (figure 4.5) to give a predicted signal output. The ratio of measured to theoretical signal output yields the experimental value of $\Sigma|R_e/ea_o|^2$.

Before comparison with the theoretical signal, all of the experimental signals were first corrected to account for the presence of

weak oblique shocks in the radiometer viewpath (section 4.2.4). This correction was approximately 2 percent. For the measurements taken in the infrared region, the experimental signal was also corrected for atomic line radiation occurring in the bandpass of interest. The integrated intensity due to spontaneous emission of a single atomic line is calculated from

$$E = \frac{N_u h\nu A_{u\ell}}{4\pi} , \ W/cm^3 \cdot sr. \qquad (3.90)$$

All of the allowed transitions for ArI and CI listed by Wiese et al. (1966) were included in the calculations. The Einstein A coefficients, $A_{u\ell}$, for these lines were also taken from Wiese et al.

The partition function used in the calculation of the number of atoms in the upper state, N_u, was identical to the one used in the computation of the species concentrations. As was discussed for molecules, the integrated intensity of individual atomic lines is summed and then folded with the instrument functions to give a predicted signal output. This output is subtracted from the measured output before comparison with the theoretical signal based solely on molecular radiation. The largest correction for atomic line radiation was 1.2 percent.

All theoretical calculations are based on optically thin approximations. This assumption was justified by comparing synthetic spectra based on the present $\Sigma|R_e/ea_o|^2$ measurements with black-body curves. The black-body intensities were always at least an order of magnitude greater than the peak spectral intensities. Line widths used in these calculations were derived from the formulas given by Arnold et al. (1969) and neglected instrument broadening.

Chapter 4

Description of Experimental Technique

This chapter contains a detailed description of the experimental facility and instrumentation used in the present work. The first section describes the shock-tube facility and its operational procedures. Section 4.2 covers the instrumentation and calibration procedures used in the experimental program to obtain reliable measurements. The third section (4.3) outlines the initial test conditions, and section 4.4 presents samples of the experimental data. Survey spectra and oscillograms of the spectral emission for each of the band systems measured are shown.

4.1 Shock-Tube Facility and Operation

4.1.1 Idealized Shock-Tube Flow

Several advantages are gained by using a shock tube to provide a heated sample of gas. The gas sample is raised nearly instantaneously to a high temperature, pressure, and density; the gas equilibrates rapidly and maintains this state for a short period of time; and the state of the shocked gas can be calculated very accurately. A brief description of the wave pattern and state of the gas inside a conventional constant-area shock tube is given below. For additional details of this subject, the reader is referred to the work of Gaydon and Hurle (1963) and Zel'dovich and Raizer (1966).

A sketch of a simple shock tube and an accompanying distance-time (x-t) diagram showing the paths of the waves is shown in figure 4.1. Initially there are two regions of gas at vastly different

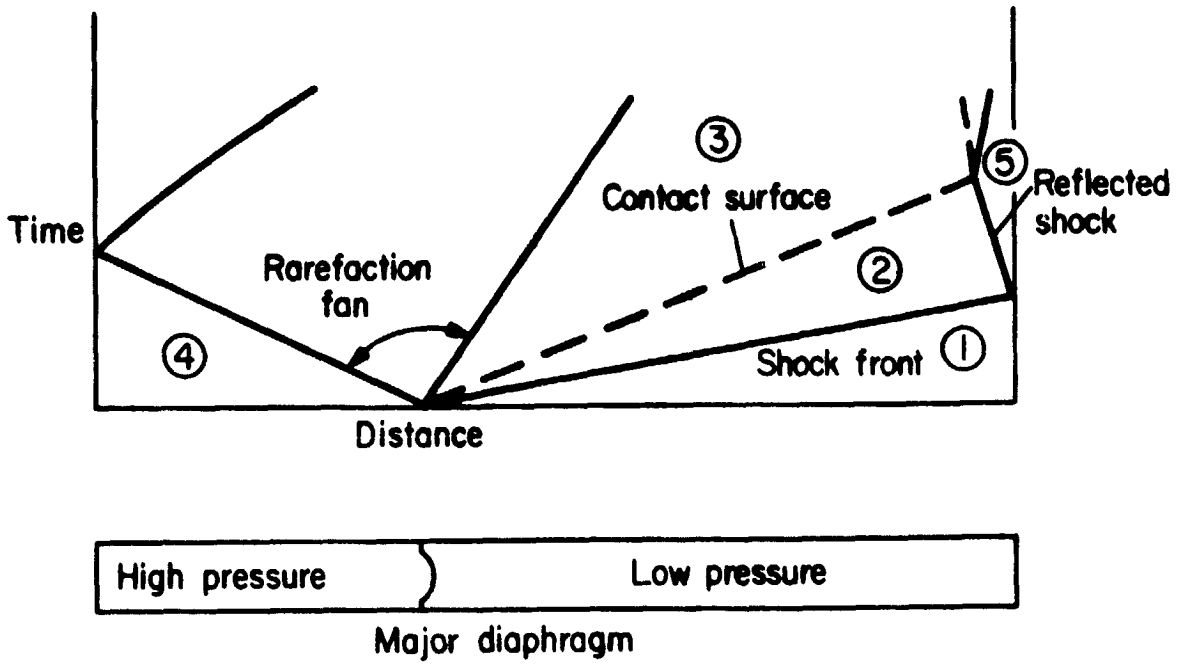

Figure 4.1.- A distance-time diagram showing the progress of the flow in a conventional shock tube.

pressures separated by a diaphragm. The gas in the low pressure side (conditions "1") is the experimental sample, while the gas in the high pressure side (conditions "4") is known as the driver gas.

Upon bursting of the diaphragm which is assumed to open instantaneously, the driver gas expands into the test gas, compressing it and forming a shock wave which propagates through it. Because of this compression, the test gas behind the incident shock wave (conditions "2") has undergone a substantial increase in temperature, pressure, and density. Since the initial conditions, "1", and the composition of the test gas are known, the velocity of the shock wave is all that is required in order to calculate the conditions "2" immediately behind the shock. This numerical procedure uses the Rankine-Hugoniot equations and was outlined in section 3.5.

As the shock wave propagates through the test gas, an expansion or rarefaction wave simultaneously travels into the high pressure section at a velocity equal to the local speed of sound. The surface separating the two gases is known as the contact surface.

The above description is an idealized picture of shock-tube flow. In reality, the shock tube performs somewhat differently, for example, the contact surface is usually not an abrupt boundary since diffusion and other processes tend to mix the particles from both regions. This mixing in addition to the formation of a cool boundary layer on the shock-tube wall behind the incident shock tend to reduce the test time, that is, the length of the test gas free of contamination divided by the shock velocity. Ideally the shock wave propagates at a constant velocity while in normal operation most shock waves tend to slow down due to viscous effects as the shock moves along the tube.

4.1.2 Shock-Tube Facility

The facility used in the experimental program is a combustion-driven shock tube and is located at Ames Research Center, Moffett Field, California. A photograph showing an overall view of the facility is presented as figure 4.2. The driver section (combustion chamber), which is the largest diameter portion of the shock tube, is shown in the foreground and is 1.27 m long. It has an inside diameter of 16.3 cm. A preformed stainless-steel diaphragm (known as the primary diaphragm and not shown in the photograph) separates the driver and driven tubes. The driven tube is 10.3 m long and has an inside diameter of 16.8 cm. This tube, shown in figure 4.2 extending from the center of the photograph to the upper left-hand corner, is coupled to a stainless-steel

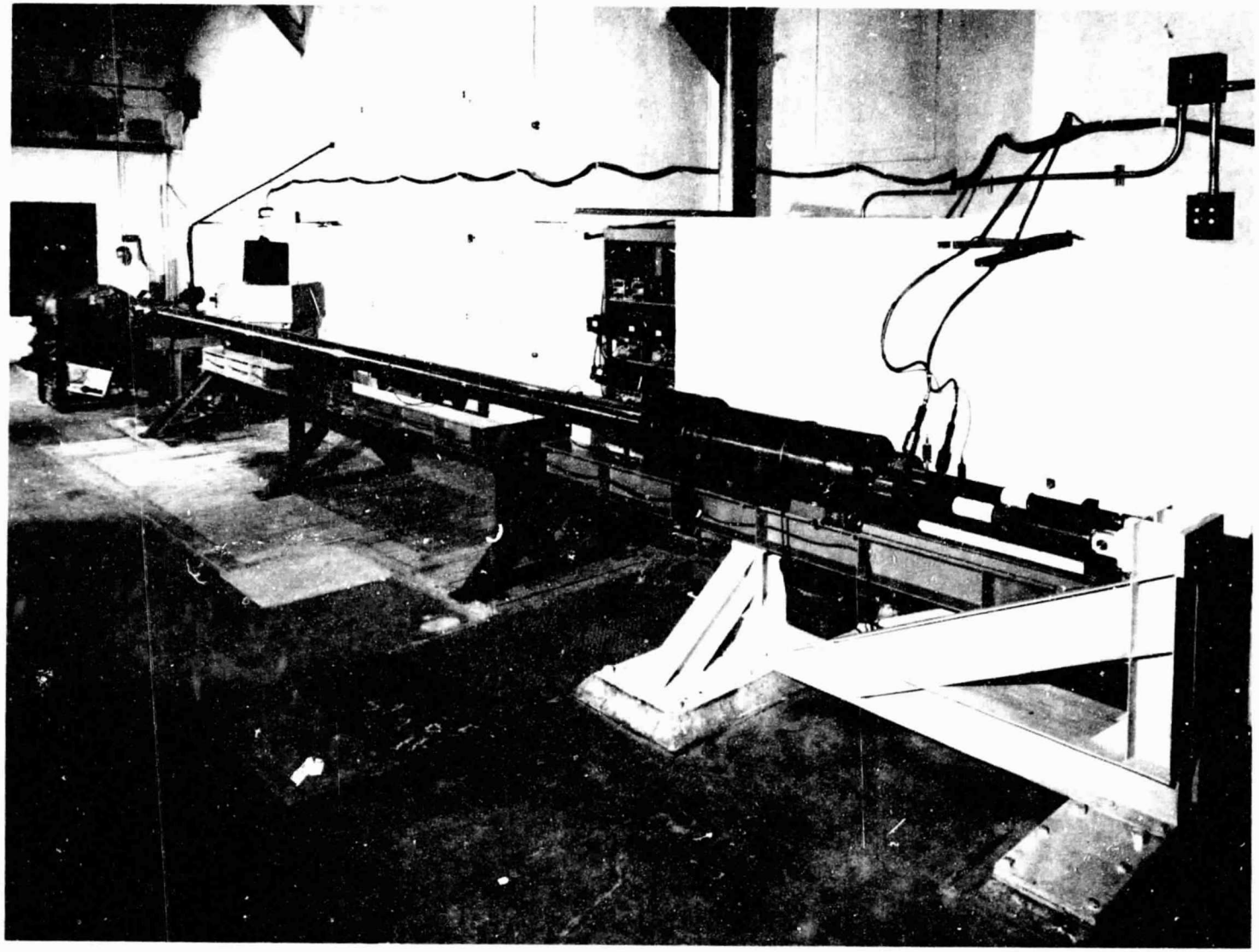

Figure 4.2.- Photograph of the combustion-driven shock-tube facility located at Ames Research Center, Moffett Field, California.

dump tank (extreme left of photograph) which is approximately 1 m in diameter and 2 m long. A flat thin prescored stainless-steel diaphragm separates the dump tank from the driven tube. The driven tube contains a test section whose centerline is 9.2 m from the primary diaphragm. The test section consists of four ports 5 cm in diameter and 90° apart. These ports can be used for obtaining either photographic, spectrographic, or radiometric data. Six additional ports at various locations along the shock tube and nominally 1 m apart are used to accommodate positive ion sensors which are used in determining the velocity of the shock wave.

The shock tube represents a relatively tight vacuum system A Welch two-stage rotary vacuum pump is used to routinely evacuate the driven tube to a pressure of less than 10^{-3} torr. The leak rate of this section is nominally 5×10^{-5} torr/min.

A continuous flow-through system for loading the test gas has been incorporated into this facility. The initial pressure in the driven tube is set by adjusting the bleed-in and pump-out rates until the predetermined pressure is obtained. Pure test gas flows through the tube until approximately 6 sec before the shock tube is fired when two solenoid operated valves at the bleed-in and pump-out locations terminate the process. Mock tests in which the shock tube was not fired verified that the gas pressure in the driven tube did not change as a result of terminating the gas flow. In this work, both the flow-through loading technique and simply loading the tube to the desired pressure were used. The radiometric and spectrographic results

from these tests were essentially identical. Therefore to minimize costs, most of the tests were performed by loading the test gas to a desired pressure and firing.

The energy for initiating combustion is provided by a 20 MFD capacitor charged to 5 KV. In order to promote uniform combustion in the combustible gases, this energy is discharged into a 10 mil tungsten glow wire positioned at the centerline and extending the entire length of the combustion chamber.

4.1.3 Shock-Tube Operation

In the following paragraphs, the procedures for cycling the shock tube through a typical test are presented. A thorough cleaning of the entire shock tube with acetone wetted cloths was the first step. All port windows including those in the splitter plates (see next section) were either cleaned or replaced. At this point the radiometric and/or spectrographic instrumentation was carefully aligned about the test section. Wavelength calibrations and band-pass measurements of the radiometers were also performed.

Both the glow wire and a powder-driven squib-ignited punch which is used to open the primary diaphragm were installed. The shock tube was then assembled using diaphragms which divide the tube into three sections: combustion chamber, driven tube, and dump tank. All three chambers were then evacuated. The driven tube was then purged by filling it with test gas to a pressure which was nominally twice the initial pressure, P_1, and reevacuating. It should be noted that a dry-ice cold trap was used on the test gas bleed-in line to remove moisture. The test gas was then loaded to the desired initial pressure.

Next, the combustion chamber was loaded with a combustible 1:3:8 mix of oxygen, hydrogen, and helium. With the completion of this task, the shock tube was ready to be fired. This was accomplished by discharging the energy from the 20 MFD capacitor into the glow wire. This process ignited the combustible gases which heated the mixture and caused the pressure to increase approximately six fold. Shortly after the peak pressure was achieved in the combustion chamber, the punch pierced the primary diaphragm at its center and the weakened diaphragm was forced open by the high pressure gas. This gas rushed into the driven tube and created a shock wave which propagated through the gas heating it. Ion sensors spaced along the tube detected the arrival of the shock and recorded information from which the shock velocity could be deduced. The shock wave passed through the test section where the radiation from the shock-heated gas was measured and then reflected off of the secondary diaphragm. The initial contact weakened the diaphragm and the subsequent higher pressure opened the diaphragm and the gases flowed into the dump tank ending the test. A description of the instrumentation used to determine both the thermodynamic and spectroscopic properties of the gas mixture is given in section 4.2.

4.2 Instrumentation

4.2.1 Pressure Measuring Devices

A 0-5000 μHg Stokes McLeod vacuum gage was used to monitor the minimum driver tube pressure and leak rate. A 0-20 torr Wallace and Tiernan vacuum gage was used to set the initial pressure in the driven tube. Both gages were calibrated by direct comparison with a reference standard traceable to the National Bureau of Standards. A

piezo-electric pressure transducer mounted in the breech plug of the combustion chamber was used to measure the driver pressures.

Figure 4.3 is an oscillogram showing the pressure history in the combustion chamber. The oscillogram sweep was started at time-zero. Approximately 35 msec later (indicated by the first small pulse on the pressure record), the energy was discharged into the glow wire. The combustion process heated the gas and caused a rapid increase in pressure in the chamber. Some 65 msec after time-zero and after the pressure had reached an essentially constant value, the punch was fired (indicated by the second small pulse on the oscillogram). The sudden decrease in pressure is caused by the arrival of the expansion wave at the breech end of the combustion chamber.

4.2.2 Shock Detectors

Shock speeds were determined from time-of-arrival measurements made at six locations along the driven tube by positive ion sensors. The output of each detector was connected to a Hewlett-Packard 100 mHz electronic chronograph to record the shock time of arrival. These detectors were quite reliable and allowed the determination of shock speed to an accuracy of about 0.10 percent. A plot of the variation of shock speed with distance for a typical test is shown in figure 4.4.

4.2.3 Spectrographic Instrumentation

Spectrographs were used in some of the tests to obtain survey spectra of the shock-heated gas for identification purposes. The spectrograph viewpath was normal to the shock-tube axis. Three spectrographs were used altogether. Only one was used in any particular test and all of them employed an opaque shutter, similar to the one

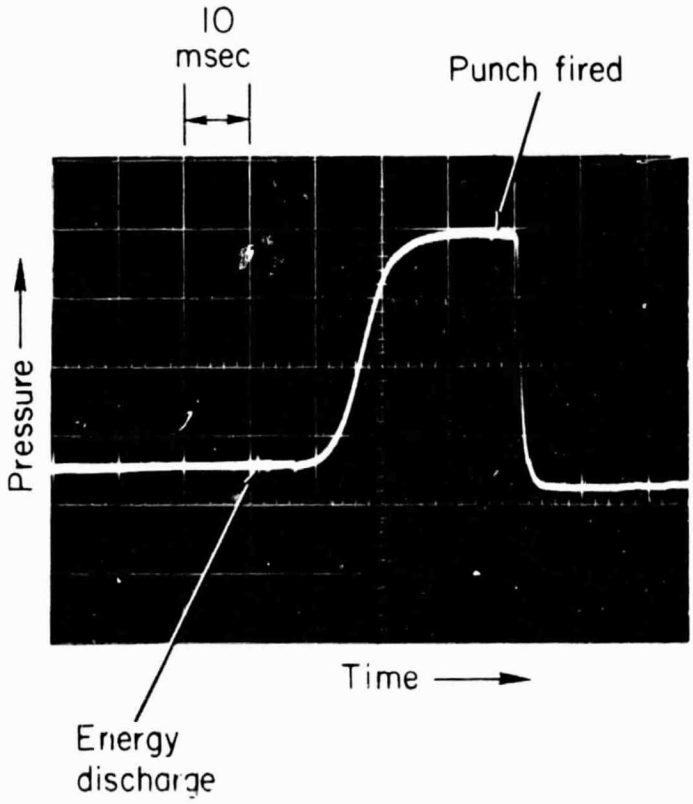

Figure 4.3.- Oscillogram of the pressure history in the combustion chamber.

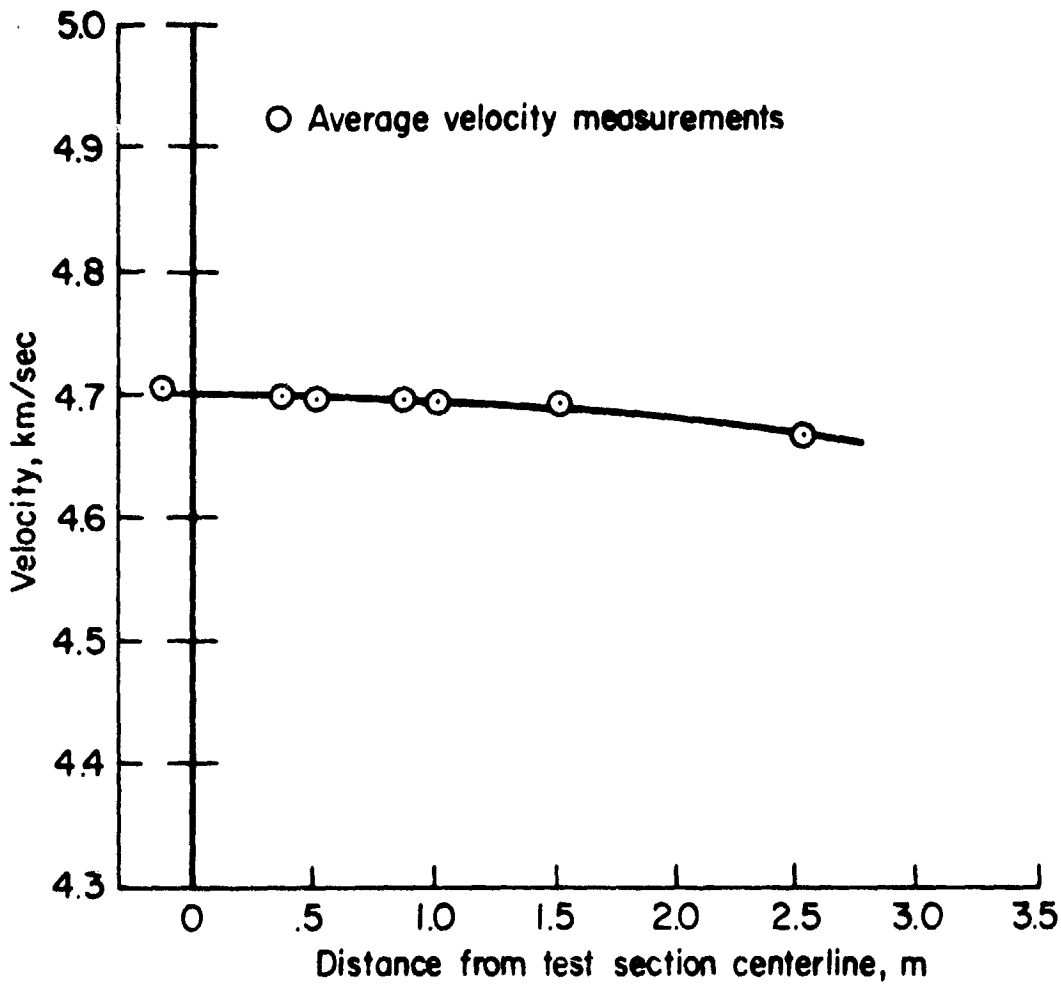

Figure 4.4.- Shock speed variation with distance for a typical test.

described by Borucki et al. (1969), to exclude the radiation from the driver gas. This shutter was explosively driven and had a closing time of 35 μsec.

To survey the ultraviolet portion of the spectrum, a Huet spectrograph model UV 24 was used. This instrument is a dual quartz prism spectrograph which has a f/3.5 aperture ratio and an 0.24-m focal length. The linear dispersion varies from 7.5 Å/mm at 2150 Å to 100.0 Å/mm at 4500 Å.

The second spectrograph, used to cover the ultraviolet and visible portions of the spectrum, was a model 75-000 Jarrell-Ash grating spectrograph. This instrument has a f/5.6 aperture ratio, a 0.75-m focal length, and a dispersion of approximately 20 Å/mm. The 600 lines/mm grating is blazed for 5000 Å.

The final spectrograph, used in the infrared, was a stigmatic f/2.5 grating instrument with a dispersion of about 50 Å/mm. The grating has 600 lines/mm and is blazed for 7500 Å. This instrument was designed by Borucki (1970).

Sample spectra of the shock-heated gas obtained with these instruments are presented in section 4.4.

4.2.4 Radiometric Instrumentation

A. General description of radiometers

Absolute intensities of selected spectral features of the radiation were measured behind the incident shock wave as a function of time by absolutely and spectrally calibrated narrow band-pass radiometers. The radiometers consisted of photomultiplier tube detectors coupled to Bausch and Lomb 1/4-m monochromators or to interference filters which

acted as dispersive elements. The interference filters (used in the infrared) incorporated a Corning 2-64 sharp cut-off filter to exclude light below 6400 Å. Below 3000 Å, an additional narrow band-pass interference filter was used in connection with the monochromators to exclude stray light.

Figure 4.5 is a sketch of the radiometric instrumentation arrangement about the shock-tube test section. As illustrated in the figure, the radiometers viewed the flow through narrow (0.5 mm) slits in splitter plates. Quartz windows were flush mounted on the surface of the splitter plates directly in front of the slits so that the entire surface of the splitter plate was completely smooth. The slits were normally positioned so that the portion of the splitter plate mounted on the opposite wall visible to the radiometer was blackened. Additional radiometer units consisting of one or five radiometers and mounted on the top and opposite side of the shock tube are not shown in figure 4.5 for clarity. Thus a total of four splitter plates were mounted in the shock tube with the distance between the plates maintained at 11 cm. The actual number of radiometer units used each test varied depending on the strength of the band system being measured. Measurements of the Freymark and Mulliken systems, for example, were made with single close-coupled radiometers mounted on the side and top of the tube.

The splitter plates were used to exclude from the radiometer viewpath the relatively thick variable temperature boundary layer on the shock-tube wall, replacing it by the thinner splitter-plate boundary layer. These plates and their accompanying struts were designed according to the following criteria: (1) the strut had to be long enough

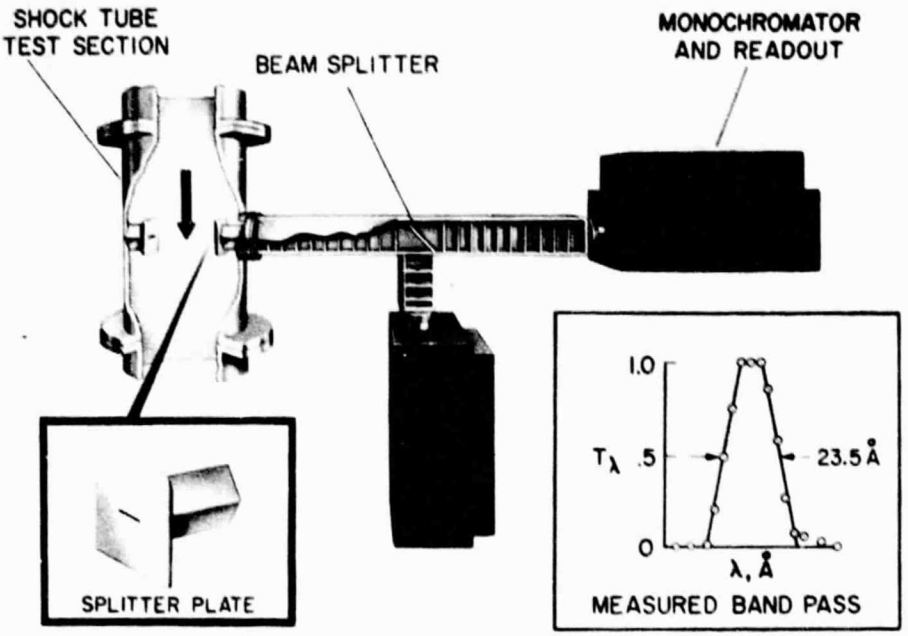

Figure 4.5.- Sketch of a two-channel radiometer unit coupled to the shock tube. The radiometer bandpass featured in the inset is typical of those resulting from the 1/4-m monochromator dispersive elements.

to completely reject the wall boundary layer, and (2) the splitter plate had to be large enough to keep the flow disturbance created by the strut between the shock-tube wall and the splitter plate. Photographs of the flow over the splitter plate assembly (shown below) verified that the splitter plates succeeded in meeting these objectives.

While the function of the splitter plates was to exclude the wall boundary layer from the radiometer viewpath, it is well known (Gruszczynski, 1968 and Arnold and Nicholls, 1970) that splitter plates cause weak oblique shocks to form on top of the plates which appear in the viewpath. Figure 4.6 is a self-luminous photograph of the flow over one of the splitter plates and a diagram illustrating the flow processes. This photograph was taken with an Abtronics image converter camera (model NR-2HS). The exposure time is 0.5 μsec. With careful examination of the photograph, an oblique shock originating at the leading edge of the splitter plate can be seen. It is also apparent that there is no flow over the sides of the splitter plate.

Equilibrium calculations, using the oblique shock relations and the angle of the shock measured from photographs similar to figure 4.6, were performed to determine the effect of the presence of these shocks. The oblique shock relations can be obtained from the normal shock relations in section 3.5.2 by simply replacing the velocity u_1 by the quantity $u_1 \sin \theta$ which is the component of velocity normal to the oblique shock whose angle is given by θ. These calculations revealed that the oblique shocks on the splitter plates increased the intensity observed by the radiometers by only 2 percent.

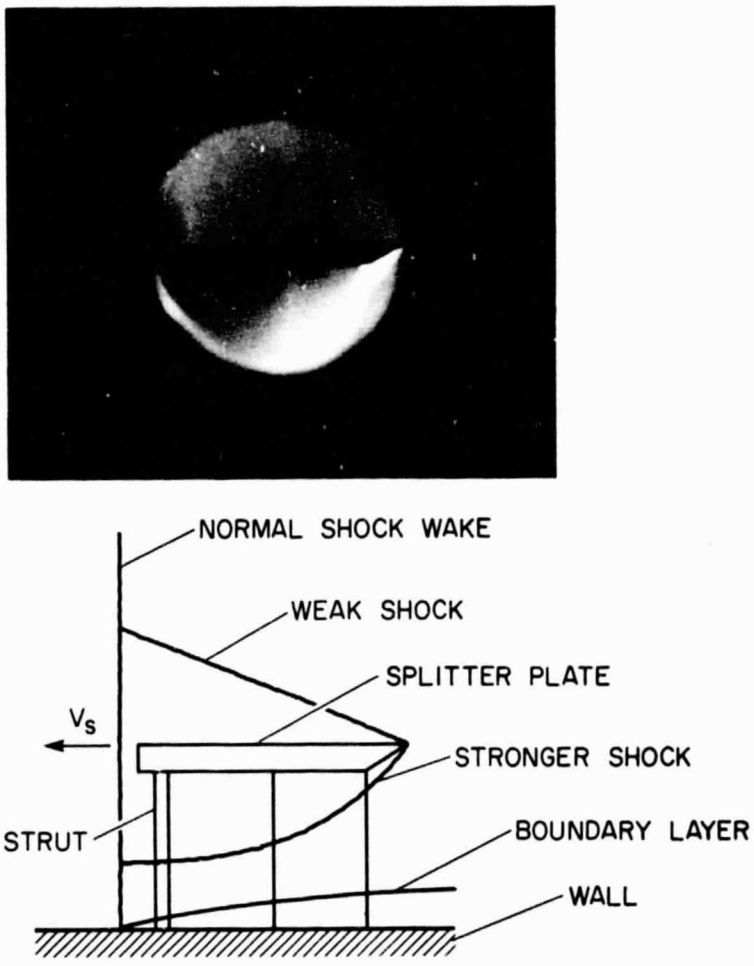

Figure 4.6.- Sketch and self-luminous photograph of the flow across a splitter plate. The strong shock below the splitter plate is clearly visible while the weak shock above the plate (depicted in the sketch) is barely visible.

B. Calibration procedures

Craig and Davy (1969) have shown that the radiometer output $V(\lambda)$ may be expressed by the following equation:

$$V(\lambda) = G(\lambda) \int_0^\infty T(\lambda)H(\lambda)d\lambda, \tag{4.1}$$

where $G(\lambda)$ is the sensitivity of the system or the calibration constant, $T(\lambda)$ is the normalized spectral response of the radiometer, and $H(\lambda)$ is the spectral irradiance incident on the radiometer. For the response to a calibration source, the quantity $H(\lambda)$ is replaced by the spectral irradiance from the calibration source, $L(\lambda)$, and equation (4.1) becomes

$$V_C(\lambda) = G(\lambda) \int_0^\infty T(\lambda)L(\lambda)d\lambda. \tag{4.2}$$

The ratio of radiometer response from the test to that from the calibration source is

$$\frac{V_T(\lambda)}{V_C(\lambda)} = \frac{\int_0^\infty T(\lambda)H(\lambda)d\lambda}{\int_0^\infty T(\lambda)L(\lambda)d\lambda}. \tag{4.3}$$

$H(\lambda)$ is the quantity which is to be determined in the present tests. For most radiators, it can be written as

$$H(\lambda) = H_0 h(\lambda), \tag{4.4}$$

where H_0 is a constant which gives the absolute strength of the radiator and $h(\lambda)$ is the relative spectral irradiance. Since molecular bands are the dominant radiators in this work, the quantity H_0 can be replaced by the electronic transition moment, $\Sigma|R_e/ea_0|^2$. The relative

spectral irradiance, $h(\lambda)$, was previously described in section 3.6. Substituting these quantities into equation (4.3) and rearranging, one obtains

$$\sum\left|\frac{R_e}{ea_o}\right|^2 = \frac{\int_o^\infty T(\lambda)L(\lambda)d\lambda}{\int_o^\infty T(\lambda)h(\lambda)d\lambda}\left[\frac{V_T(\lambda)}{V_C(\lambda)}\right]$$

$$= \frac{V_T(\lambda)}{G_C(\lambda)\int_o^\infty T(\lambda)h(\lambda)d\lambda} \qquad (4.5)$$

Therefore, the $\Sigma|R_e/ea_o|^2$ value can be determined from the radiometer output during a test if the calibration constant, $G_C(\lambda)$, and the spectral response, $T(\lambda)$, of the radiometer is known.

Each radiometer was calibrated absolutely against an NBS tungsten ribbon filament lamp standard or a quartz-iodine tungsten-coil filament lamp to determine $G_C(\lambda)$. The calibration source was used as an infinite wall source. The spectral irradiance of the standard lamp was extended below 2500 Å by measuring the relative output of the lamp between 2200 Å and 3000 Å (at 100 Å intervals) and matching the curves at 3000 Å. This procedure resulted in a difference of only about 5 percent at 2500 Å between the normalized curve and the calibration value provided with the lamp. It should be noted that the optical path, monochromator settings (where applicable), and photomultiplier operating voltages were identical for both calibration and experiment.

A typical normalized spectral response, $T(\lambda)$, of a radiometer using a 1/4-m Bausch and Lomb monochromator as a dispersing element is shown

in the inset on figure 4.5. This response, often referred to as a bandpass, was obtained by scanning the 5461 Å line of Hg and normalizing the output. Both the spectral response, $T(\lambda)$, and the center wavelength of the response curve are critical to the understanding of the experimental measurements. Consequently, the spectral response, which gives an accurate wavelength calibration (± 1.5 Å) was measured before every third test. The only response changes detected during this procedure were small ones.

The spectral responses of the interference filters were obtained by calibrating the transmission of each filter from 6000 to 13,000 Å. This calibration procedure (Whiting et al. 1972) incorporated a Perkin-Elmer 210 grating spectrograph and a synchronous amplifier to obtain transmission values as low as 10^{-5} of peak transmission. Transmission values for wavelengths greater than 13,000 Å were smaller than 10^{-5}. This is primarily due to the very low sensitivity of the photomultiplier photocathode surface at these wavelengths.

A detailed description of these calibrations procedures and radiometric techniques in general is contained in the work by Craig and Davy (1969). An additional check suggested by them is to determine the linear operating range of each radiometer. All of the radiometers used in the experimental work were checked for this effect. This was accomplished by selecting a filter whose transmission is well known and placing it in and out of the incident beam of light and recording the signals. The ratio of these signals gives the transmission of the filter if the radiometer is operating in the linear regime. As the transmission is repeatedly

measured with increasing intensity, an intensity level will be reached at which the calculated filter transmission begins to increase. This represents the linear limit. All of the experimentally measured signals were kept below this limit.

In order to check the radiometers used in the ultraviolet below 3000 Å for scattered light, two shock-tube tests were performed with glass windows rather than quartz windows in the splitter plates. These tests demonstrated that scattered light in the radiometers was negligible.

4.3 Initial Test Conditions

The test gas which when shock heated produced excited C_2 was nominally 85-percent argon and 15-percent acetylene (C_2H_2). The actual gas composition as certified by the supplier was routinely verified by a mass spectrometer analysis of a sample of the test gas taken from the shock-tube test section. Contaminant concentrations never exceeded 80 parts/million in any of the analyses.

The initial pressure, P_1, in the shock tube ranged from 5 to 15 torr. However, the majority of the tests were performed at a pressure of 10 torr. Shock velocities varied from approximately 4.3 to 5.0 km/sec. The shock velocity, initial loading conditions, and test gas composition were selected in order to maximize the ratio of C_2 particles to other species such as C_2, CH, and particulate carbon. Figure 4.7 is a plot of the concentration of some of the carbon-containing species as a function of velocity for an initial pressure of 10 torr. These concentrations were obtained using the thermochemistry program of Horton and Menard (1969) described in section 3.5. Particulate carbon concentrations for these

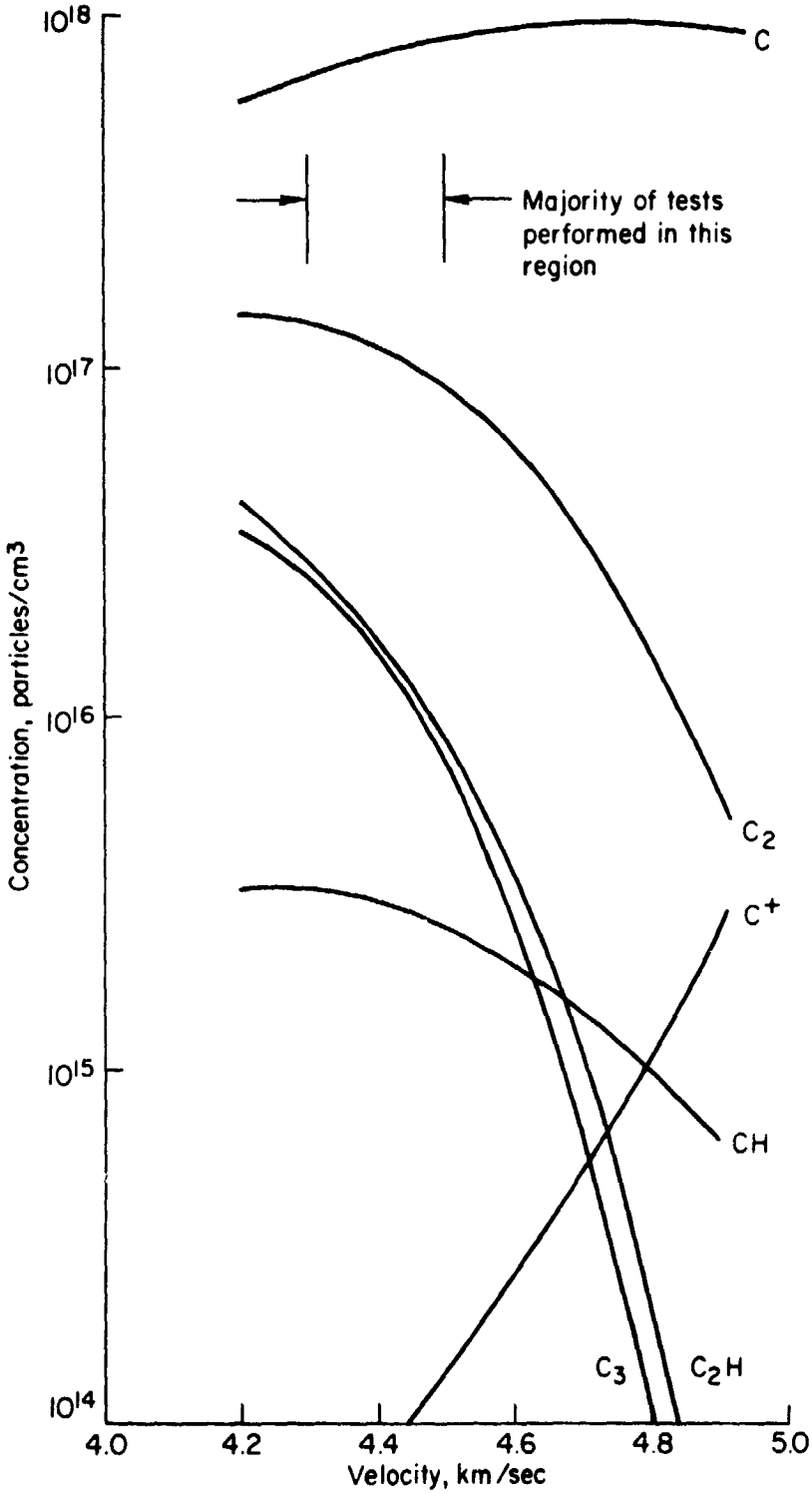

Figure 4.7.- The variation of the concentration of selected carbon-containing species as a function of shock velocity. The test gas is 85 percent Ar and 15 percent C_2H_2; P_1 = 10.0 torr. These concentrations were obtained with the thermochemistry program of Horton and Menard (1969).

conditions were quite low - less than 10^{12} particles/cm^3 and therefore do not appear on the plot. As illustrated on the figure, the majority of the shock-tube tests at this pressure were made at velocities between 4.3 and 4.5 km/sec. The C_2 concentration varies slowly over this velocity interval. Consequently, a slight error in determining the shock velocity will result in only a small error in the C_2 particle concentration.

Note that the species concentrations obtained from the program of Horton and Menard (1969) are compatible with those obtained from the NASA Lewis program (McBride and Gordon, 1967).

4.4 Sample Spectrographic and Radiometric Data

4.4.1 Spectrographic Data

Photographic survey spectra of the shock-heated gas were obtained to verify the purity of the test gas, to demonstrate that C_2 was the dominant radiator in the radiometer bandpass, and to identify the C_2 emission. Sample survey spectra obtained with the spectrographs described in section 4.2.3 are displayed in figures 4.8 to 4.10. These exposures were each obtained from a single shock-tube test. As mentioned in section 4.2.3, the spectrographs were equipped with explosively driven capping shutters with a closing time of 35 μsec. Therefore these spectra represent a time integrated exposure of the shock-heated gas. It will be shown below that the shock-tube test time exceeds 35 μsec for all of the test conditions utilized and consequently these spectra are from the shock-heated test gas only.

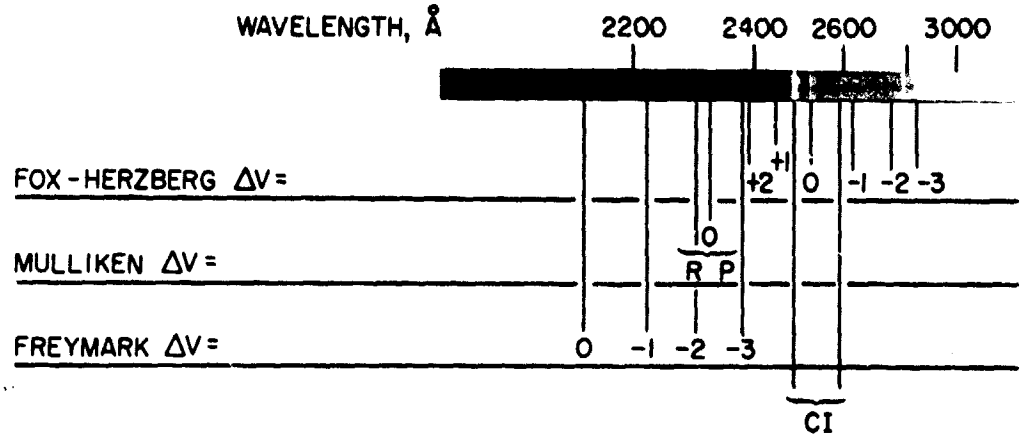

Figure 4.8.- Identified survey spectrum of the shock-heated Ar and C_2H_2 in the ultraviolet region. This spectrum was obtained with a Huet UV 24 spectrograph. The path length was 33.6 cm (double-pass viewpath) and the exposure is from a single shock-tube test. The spectrum was recorded on a type 103-0 plate.

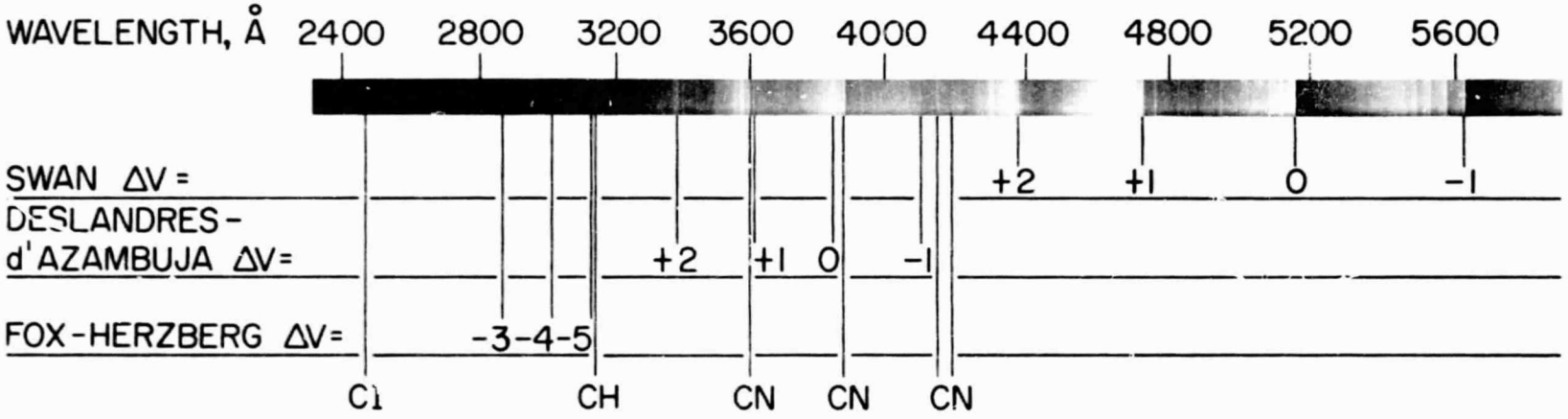

Figure 4.9.- Identified survey spectrum of the shock-heated Ar and C_2H_2 in the ultraviolet and visible regions. This spectrum was obtained with a Jarrell-Ash model 75-000 spectrograph. The path-length was 16.8 cm and the exposure is from a single shock-tube test. The spectrum was recorded on Tri-X panchromatic film.

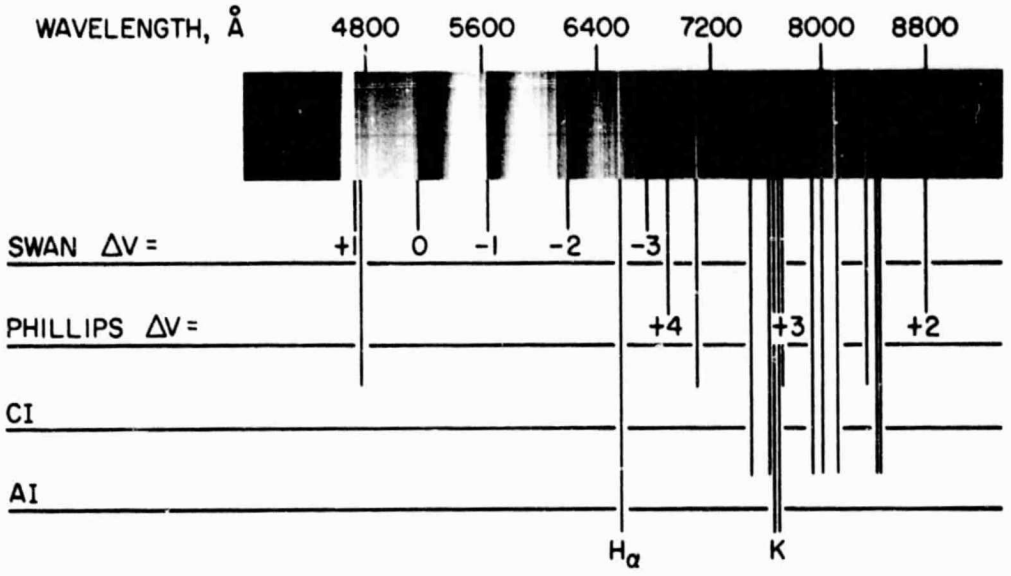

Figure 4.10.- Identified survey spectrum of the shock-heated Ar and C_2H_2 in the visible and infrared regions. This spectrum was obtained with a stigmatic-grating spectrograph which was constructed in-house. The path-length was 16.8 cm and the exposure is from a single shock-tube test. The spectrum was recorded on high-speed infrared film.

Six of the band systems of interest - the Freymark, Mulliken, Fox-Herzberg, Deslandres-d'Azambuja, Swan, and Phillips systems - are readily identified in these spectra. The $\Delta v = 0, -1, -2$, and -3 sequences of the Freymark system appear in figure 4.8. The Mulliken system is a headless system (section 3.4.5) and does not have discrete structure. Only the $\Delta v = 0$ sequence appears since it is the strongest radiating sequence of the system (see figure 3.9). This sequence in figure 4.8 resembles a doublet consisting of diffuse lines, when in reality the structure consists of R and P branches. Six sequences - $\Delta v = +2, +1, 0, -1, -2, -3$ - of the Fox-Herzberg system are also identifiable in the spectrum in figure 4.8. Additional sequences ($\Delta v = -4$ and -5) of the Fox-Herzberg are seen in figure 4.9. The Deslandres-d'Azambuja system is represented by four sequences ($\Delta v = +2, +1, 0$, and -1). The $\Delta v = +1$ and 0 sequences of this system are badly overlapped by the CN violet system which appears as a contaminant in the radiating test gas. Several sequences of the dominant Swan system appear in the spectra in figures 4.9 and 4.10. The Phillips system is identifiable by the presence of the $\Delta v = +4, +3$, and +2 sequences. The only other band system of importance to this study is the Ballik-Ramsay system. Since the short wavelength limit of this system is about 11,000 Å, no attempt was made to record it photographically.

In addition to the C_2 band systems, several atomic lines of C I and Ar I as well as the H_α line have been identified. The Messerle-Krauss system which radiates in the 3100-3400 Å spectral region could not be detected in these spectra.

These spectra demonstrate that the shock-heated test gas is virtually contaminant free. With the exception of a few potassium lines (whose origin is probably the shock-tube walls), the only observed radiating contaminant is the prolific CN radical. An estimate of the CN concentration was performed by integrating the intensity of the CN radiation at 3883 and 3590 Å from a densitometer trace of the spectrographic plate and comparing with the absolute intensity measurements of the nearby Deslandres-d'Azambuja system. The CN concentration was estimated to be approximately 10^{13} particles/cm^3 which is four orders of magnitude less than the typical C_2 concentration (figure 4.7).

Spectra similar to those displayed in figures 4.8 to 4.10 were used to select the band-pass location and width to assure that C_2 was the dominant radiator in the radiometer bandpass. These measurements are discussed in the next section.

4.4.2 Radiometric Data

Absolute intensities of selected spectral regions of the radiation behind the incident shock were measured by calibrated radiometers. These radiometers (section 4.2.4) consisted of dispersing elements and photomultiplier tube detectors. The output of each detector was amplified, displayed on an oscilloscope, and photographed. Sample oscillograms of the radiation signal for each of the band systems measured in this study are presented in this section.

Oscillograms from a radiometer whose bandpass was centered at 5165 Å (the $\Delta v = 0$ sequence of the Swan system) are displayed in figure 4.11. The oscillograms in figures 4.11 (a) and (b) were obtained from tests in which the initial pressure was 5.0 and 10.0 torr,

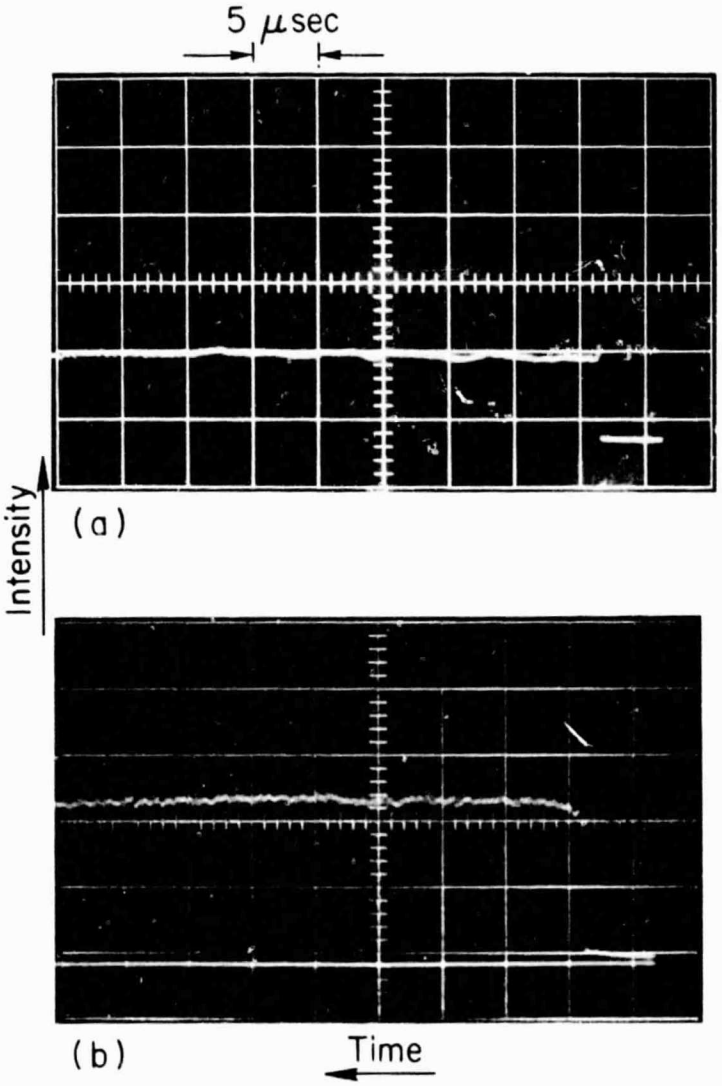

Figure 4.11.- Sample oscillograms from the radiometer whose bandpass was centered at 5165 Å (the $\Delta v = 0$ sequence of the Swan system); (a) P_1 = 5.0 torr, (b) P_1 = 10.0 torr.

respectively. The initial sharp rise in the traces represents the passage of the luminous shock front past the slit. In figure 4.11(a), an initial overshoot attributed to nonequilibrium processes is followed by a rapid relaxation to an essentially constant level of intensity. This level indicates that the shock-heated gas had equilibrated.

The nonequilibrium overshoot vanished as the pressure was increased to 10 torr (fig. 4.11(b)). The absence of this phenomenon indicated that the time required for the gas to equilibrate was shorter than the rise time of the instrumentation. The radiometer electronics (photo-tube and amplifier) had a rise time of 40 nsec and the signal from this unit was displayed on an oscilloscope which had a rise time of 25 nsec. However, the optical rise time of the radiometer was about 0.11 μsec. This rise time was due primarily to the time it took the shock wave to move across the slit in the splitter plate.

Additional oscillograms of the radiation signal from the Freymark, Mulliken, Fox-Herzberg, Deslandres-d'Azambuja, Phillips, and Ballik-Ramsay systems are displayed in figure 4.12. These oscillograms which were obtained from tests with 10 torr initial pressure, are similar to that of the Swan system and indicate that for the present study the gas had reached equilibrium.

Oscillograms similar to those just presented can also be used to determine the approximate facility flow time. For an initial pressure of 5.0 torr, oscillograms with slower sweep rates revealed that the intensity behind the shock front remained almost constant for about 80 μsec and then began to gradually decrease. This value is somewhat

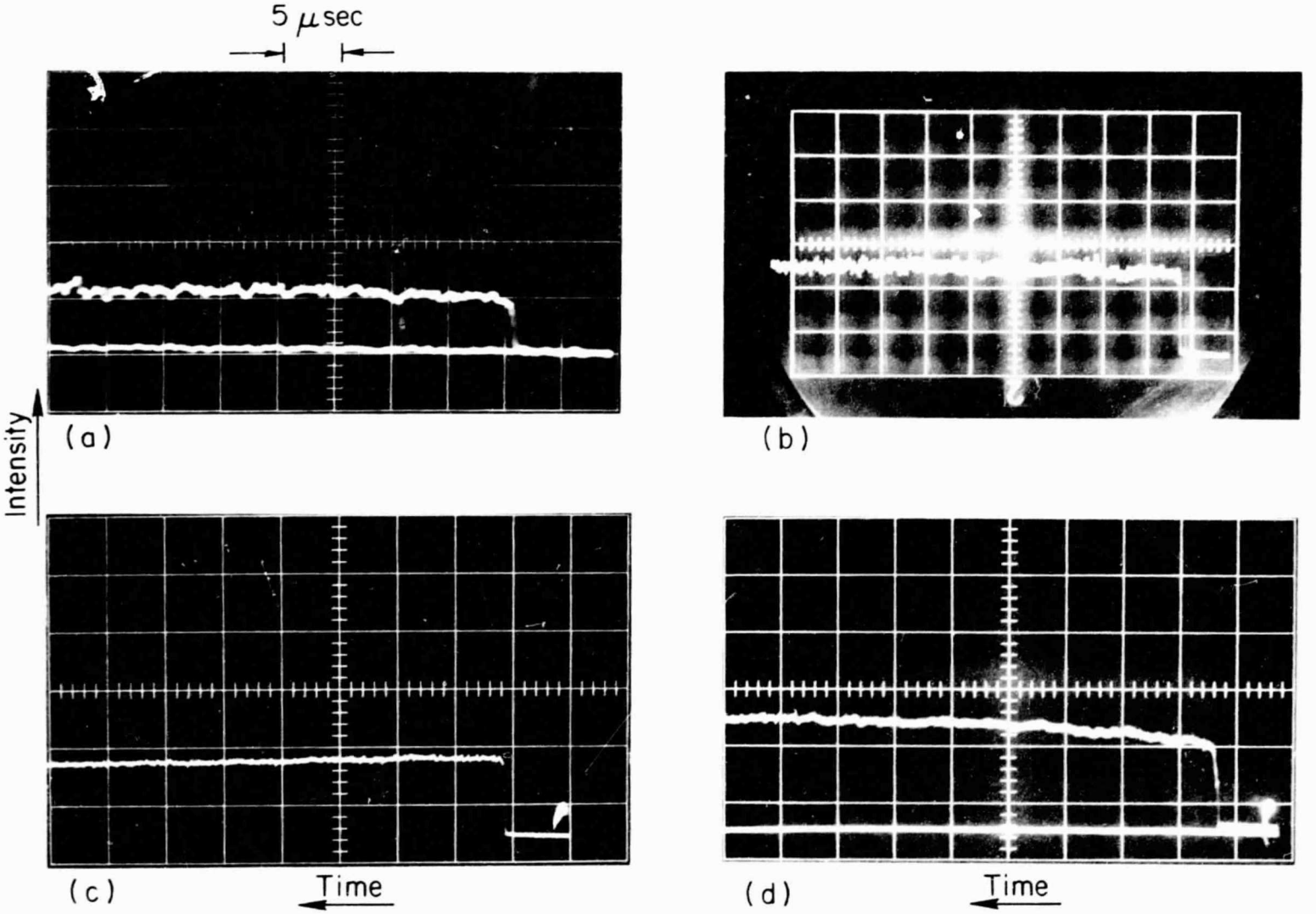

Figure 4.12.- Oscillograms of the radiation signal from the (a) Ballik-Ramsay system, (b) Phillips system, (c) Deslandres-d'Azambuja system, (d) Fox-Herzberg system.

less than the predicted test time of 130 μsec, based on Mirels' (1963) laminar boundary-layer theory. This observed difference between the experimental and theoretical test time is probably due primarily to mixing at the contact surface (figure 4.1).

Chapter 5

Electronic Transition Moments Measurements and Results

The object of the experimental program described in this thesis was to measure the absolute strength of the band systems of the C_2 molecule in the spectral region between 0.2 and 1.2 μ. The results of these measurements are given in this chapter in terms of the electronic transition moments squared values, $\Sigma|R_e/ea_o|^2$. These values were obtained using the synthetic spectrum analysis technique described in section 3.6.

The first section of this chapter deals with the spectral location of the radiometers and the dominant Δv sequence of each electronic transition selected for measurement. The absolute strengths of the Ballik-Ramsay, Phillips, Swan, Deslandres-d'Azambuja, Fox-Herzberg, Mulliken, and Freymark systems are presented in section 5.2. An error analysis leading to an estimate of the accuracy to which the $\Sigma|R_e/ea_o|^2$ values have been determined is presented in section 5.3.

5.1 Spectral Measurements

Survey spectra were used to select the strongest radiating Δv sequences which were free of contaminant radiation for radiometric measurement. Densitometer traces of some of these spectra are shown in figures 5.1 to 5.3. The sequences selected for measurement are indicated in the figures by the short horizontal lines. The length of these lines represent the approximate width of the bandpass of the radiometer assigned to measure a given spectral feature. Table 5.1 contains the wavelengths at which the radiometer bandpasses were centered, the bandpass of each, and the dominant Δv sequence in the bandpass for each band system.

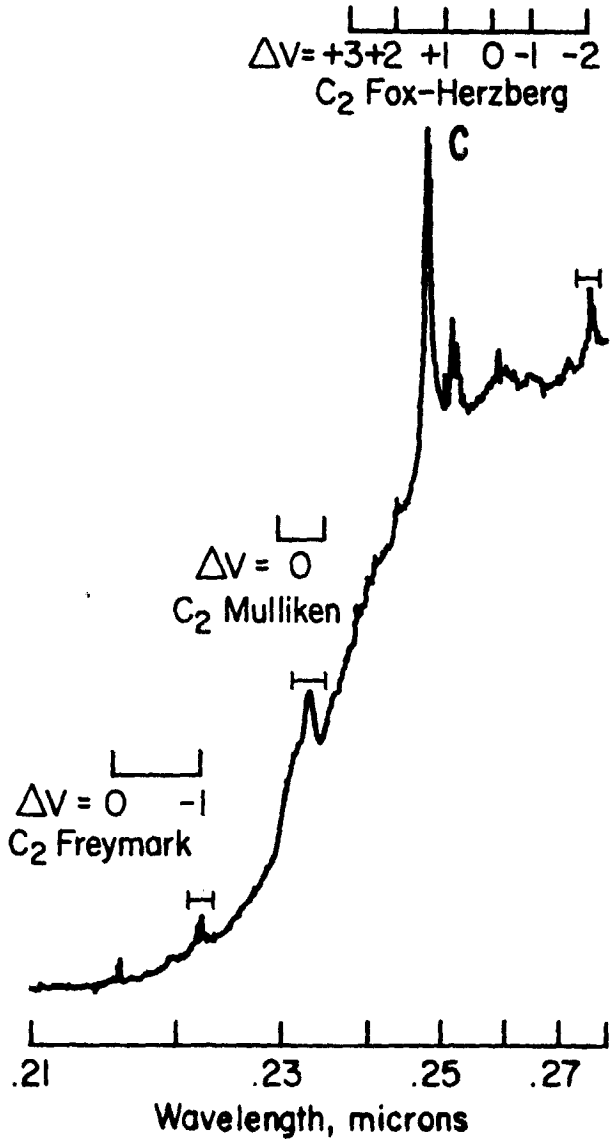

Figure 5.1.- Densitometer trace of the ultraviolet survey spectrum. The small horizontal bars (⊢) indicate the spectral location and width of the radiometers.

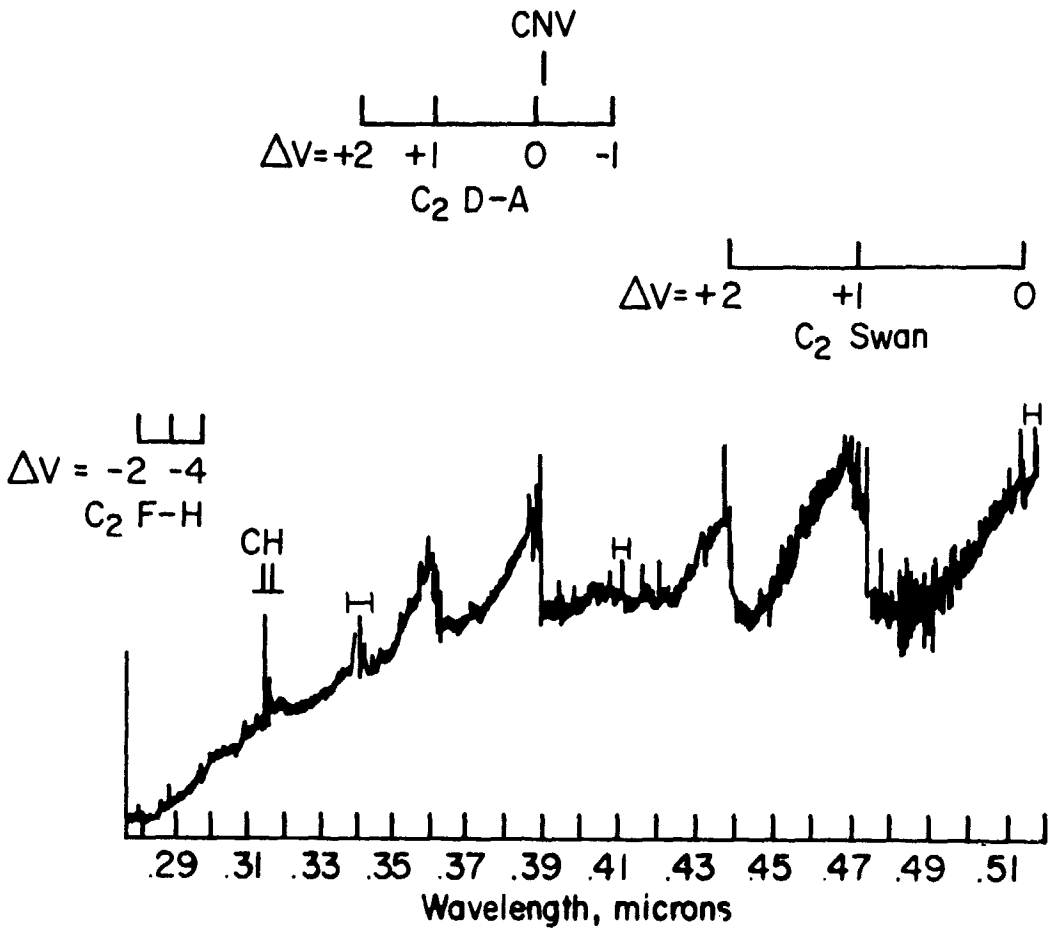

Figure 5.2.- Densitometer trace of the visible survey spectrum. The small horizontal bars (⊢⊣) indicate the spectral location and width of the radiometers.

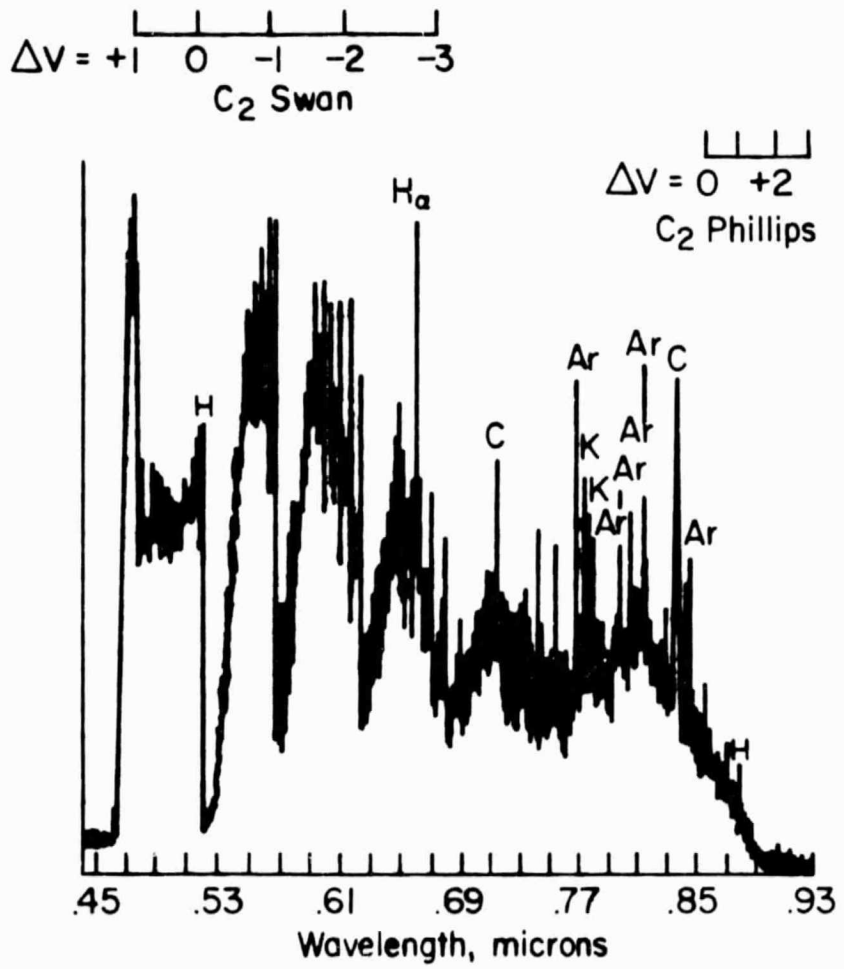

Figure 5.3.- Densitometer trace of the infrared survey spectrum. The small horizontal bars (⊢⊣) indicate the spectral location and width of the radiometers.

Table 5.1 Radiometer Settings and Information.

Band system	Band-pass centerline, Å	Dominant Δv sequence in bandpass	Band-pass width, Å
Swan d $^3\pi_g$ - a $^3\pi_u$	5165	0	19
Phillips A $^1\pi_u$ - X $^1\Sigma_g^+$	12,140 8750	0 +2	110 20
Deslandres-d'Azambuja C $^1\pi_g$ - A $^1\pi_u$	4090 3400	-1 +2	19 28
Fox-Herzberg e $^3\pi_g$ - a $^3\pi_u$	2775	-2	30
Mulliken D $^1\Sigma_u^+$ - X $^1\Sigma_g^+$	2315	0	30
Freymark E $^1\Sigma_g^+$ - A $^1\pi_u$	2218	-1	30
Ballik-Ramsay b $^3\Sigma_g^-$ - a $^3\pi_u$	11,970	+2	92

The radiometers which are described in Chapter 4 were always used in pairs with one centered on the bandhead of interest and the other just off the bandhead to measure the backgrcund radiation. The bandhead-to-background intensity ratios were essentially constant for a given band system. These ratios did, however, vary from about 8 to 1 for the Swan system to approximately 1.4 to 1 for the Freymark system.

5.2 Electronic Transition Moment Results

The spectral measurements described above were converted to electronic transition moments by using the synthetic spectrum data analysis technique previously discussed in Chapter 3. As stated, a synthetic spectrum was produced by calculating the intensity (equation (3.1)) of each rotational line, distributing this intensity in the spectrum by a Voigt profile and then summing. This spectrum was then folded with the measured instrument profile (Chapter 4) to predict a theoretical signal output. The ratio of measured (corrected for background radiation) to theoretical signal output yields the experimental value of $\Sigma|R_e/ea_o|^2$.

The final results of the measurements performed during this work are displayed in table 5.2. The $\Sigma|R_e/ea_o|^2$ values in column four are the average of the individual electronic transition moments deduced from several experimental tests. A complete listing of the $\Sigma|R_e/ea_o|^2$ values from each test as well as the pertinent thermochemical quantities for each test is contained in appendix E. The values of $\Sigma|R_e/ea_o|^2$ represent an average for a given Δv sequence. This is because the bandpass often includes contributions from two or more vibrational transitions of a particular band. Note that the $\Sigma|R_e/ea_o|^2$ values listed in table 5.2 are valid for the specific wavelength (or internuclear separation) at which they were determined but are not necessarily valid for the entire band system.

Although two sequences of the Deslandres-d'Azambuja and Phillips systems were measured, no attempt was made to measure systematically the variation of $\Sigma|R_e/ea_o|^2$ with internuclear separation.

Table 5.2 The Experimental Values of the Electronic Transition Moments.

C_2 band system	Δv	λ, Å	$\Sigma\|R_e/ea_o\|^2$, A.U.
Swan, $d\ ^3\pi_g - a\ ^3\pi_u$	0	5165	3.52 ± 0.50
Phillips, $A\ ^1\pi_u - X\ ^1\Sigma_g^+$	0	12,140	0.36 ± 0.08
	+2	8750	0.40 ± 0.10
Deslandres-d'Azambuja, $C\ ^1\pi_g - A\ ^1\pi_u$	-1	4090	0.93 ± 0.18
	+2	3400	0.91 ± 0.18
Fox-Herzberg, $e\ ^3\pi_g - a\ ^3\pi_u$	-2	2775	0.40 ± 0.10
Mulliken, $D\ ^1\Sigma_u^+ - X\ ^1\Sigma_g^+$	0	2315	0.13 ± 0.05
Freymark, $E\ ^1\Sigma_g^+ - A\ ^1\pi_u$	-1	2218	2.26 ± 1.13
Ballik-Ramsay, $b\ ^3\Sigma_g^- - a\ ^3\pi_u$	+2	11,970	0.65 ± 0.15

5.3 Error Analysis

An estimate of the accuracy to which the $\Sigma|R_e/ea_o|^2$ values have been determined has also been included in table 5.2. This uncertainty was obtained by summing estimates of individual experimental sources of error and therefore represents the maximum error possible due to

experimental uncertainties. Individual sources of error with their accompanying estimate of accuracy include:

Shock velocity, ±0.1 percent

Initial pressure, ±2.0 percent

Gas composition, ±0.03 percent

Band-pass position, ±2 Å

Absolute calibration, typically ±5 percent

Signal deflection on oscillogram, ±4 percent.

The uncertainity in the absolute calibration was larger (±10 percent) for the systems which lie below 2500 Å. This results from the additional uncertainties introduced by extending the calibration curves to 2200 Å. The large uncertainity in the Freymark system results from this additional error as well as the small bandhead-to-background signal ratio.

No attempt was made to estimate the uncertainties which would arise from errors in the spectroscopic or thermochemical constants. The information contained in appendix D is sufficient to allow a rapid re-evaluation of the data for any significant changes in these constants.

Chapter 6

Discussion and Conclusions

In this chapter, the electronic transition moments presented in the preceding chapter are compared with the results found in the literature and summarized earlier in section 2.5. A critical comparison with both experimental and theoretical results are given in section 6.1, and the final conclusions are presented in section 6.2.

6.1 Comparison With Other Results

A comparison of the final results of this study with both experimental and theoretical results found in the literature is presented below for each band system. Most of the results cited in the literature are defined in terms of various absolute intensity parameters and care must be used in interpreting them. The original references were consulted in order to determine the manner in which the results were defined. These results were then converted to $\Sigma|R_e/ea_o|^2$ values by using a consistent set of defining equations. The defining relations were taken from Schadee (1967) and Tatum (1967) and are reproduced in appendix A.

6.1.1 The Swan System, d $^3\pi_g$ - a $^3\pi_u$

The Swan system has been studied extensively in the past to obtain electronic transition moment data. Table 6.1 presents a comparison of the present experimental value (3.52 ± 0.50) with others in the literature. Only measurements of the $\Delta v = 0$ sequence (5165 Å) are included. The present results agree excellently with the shock-tube measurements of Arnold (1968) and Fairbairn (1966). Both of these measurements were

Table 6.1 Measurements of the Electronic Transition Moments of the Swan System. Only Measurements of the $\Delta v = 0$ Sequence (5165 Å) are Included.

Experimenter	Method	$\Sigma\|R_e/ea_o\|^2$, A.U.
Present results	Shock tube	3.52 ± 0.50
Arnold (1968)	Shock tube	3.56 ± 0.50
Fairbairn (1966)	Shock tube	3.36 ± 1.20
Harrington et al. (1966)	Shock tube	2.95 ± 0.92
Sviridov et al. (1965)	Shock tube	2.24 ± 0.81
Sviridov et al. (1966)	Shock tube	2.85 ± 0.20
Hicks (1957)	King furnace	2.64
Hagen (1963)	King furnace	0.71 ± 0.40
Jeunehomme and Schwenker (1965)	Laser excitation	0.60 ± 0.02
Fink and Welge (1967)	Phase shift	2.24 ± 0.70
Wentink et al. (1967)	Laser excitation	>1.35

also made behind the incident shock. Arnold used a test gas consisting of CO_2 and Ar, while Fairbairn used a variety of test gases which consisted of one or more of the following: C_2H_2, C_2N_2, CO, and Ar. Additional shock-tube measurements by Harrington et al. (1966), Sviridov et al. (1965), and Sviridov et al. (1966) obtained in the reflected shock region are in fair agreement with the present results. Harrington et al. used fluoro-carbon as a test gas, while Sviridov et al. used pure CO and mixtures of CO with Ar.

There exists an almost uniform discrepancy (albeit small) between the incident and reflected shock measurements. This discrepancy appears to be more than a coincidence and may result from a common error in calculating the jump conditions across the shock. If this hypothesis were true, one would suspect the reflected shock properties since they are more complicated to predict than the single jump properties across an incident shock. Fairbairn (1966) has suggested that the uncertain bond energies in the fluoro-carbon system might be another source of error in the data of Harrington et al.

The data of Hagan (1963) obtained in a King furnace displays an extremely large scatter with $\Sigma|R_e/ea_o|^2$ values ranging from 0.32 to 4.37. This large scatter is suggestive of nonequilibrium conditions which is the major disadvantage of King furnaces. The value (0.71) recommended by Hagan is clearly too small. Similar measurements in a King furnace by Hicks (1957), however, agree reasonably well with the shock-tube results. Note that the value of 3.45 reported by Hicks has been adjusted to 2.64 to account for the newer values of the heat of sublimation of C_2 (Fairbairn, 1966).

Jeunehomme and Schwenker (1965) and Wentink et al. (1967) have used the laser excitation technique to obtain radiative lifetime measurements of the upper state of the Swan system. Both measurements were made in the hot vapor arising from graphite being heated by a laser beam. Wentink et al. discuss two major problems of this technique which lead them to conclude that their results usually gives only a lower limit to the $\Sigma|R_e/ea_o|^2$ value. These problems are: (1) the temperature and

pressure behavior of the blowoff vapor is complex and not well understood; and (2) the high velocity of the blowoff vapor produces a time variation of the density of the blowoff vapor in the field of view of the instrumentation optics. Fairbairn in discussing the data of Jeunehomme and Schwenker suggested the possibility of formation of molecules in the upper state during the decay process as an additional source of error. It now seems justified to assume that the results of Jeunehomme and Schwenker and Wentink et al. in table 6.1 are incorrect.

The lifetime measurements of Fink and Welge (1967) using the phase-shift method agree with the lower bounds of the shock-tube data and are thus in fair agreement with the present results. In this work, the lower state molecules were excited by electron bombardment of C_2H_2 at low (10^{-3} torr) pressures. These results are based on the critical assumption that the excited state formation time is very short compared to the radiative lifetime. This assumption as Fink and Welge point out is not trivial, and represents a potential source of error in the lifetime measurement data.

Arnold (1968) concludes that the correct $\Sigma|R_e/ea_o|^2$ value of the $\Delta v = 0$ sequence of the Swan system is probably bounded by the shock-tube measurements listed in table 6.1. The results from the present tests support that conclusion and indicate that the correct value lies near the upper bound of these measurements.

The results of various theoretical efforts to predict the absolute strength of the Swan system are listed in table 6.2. Clementi (1960) has calculated the strength of several of the band systems of C_2. He

Table 6.2 Theoretical Predictions of the Absolute Strength of the Swan System.

Reference	$\Sigma\|R_e/ea_o\|^2$, A. U.	Remarks
Clementi (1960)	1.14	$\Sigma\|R_e/ea_o\|^2$ value modified to account for the statistical weight of the upper level omitted from defining-equation
Shull (1951)	4.24	Same as above.
Stephenson (1951)	4.06	
Lyddane, Rogers, and Roach (1941)	3.39	
Spindler (1965)	5.04	Based on Jeunehomme's lifetime measurements of the $d\ ^3\pi_g$ state
Coulson and Lester (1955)	33.92	
Results of this work	3.52 ± 0.50	Experimental measurement of the $\Delta v = 0$ sequence (5165 Å)

used the dipole-moment operator method and obtained a $\Sigma|R_e/ea_o|^2$ value of 1.14 for the Swan system. As noted in table 6.2, Clementi omitted the statistical weight of the upper state from his defining equation. Consequently, the $\Sigma|R_e/ea_o|^2$ value credited to him on table 6.2 has been modified to account for this factor. A similar correction was also made to the results of Shull (1951). Shull, Stephenson (1951), Lyddane et al. (1941), and Coulson and Lester (1955) all used the dipole-moment operator method. Spindler's (1965) prediction is based on the lifetime

measurement of the upper state by Jeunehomme. The early work of Lyddane et al., Stephenson, and Shull agrees surprisingly well with the higher values reported from shock-tube tests. These theoretical papers, however, also contain predictions of the absolute strengths of other band systems of C_2, CN, and N_2. Experimental measurements of the strengths of these band systems indicates that only the predictions of Stephenson are consistently accurate. Since these calculations are quite old and based on hydrogen-ion approximated wave functions, it is clear that there is still much progress to be made in the field of theoretical computations of basic molecular properties.

A new measurement of the relative spectral intensity distribution of the Swan system was recently reported by Danylewych (1972) and Danylewych and Nicholls (1974). This work contains a valuable plot comparing all of the past measurements of the variation of spectral intensity of the Swan system.

6.1.2 The Fox-Herzberg System, $e\ ^3\pi_g - a\ ^3\pi_u$

The value of $\Sigma|R_e/ea_o|^2$ for the $\Delta v = +2$ sequence (2775 Å) of the Fox-Herzberg system was found to be 0.40 ± 0.10. Sviridov et al. (1966), also using a shock tube but obtaining measurements in the reflected shock region, placed an upper limit 0.55 on the $\Sigma|R_e/ea_o|^2$ value. These measurements were made in mixtures of CO and Ar. Wentink et al. (1967) using the laser excitation technique placed a lower limit of 0.45 on the $\Delta v = 0$ sequence (2512 Å). (See section 6.1.1 for a discussion of this work.) The excellent agreement between these three

measurements may be fortuitous since two of them represent limits. The results however are compatible.

Clementi's (1960) prediction of 57.80 is obviously unreliable. This value has been reduced by a factor of six to account for the statistical weight of the upper level missing from the equation defining the absolute strength in his paper.

6.1.3 The Deslandres-d'Azambuja System, $C\ ^1\pi_g - A\ ^1\pi_u$

Values of 0.91 ± 0.18 and 0.93 ± 0.18 for the $\Delta v = +2$ (3400 Å) and -1 (4090 Å) sequences, respectively, were obtained in the present work. The sequence at 3852 Å was not measured since the $\Delta v = 0$ sequence of CN violet (which was observed as a slight contaminant) overlaps this wavelength region. Wentink et al. (1967) quote a lower bound of 0.18 for the $\Delta v = 0$ sequence.

Stephenson (1951), Shull (1951), and Clementi (1960) have all used the dipole moment operator method to predict $\Sigma|R_e/ea_o|^2$ values of 1.35, 3.97, and 1.12, respectively. Stephenson's prediction is greater (46 percent) than the experimental value. However, as discussed above, his predictions are consistently 20 to 50 percent higher than the experimental values. While Clementi's prediction agrees quite well with the experimental value, it appears to be a coincidence since his predictions of the other C_2 band strengths are not supported by experimental measurements nor do they show a consistent difference with the experimental results. Shull's value of 3.97 is too high. Once again the results of Clementi and Shull have been modified (section 6.1.1) to

account for the incorrect definition of the absolute strength used by them.

As stated earlier, a detailed study to determine the variation of $\Sigma|R_e/ea_o|^2$ with internuclear separation, r, was not undertaken. However the results of the present tests indicate that the $\Sigma|R_e/ea_o|^2$ value does not vary with r over the range of r (and λ) appropriate to the two sequences of the Deslandres-d'Azambuja system that were measured.

6.1.4 The Mulliken System, D $^1\Sigma_u^+$ - X $^1\Sigma_g^+$

A value of 0.13 ± 0.05 was measured for the $\Sigma|R_e/ea_o|^2$ value of the $\Delta v = 0$ sequence (2315 Å) of the Mulliken system. Smith (1969) measured the radiative lifetime of the same sequence using the phase shift method. He produced C_2 spectra by focusing high energy electrons on ethylene or benzene. Smith obtained a $\Sigma|R_e/ea_o|^2$ value of 0.42 ± 0.05. These lifetime measurements are based on the nontrivial assumption that the excited state formation time is very short compared to the radiative lifetime. This assumption was not verified by Smith and represents a potential source of substantial error. It is interesting to note also that Smith was unable to detect the Freymark, Fox-Herzberg, and Deslandres-d'Azambuja systems contained in the spectral region he examined. Clementi's (1960) prediction for this system is 0.78.

6.1.5 The Phillips System, A $^1\pi_u$ - X $^1\Sigma_g^+$

The $\Sigma|R_e/ea_o|^2$ value for the $\Delta v = 0$ (12,140 Å) and +2 (8750 Å) sequences was determined in the present tests to be 0.36 ± 0.08 and 0.40 ± 0.10, respectively. These measurements were obtained using the

two types of radiometers described in section 4.2.4. The $\Delta v = +2$ sequence was measured with the 1/4-m monochromator type. Hicks (1957) has also measured the $\Delta v = +2$ sequence using a King furnace as a source. His measurement was not an absolute determination per se but was taken relative to the (1,0) state of the Swan system. This measurement yields a $\Sigma|R_e/ea_o|^2$ value of 0.68 with a factor of three uncertainty. Considering the gross uncertainty in Hicks' result, it would be premature to form any conclusion pertaining to the absolute strength of this sequence. However, the two sets of measurements do agree satisfactorily. Clementi's (1960) prediction of the $\Sigma|R_e/ea_o|^2$ value for this system is 0.13.

Based on the measurements of the $\Delta v = 0$ and +2 sequences, the $\Sigma|R_e/ea_o|^2$ of this system appears to have a weak dependence on the internuclear separation.

6.1.6 The Ballik-Ramsay System, b $^3\Sigma_g^-$ - a $^3\pi_u$

A $\Sigma|R_e/ea_o|^2$ value of 0.65 ± 0.15 was measured for the $\Delta v = +2$ sequence (11970 Å) of this system. There are no other existing measurements of this system known to the author. Clementi (1960) has predicted a value of 1.21.

6.1.7 The Freymark System, E $^1\Sigma_g^+$ - A $^1\pi_u$

The $\Sigma|R_e/ea_o|^2$ value for the $\Delta v = -1$ sequence (2218 Å) was determined to be 2.26 ± 1.13. There are no other measurements or predictions of the strength of this system known to the author.

A summary of the results presented in sections 6.1.2 to 6.1.7 is given in table 6.3. The results of the present effort (excluding the

Table 6.3 Experimental and Theoretical Results of the Absolute Strength of the Band Systems (Excluding the Swan System) of the C_2 Molecule.

Band system	Results in literature, $\Sigma\|R_e/ea_o\|^2$, A.U.		Results of this work $\Sigma\|R_e/ea_o\|^2$, A.U., [$\Delta v/\lambda$(Å)]
	Theoretical	Experimental [$\Delta v/\lambda$(Å)]	
Ballik-Ramsay, b $^3\Sigma_g^-$ - a $^3\pi_u$	1.21-Clementi (1960)		0.65 ± 0.15 (+2/11,970)
Phillips, A $^1\pi_u$ - X $^1\Sigma_g^+$	0.13-Clementi (1960)	0.68-Hicks (1957) (+2/8750)	0.40 ± 0.10 (+2/8750)
Deslandres-d'Azambuja, C $^1\pi_g$ - A $^1\pi_u$	1.12-Clementi (1960) 3.97-Shull (1951) 1.35-Stephenson (1951)	>0.18-Wentink et al. (1967) (0/3852)	0.91 ± 0.18 (+2/3400)
Fox-Herzberg, e $^3\pi_g$ - a $^3\pi_u$	57.80-Clementi (1960)	<0.55-Sviridov et al. (1965) >0.45-Wentink et al. (1967) (0/2512)	0.40 ± 0.10 (-2/2775)
Mulliken, D $^1\Sigma_u^+$ - X $^1\Sigma_g^+$	0.78-Clementi (1960)	0.42-Smith (1969) (0/2315)	0.13 ± 0.05 (0/2315)
Freymark, E $^1\Sigma_g^+$ - A $^1\pi_u$			2.26 ± 1.13 (-1/2218)

Swan system) are compared with the experimental and theoretical results found in the literature.

6.2 Conclusions

A systematic study of the absolute strength of seven of the band systems of the C_2 molecule in the spectral region 0.2 to 1.2 μ has been made. Experimental measurements of the strength of the Ballik-Ramsay, Phillips, Swan, Deslandres-d'Azambuja, Fox-Herzberg, Mulliken, and Freymark systems were performed.

A combustion-driven shock tube was used to heat the test gas of 85-percent Ar and 15-percent C_2H_2 to temperatures of approximately 6000 °K. Measurements of the absolute intensity of the equilibrium radiation in selected spectral regions were obtained with spectrally and absolutely calibrated narrow pass-band radiometers. The measurements were made behind the incident shock.

The absolute intensity measurements were converted to electronic transition moments by a synthetic spectrum analysis. The values deduced from this work are as follows:

System	λ(Å)	$\Sigma\lvert R_e/ea_o\rvert^2$, A.U.
Ballik-Ramsay ($\Delta v = +2$)	11,970	0.65 ± 0.15
Phillips ($\Delta v = 0$)	12,140	0.36 ± 0.08
($\Delta v = +2$)	8750	0.40 ± 0.10
Swan ($\Delta v = 0$)	5165	3.52 ± 0.50
Deslandres-d'Azambuja ($\Delta v = +2$)	3400	0.91 ± 0.18
($\Delta v = -1$)	4090	0.93 ± 0.18
Fox-Herzberg ($\Delta v = +2$)	2775	0.40 ± 0.10

System	(Å)	$\Sigma\|R_e/ea_o\|^2$, A.U.
Mulliken ($\Delta v = 0$)	2315	0.13 ± 0.05
Freymark ($\Delta v = -1$)	2218	2.26 ± 1.13

These results are valid for the specific sequence (or wavelength) at which they were determined but are not necessarily valid for the entire band system.

APPENDIX A

Absolute Intensity Relationships

The relationships between the various absolute intensity parameters are given herein. Complete descriptions of these relations can be found in the papers of Schadee (1967) and Tatum (1967).

A wavelength-dependent electronic absorption f number, $f_{e\ell}(\lambda)$, is related to the $\Sigma|R_e/ea_o|^2$ value by

$$f_{e\ell}(\lambda) = \frac{8\pi^2 m_e c}{3he^2\lambda} \frac{\Sigma|R_e/ea_o|^2}{(2 - \delta_{o,\Lambda''})(2S'' + 1)}, \text{ dimensionless.}$$

The band oscillator strength, $f_{v'v''}$ (written for absorption), and the band Einstein coefficient, $A_{v'v''}$, are related to the electronic transition moment by

$$f_{v'v''} = \frac{8\pi^2 m_e c}{3he^2} \frac{q_{v'v''}}{\lambda_{v'v''}} \frac{\Sigma|R_e(\bar{r}_{v'v''})|^2}{(2 - \delta_{o,\Lambda''})(2S'' + 1)}, \text{ dimensionless}$$

and

$$A_{v'v''} = \frac{64\pi^4\nu^3}{3hc^3} q_{v'v''} \frac{\Sigma|R_e(\bar{r}_{v'v''})|^2}{(2 - \delta_{o,\Lambda'})(2S' + 1)}, \text{ sec}^{-1}.$$

The band strength, $S_{v'v''}$, is related to the $\Sigma|R_e/ea_o|^2$ through

$$S_{v'v''} = q_{v'v''}\, \Sigma|R_e/ea_o|^2, \text{ A.U.}$$

The mean radiative lifetime $\tau_{v'}$ (written for the upper state) is given by

$$\frac{1}{\tau_{v'}} = \frac{64\pi^4}{3hc^3(2 - \delta_{o,\Lambda'})(2S' + 1)} \sum_{v''} \nu^3 q_{v'v''}\, \Sigma|R_e(\bar{r}_{v'v''})|^2, \text{ sec}^{-1}$$

$$= \sum_{v''} A_{v'v''}, \text{ sec}^{-1}$$

APPENDIX B

Band Origins

The band origins of the seven C_2 bands systems of interest in this work are tabulated in this appendix (tables B-1 through B-7). In section 3.1.2, the band origin, $\bar{\nu}_o$, was defined as:

$$\bar{\nu}_o(v',v'')(cm^{-1}) = (T_e' - T_e'') + [G'(v') - G''(v'')] = 10^8/\lambda_o(\text{Å})$$

where T_e and $G(v)$ are the electronic and vibrational term energies, respectively. The electronic term energies are listed in table 2.1 and the vibrational term energies were calculated from equation (3.11) using the vibrational constants also listed in table 2.1. These band origins are calculated in vacuo and are listed in Å units.

TABLE B-1. BAND ORIGINS (Å, IN VACUO) OF THE FREYMARK SYSTEM

v' \ v''	0	1	2	3	4	5	6	7	8	9	10
0	2142.78	2218.08	2297.58	2381.60	2470.52	2564.73					
1	2072.09	2142.41	2216.49	2294.59	2377.01	2464.10					
2	2009.04	2075.09	2144.50	2217.53	2294.42	2375.45					
3	1952.63	2014.95	2080.34	2148.99	2221.13	2296.98					
4		1961.08	2022.97	2087.83	2155.85	2227.24					
5			1971.52	2033.07	2097.52	2165.04					
6				1983.94	2045.26	2109.41					
7											
8											
9											
10											

TABLE B-2. BAND ORIGINS (Å, IN VACUO) OF THE MULLIKEN SYSTEM

v' \ v''	0	1	2	3	4	5	6	7	8	9	10
0	2313.34	2415.46	2525.20								
1	2220.78	2314.73	2415.32	2523.19							
2	2136.62	2223.44	2316.09	2415.10	2521.02						
3		2140.36	2226.09	2317.40	2414.75	2518.65					
4			2144.10	2228.67	2318.57	2414.20	2516.00				
5				2147.79	2231.15	2319.57	2413.39	2513.01			
6					2151.38	2233.47	2320.33	2412.27	2509.63		
7						2154.83	2235.57	2320.79	2410.77	2505.77	
8							2158.08	2237.40	2320.62	2408.83	2501.40
9								2161.09	2238.90	2320.62	2406.41
10									2163.80	2240.04	2319.87

TABLE B-3. BAND ORIGINS (Å, IN VACUO) OF THE FOX-HERZBERG SYSTEM

v' \ v''	0	1	2	3	4	5	6	7	8	9	10
0	2512.15	2618.59	2732.70	2855.31	2987.35	3129.91	3284.23				
1	2448.36	2549.35	2657.39	2773.19	2897.57	3031.50	3176.05	3332.48			
2	2390.77	2486.97	2589.68	2699.53	2817.26	2943.70	3079.81	3226.68	3385.59		
3	2337.82	2429.72	2527.66	2632.21	2744.01	2863.83	2992.49	3130.97	3280.37	3441.97	
4	2288.19	2376.16	2469.74	2569.46	2675.89	2789.70	2911.65	3042.58	3183.48	3335.46	3499.81
5		2325.05	2414.58	2509.80	2611.25	2719.52	2835.28	2959.29	3092.41	3235.62	3390.06
6											
7											
8											
9											
10											

TABLE B-4. BAND ORIGINS (Å, IN VACUO) OF THE DESLANDRES-d'AZAMBUJA SYSTEM

v' \ v''	0	1	2	3	4	5	6	7	8	9	10
0	3850.62	4100.77	4381.01	4697.00	5055.89	5466.84					
1	3605.65	3824.08	4066.66	4337.53	4641.81	4985.91	5378.03				
2	3397.79	3591.09	3804.19	4040.21	4302.94	4597.04	4928.34	5304.19			
3	3222.11	3395.42	3585.32	3794.22	4025.01	4281.22	4567.15	4888.13	5250.85		
4	3074.63	3232.06	3403.66	3591.36	3797.47	4024.71	4276.40	4556.56	4870.17	5223.39	
5	2952.23	3097.07	3254.29	3425.48	3612.48	3817.53	4043.27	4292.79	4570.03	4879.68	5227.56
6		2987.50	3133.53	3291.94	3464.28	3652.41	3858.49	4085.12	4335.40	4613.10	4922.81
7			3038.71	3187.45	3348.76	3524.23	3715.72	3925.43	4155.98	4410.49	4692.76
8				3109.81	3263.16	3429.56	3610.63	3808.34	4024.96	4263.21	4526.38
9					3205.97	3366.44	3540.75	3730.67	3938.30	4166.12	4417.09
10						3334.35	3505.27	3691.30	3894.45	4117.08	

TABLE B-5. BAND ORIGINS (Å, IN VACUO) OF THE SWAN SYSTEM

v' \ v''	0	1	2	3	4	5	6	7	8	9	10
0	5160.37	5630.49	6185.91	6851.93	7664.92	8679.21					
1	4732.13	5124.49	5580.53	6116.91	6756.69	7532.68	8493.16				
2	4376.68	4710.23	5092.76	5535.76	6054.59	6670.34	7412.66	8324.69			
3	4077.61	4365.64	4692.31	5065.82	5496.87	5999.70	6593.61	7305.55	8174.21		
4	3823.15	4075.24	4358.49	4678.93	5044.28	5464.55	5952.93	6527.21	7211.96	8042.10	
5	3604.63	3827.88	4076.74	4355.76	4670.69	5028.80	5439.47	5914.99	6471.84	7132.54	7928.76
6		3615.31	3836.49	4082.60	4358.02	4668.20	5020.02	5422.33	5886.64	6428.25	7067.94
7			3629.90	3849.47	4093.39	4365.86	4672.09	5018.64	5413.87	5868.62	6397.20
8				3648.92	3867.36	4109.69	4379.92	4683.08	5025.42	5414.90	5861.80
9					3672.90	3890.79	4132.15	4400.92	4701.92	5041.19	5426.33
10						3702.46	3920.37	4161.50	4429.64	4729.50	5066.90

TABLE B-6. BAND ORIGINS (Å, IN VACUO) OF THE PHILLIPS SYSTEM

v' \ v''	0	1	2	3	4	5	6	7	8	9	10
0	12094.60	15526.30	21545.02								
1	10149.90	12461.30	16062.70	22443.55							
2	8762.53	10433.23	12844.36	16623.61	23387.17						
3	7723.30	8992.51	10728.31	13243.02	17207.39						
4	6916.07	7916.65	9231.59	11034.62	13656.17	17811.56					
5	6271.20	7082.94	8117.42	9479.39	11351.36	14082.23					
6	5744.41	6418.17	7256.09	8325.33	9735.35	11677.49					
7	5306.16	5875.94	6570.60	7435.32	8539.98	9998.73	12011.65				
8	4936.03	5425.43	6012.33	6728.34	7620.32	8760.83	10268.59	12352.06			
9	4619.43	5045.34	5549.08	6153.46	6891.17	7810.70	8987.19	10543.71	12696.61		
10	4345.65	4720.54	5158.68	5677.04	6299.17	7058.78	8005.93	9218.19	10822.61	13042.64	

TABLE B-7. BAND ORIGINS (Å, IN VACUO) OF THE BALLIK-RAMSAY SYSTEM

v' \ v''	0	1	2	3	4	5	6	7	8	9	10
0	17753.47	24908.51									
1	14122.62										
2	11755.34										
3	10090.18	12058.92									
4	8855.42	10336.44	12376.48								
5	7903.53	9062.43	10593.34	12708.80							
6	7147.50	8082.18	9277.96	10861.42	13056.68						
7				9502.42	11141.26						
8					9736.24	11433.47					
9						9979.89	11738.69				
10							10233.85	12057.60			
11								10498.62	12390.92		

APPENDIX C

Franck-Condon Factors

The Franck-Condon factors used in the data reduction in this study are listed in this appendix. These factors were defined in section 3.2 by

$$q_{v'v''} = \int |\psi_{v'}\psi_{v''}\, dr|^2$$

where the ψ's represent the vibrational wave functions. The factors listed herein are based on Klein-Dunham potentials and were taken from the work of McCallum, Jarmain, and Nicholls (1970).

TABLE C-1. FRANCK-CONDON FACTORS FOR THE BALLIK-RAMSAY SYSTEM

v' \ v''	0	1	2	3	4	5	6	7	8	9	10
0	6.3400E-01	3.0600E-01	5.4900E-02	4.7600E-03	2.0500E-04	2.9400E-06	1.6400E-09	1.4000E-08	2.9400E-11	3.4900E-09	9.3000E-10
1	2.6900E-01	1.8700E-01	3.9500E-01	1.3100E-01	1.6400E-02	9.1800E-04	1.9400E-05	5.4100E-08	8.3600E-09	2.8100E-10	8.4300E-10
2	7.4300E-02	2.9500E-01	2.2000E-02	3.6400E-01	2.0600E-01	3.5800E-02	2.5000E-03	6.4400E-05	2.4100E-07	2.0100E-08	5.0500E-10
3	1.7400E-02	1.4500E-01	2.1900E-01	4.0900E-03	2.8000E-01	2.6700E-01	6.1900E-02	5.2700E-03	1.6400E-04	9.8500E-07	3.5300E-09
4	3.7900E-03	4.8800E-02	1.8100E-01	1.2500E-01	4.6600E-02	1.8500E-01	3.0600E-01	9.3400E-02	9.6200E-03	3.4200E-04	2.1800E-06
5	7.9800E-04	1.3800E-02	8.4000E-02	1.8000E-01	5.0900E-02	1.0000E-01	1.0300E-01	3.2300E-01	1.2800E-01	1.5700E-02	6.2200E-04
6	1.6200E-04	3.5500E-03	3.0000E-02	1.1300E-01	1.5100E-01	9.9900E-03	1.4000E-01	4.3800E-02	3.2000E-01	1.6400E-01	2.3700E-02
7	3.1900E-05	8.5500E-04	9.2000E-03	5.0000E-02	1.2900E-01	1.0900E-01	1.7300E-04	1.5700E-01	1.0100E-02	2.9700E-01	2.0100E-01
8	6.7400E-06	2.0600E-04	2.6700E-03	1.8500E-02	7.0300E-02	1.3000E-01	6.5900E-02	1.2500E-02	1.5200E-01	1.3800E-07	2.6300E-01
9	1.5000E-06	4.9400E-05	7.3500E-04	6.1500E-03	3.0600E-02	8.7000E-02	1.1700E-01	3.0700E-02	3.6700E-02	1.3100E-01	8.1900E-03
10	3.5200E-07	1.2100E-05	2.0000E-04	1.9300E-03	1.1700E-02	4.4300E-02	9.7200E-02	9.4700E-02	8.4000E-03	6.3100E-02	1.0100E-01

TABLE C-2. FRANCK-CONDON FACTORS FOR THE PHILLIPS SYSTEM

v' \ v''	0	1	2	3	4	5	6	7	8	9	10
0	4.1200E-01	3.9800E-01	1.5500E-01	3.1100E-02	3.4300E-03	2.0500E-04	5.8900E-06	6.0400E-08	2.8200E-11	6.9300E-12	2.7200E-15
1	3.3100E-01	5.5300E-03	2.8900E-01	2.7100E-01	8.8600E-02	1.3600E-02	1.0300E-03	3.5600E-05	4.0200E-07	9.5800E-11	1.8100E-11
2	1.6200E-01	1.7200E-01	5.8100E-02	1.1500E-01	3.0200E-01	1.5600E-01	3.2200E-02	3.0400E-03	1.2200E-04	1.5200E-06	1.1100E-10
3	6.3100E-02	1.9900E-01	3.1700E-02	1.4300E-01	1.6700E-02	2.6300E-01	2.1600E-01	5.9100E-02	6.7900E-03	3.1500E-04	4.1500E-06
4	2.1600E-02	1.2600E-01	1.3800E-01	1.2300E-03	1.5600E-01	2.7900E-03	1.8900E-01	2.5900E-01	9.2600E-02	1.2800E-02	6.7300E-04
5	6.8800E-03	6.0200E-02	1.4500E-01	5.7700E-02	3.6800E-02	1.1400E-01	3.7300E-02	1.1100E-01	2.7800E-01	1.3000E-01	2.1300E-02
6	2.0900E-03	2.4600E-02	9.6100E-02	1.2000E-01	8.8500E-03	8.1500E-02	5.7300E-02	8.3000E-02	4.8700E-02	2.7500E-01	1.6800E-01
7	6.1500E-04	9.1700E-03	4.9900E-02	1.1200E-01	7.3100E-02	1.6900E-03	1.0300E-01	1.5500E-02	1.1600E-01	1.1800E-02	2.5300E-01
8	1.7800E-04	3.2100E-03	2.2500E-02	7.4200E-02	1.0400E-01	2.9200E-02	2.2600E-02	9.6100E-02	1.1100E-04	1.2600E-01	2.5700E-05
9	5.1400E-05	1.0800E-03	9.2400E-03	4.0200E-02	8.8700E-02	7.7700E-02	4.1200E-03	5.1200E-02	6.9600E-02	8.2600E-03	1.1400E-01
10	1.4900E-05	3.5600E-04	3.5800E-03	1.9300E-02	5.7900E-02	8.8500E-02	4.4600E-02	1.3700E-03	7.1500E-02	3.8000E-02	3.0000E-02

TABLE C-3. FRANCK-CONDON FACTORS FOR THE SWAN SYSTEM

v' \ v''	0	1	2	3	4	5	6	7	8	9	10
0	7.2400E-01	2.2000E-01	4.6000E-02	8.4500E-03	1.5100E-03	2.7900E-04	5.5700E-05	1.2400E-05	3.1500E-06	9.1400E-07	2.9900E-07
1	2.4600E-01	3.3000E-01	2.8700E-01	1.0200E-01	2.6700E-02	6.2500E-03	1.4400E-03	3.4500E-04	8.9900E-05	2.5900E-05	8.3900E-06
2	2.9000E-02	3.7000E-01	1.1700E-01	2.6500E-01	1.4600E-01	5.1700E-02	1.5300E-02	4.2700E-03	1.2100E-03	3.6200E-04	1.1800E-04
3	1.3500E-03	7.4700E-02	4.1200E-01	2.2300E-02	2.0200E-01	1.6700E-01	7.7600E-02	2.8400E-02	9.4600E-03	3.1100E-03	1.0600E-03
4	1.2900E-05	4.6900E-03	1.2800E-01	4.0200E-01	1.7500E-05	1.2900E-01	1.6500E-01	9.8800E-02	4.4100E-02	1.7300E-02	6.5500E-03
5	3.1400E-07	3.9900E-05	1.0000E-02	1.8300E-01	3.6400E-01	1.4800E-02	6.7200E-02	1.4200E-01	1.1000E-01	5.9500E-02	2.7300E-02
6	5.7100E-08	3.2600E-06	6.1100E-05	1.7000E-02	2.3500E-01	3.1500E-01	4.2500E-02	2.4700E-02	1.0900E-01	1.1000E-01	7.1600E-02
7	1.8800E-11	3.7900E-07	1.7800E-05	4.6300E-05	2.4600E-02	2.8400E-01	2.6500E-01	6.8000E-02	3.5800E-03	7.1800E-02	9.8400E-02
8	2.6900E-10	1.4300E-09	1.3700E-06	6.7300E-05	3.7500E-06	3.1800E-02	3.2800E-01	2.2200E-01	8.3400E-02	7.5400E-04	3.9500E-02
9	2.3300E-11	1.9600E-09	3.5100E-08	2.8900E-06	1.9600E-04	7.2800E-05	3.6800E-02	3.6900E-01	1.9100E-01	8.6100E-02	1.0300E-02
10	1.0300E-12	1.4200E-11	1.5200E-08	3.4500E-07	3.5300E-06	4.6500E-04	7.0500E-04	3.7800E-02	4.0500E-01	1.7300E-01	7.7600E-02

TABLE C-4. FRANCK-CONDON FACTORS FOR THE DESLANDRES-d'AZAMBUJA SYSTEM

v' \ v''	0	1	2	3	4	5	6	7	8	9	10
0	7.3500E-01	2.1500E-01	4.1900E-02	6.6200E-03	9.8500E-04	1.5400E-04	2.8800E-05	7.4100E-06	2.8100E-06	1.4000E-06	7.6100E-07
1	2.3600E-01	3.5500E-01	2.8500E-01	9.6000E-02	2.2200E-02	4.5000E-03	9.3500E-04	2.2900E-04	7.1800E-05	2.9600E-05	1.5200E-05
2	2.7800E-02	3.5900E-01	1.4600E-01	2.6400E-01	1.4100E-01	4.5200E-02	1.2200E-02	3.2600E-03	1.0000E-03	3.7900E-04	1.7500E-04
3	1.0800E-03	6.8000E-02	4.1500E-01	4.8200E-02	1.9600E-01	1.6200E-01	7.0000E-02	2.4800E-02	8.4200E-03	3.1600E-03	1.3800E-03
4	2.5400E-06	2.4900E-03	1.0800E-01	4.4000E-01	1.1600E-02	1.1500E-01	1.5800E-01	8.8100E-02	4.0800E-02	1.7100E-02	7.8300E-03
5	1.0500E-05	1.4000E-04	2.5100E-03	1.4000E-01	4.6100E-01	2.4600E-03	4.4800E-02	1.3300E-01	8.9100E-02	5.5400E-02	2.7900E-02
6	1.8200E-07	7.0000E-05	1.1900E-03	4.6300E-04	1.5000E-01	4.8500E-01	1.9600E-03	3.7100E-03	1.0100E-01	6.6900E-02	6.3000E-02
7	3.0600E-07	1.0500E-06	1.7100E-04	5.0400E-03	2.4500E-03	1.2500E-01	4.9000E-01	7.5800E-03	1.3800E-02	7.8100E-02	2.5900E-02
8	4.4700E-09	2.9400E-06	5.6500E-05	4.6600E-05	1.1600E-02	2.8200E-02	5.6500E-02	4.0700E-01	2.0700E-02	9.1300E-02	7.4800E-02
9	3.5300E-08	3.2400E-07	4.0200E-06	4.3500E-04	8.5500E-04	9.9100E-03	8.8000E-02	2.1700E-04	1.7600E-01	1.5100E-02	1.5700E-01
10	6.0100E-09	3.0800E-08	6.8400E-06	5.2800E-05	2.5100E-04	7.4500E-03	2.2100E-03	5.9400E-02	4.5300E-02	1.8100E-03	1.0500E-02

TABLE C-5. FRANCK-CONDON FACTORS FOR THE FOX-HERZBERG SYSTEM

v' \ v''	0	1	2	3	4	5	6	7	8	9	10
0	2.1700E-03	1.7100E-02	6.1200E-02	1.3300E-01	1.9800E-01	2.1400E-01	1.7500E-01	1.1100E-01	5.5800E-02	2.2700E-02	7.6100E-03
1	8.9200E-03	5.0900E-02	1.1700E-01	1.3300E-01	6.5300E-02	2.0900E-03	3.3400E-02	1.2200E-01	1.7000E-01	1.4500E-01	8.9000E-02
2	2.0200E-02	8.2600E-02	1.1300E-01	4.5900E-02	8.9100E-04	6.1300E-02	9.4300E-02	3.3300E-02	2.1600E-03	6.8300E-02	1.4400E-01
3	3.3500E-02	9.6400E-02	6.8300E-02	7.3600E-04	4.6500E-02	7.1200E-02	8.4300E-03	2.5400E-02	8.6400E-02	5.1100E-02	1.4600E-04
4	4.5300E-02	8.9400E-02	2.3500E-02	1.4900E-02	6.6500E-02	1.4300E-02	2.0100E-02	6.8100E-02	1.7200E-02	1.4500E-02	7.8800E-02
5	4.8800E-02	6.4100E-02	2.1400E-03	3.7600E-02	3.6200E-02	2.1000E-03	5.0300E-02	1.9100E-02	1.1200E-02	5.8300E-02	1.8400E-02
6	4.4000E-02	6.8400E-02	4.9700E-03	3.1000E-02	3.3300E-02	3.2800E-03	4.9000E-02	7.5300E-03	2.9400E-02	4.7300E-02	7.7100E-05
7	5.7200E-02	5.8300E-02	3.9000E-05	4.4400E-02	9.9400E-03	2.4900E-02	3.1100E-02	5.3800E-03	4.9200E-02	3.5300E-03	4.0300E-02
8	6.4700E-02	4.1200E-02	6.0400E-03	4.2200E-02	1.7000E-06	4.0200E-02	4.5800E-03	3.2800E-02	2.0200E-02	1.7000E-02	4.3800E-02
9	6.6600E-02	2.2900E-02	1.7800E-02	2.8100E-02	7.3400E-03	3.3600E-02	2.1700E-03	3.9900E-02	2.4900E-06	4.4200E-02	4.6900E-03
10	6.7400E-02	9.5700E-02	2.9700E-02	1.2600E-02	2.1700E-02	1.5700E-02	1.8200E-02	2.0700E-02	1.4800E-02	2.9100E-02	9.4600E-03

TABLE C-6. FRANCK-CONDON FACTORS FOR THE MULLIKEN SYSTEM

v' \ v''	0	1	2	3	4	5	6	7	8	9	10
0	9.9700E-01	2.5100E-03	1.6200E-04	3.6400E-06	1.7600E-08	8.3600E-09	5.4300E-09	1.5900E-09	3.3200E-10	5.9100E-11	1.0100E-11
1	2.5900E-03	9.9300E-01	3.9400E-03	4.2100E-04	1.1800E-05	4.9000E-08	4.9700E-08	3.2300E-08	1.0600E-08	2.7900E-09	5.5200E-10
2	9.1400E-05	4.1800E-03	9.9000E-01	4.5100E-03	7.2800E-04	2.4000E-05	8.3400E-08	1.7300E-07	1.1900E-07	4.0100E-08	1.0300E-08
3	3.7500E-08	2.6500E-04	4.9200E-03	9.8900E-01	4.4300E-03	1.0500E-03	3.8700E-05	9.3100E-08	4.3900E-07	3.1300E-07	1.1100E-07
4	1.0700E-07	3.1200E-07	5.0900E-04	4.9600E-03	9.8900E-01	3.9000E-03	1.3600E-03	5.4600E-05	7.2300E-08	9.1500E-07	6.6100E-07
5	1.9400E-08	4.6600E-07	1.2700E-06	8.0400E-04	4.4700E-03	9.9000E-01	3.0900E-03	1.6600E-03	7.0400E-05	4.0600E-08	1.6200E-06
6	2.2500E-09	1.1600E-07	1.2200E-06	3.6800E-06	1.1300E-03	3.6200E-03	9.9100E-01	2.1600E-03	1.9200E-03	8.6200E-05	2.1500E-08
7	2.8800E-10	1.6700E-08	3.9200E-07	2.4200E-06	8.6200E-06	1.4700E-03	2.5900E-03	9.9200E-01	1.2700E-03	2.1600E-03	1.0300E-04
8	3.6500E-11	2.2200E-09	6.5000E-08	9.9100E-07	4.0200E-06	1.7600E-05	1.8000E-03	1.5700E-03	9.9400E-01	5.5700E-04	2.3800E-03
9	3.9400E-12	2.8100E-10	9.6200E-09	1.9300E-07	2.0700E-06	5.7700E-06	3.2400E-05	2.1000E-03	7.1700E-04	9.9400E-01	1.2000E-04
10	6.2200E-13	3.4600E-11	1.5100E-09	3.1100E-08	4.5800E-07	3.7500E-06	7.2300E-06	5.6200E-05	2.3700E-03	1.7500E-04	9.9400E-01

TABLE C-7. FRANCK-CONDON FACTORS FOR THE FREYMARK SYSTEM

v' \ v''	0	1	2	3	4	5
0	5.8100E-01	2.7100E-01	1.0200E-01	3.2800E-02	9.9600E-03	2.6700E-03
1	3.7100E-01	1.6200E-01	2.2200E-01	1.4400E-01	6.4500E-02	2.4300E-02
2	4.6900E-02	4.8200E-02	4.6800E-02	1.4000E-01	1.4300E-01	8.1700E-02
3	1.5200E-05	8.4000E-02	5.2600E-01	1.9500E-02	7.9800E-02	1.2600E-01
4	2.9400E-04	5.0800E-04	9.5600E-02	5.6300E-01	1.8400E-02	4.0500E-02
5	1.5600E-06	1.0700E-03	5.4900E-03	7.7400E-02	5.9800E-01	3.3900E-02
6	2.8100E-06	6.9300E-05	1.6300E-03	2.0800E-02	3.6800E-02	6.0800E-01

APPENDIX D

Thermochemical Calculation Data

This appendix contains a list of the species and significant constants required as input data in the thermochemical calculations of mixtures of argon and acetylene. The constants for atomic species considered in the thermochemical calculations are listed in table D-1, while those for the diatomic and polyatomic molecules are given on tables D-2 and D-3, respectively.

TABLE D-1. ATOMIC SPECIES DATA USED IN THERMOCHEMICAL CALCULATIONS

Species	Number of energy levels included	Energy level reference	Heat of formation, h_i^o, kcal/mole
C	41	Moore (1949)	169.99
C^+	36		429.54
C^{++}	20		991.69
C^-	51		144.00
H	6		51.62
H^+	0		365.03
H^-	16	Moore (1949)	344.00
Ar	59		0.0
Ar^+	28		363.34
Ar^{++}	41		1000.28
e^-	0		0.0

TABLE D-2. DIATOMIC MOLECULAR DATA USED IN THERMOCHEMICAL CALCULATIONS

Species	Energy levels included	Energy level reference	Heat of formation, h_i^o, kcal/mole
C_2	X $^1\Sigma_g^+$, a $^3\pi_u$, b $^3\Sigma_g^-$, A $^1\pi_u$, c $^3\Sigma_u^+$, d $^3\pi_g$, C $^1\pi_g$, e $^3\pi_g$, D $^1\Sigma_u^+$, E $^1\Sigma_g^+$	Ballik and Ramsay (1963)	196.00
H_2	X $^1\Sigma_g^+$	Herzberg (1950)	0.0
CH	X $^2\pi$, A $^2\Delta$, B $^2\Sigma^-$, C $^2\Sigma^+$	Herzberg (1950)	141.60

TABLE D-3. POLYATOMIC MOLECULAR DATA USED IN THERMOCHEMICAL CALCULATIONS

Species	Ground state	Number of vibrational frequencies included	Reference	Heat of formation, h_i^o, kcal/mole
C_3	$^1\Sigma_g^+$	4	McBride et al. (1963)	188.00
C_2H	$^2\pi$	4	JANAF Tables (1971)	116.70
CH_2	$^3\Sigma_g^-$	4	McBride et al. (1963)	95.00
CH_3	$^2A_2''$	6	McBride et al. (1963)	33.40
C_2H_2	$^1\Sigma_g^+$	7	Herzberg (1966)	54.33

APPENDIX E

Tabulation of Individual Test Conditions and Data

This appendix contains a complete list of the pertinent thermochemical quantities, the measured absolute value of the spectral emission in the radiometer bandpass, and the $\Sigma|R_e/ea_o|^2$ value deduced for each test. The average of the absolute strength factors, $\Sigma|R_e/ea_o|^2$, given in tables E-1 to E-7 for the Swan, Fox-Herzberg, Deslandres-d'Azambuja, Mulliken, Phillips, Freymark, and Ballik-Ramsay systems, respectively, were reported earlier in table 5.2.

The critical radiometer settings (band-pass center location and width) for each system may be found in section 5.1. The $\Sigma|R_e/ea_o|^2$ value was deduced from the absolute measurements (column 6) by use of the synthetic spectrum calculations described in section 3.5. These calculations included all of the vibrational bands for which Franck-Condon factors are listed in appendix C.

TABLE E-1. TABULATION OF SHOCK-TUBE DATA FOR THE C_2 SWAN SYSTEM

Test	P_1, torr	V_s, km/sec	T_2, °K	N_{C_2}, parts/cm^3	I_λ, W/cm^2·μ·sr	$\Sigma\|R_e/ea_o\|^2$, A.U.
1	5.0	4.83	6610	3.30^{15}	1778	3.69
2		4.84	6660	3.18^{15}	1742	3.74
3		4.82	6560	3.42^{15}	1665	3.34
4		4.82	6560	3.42^{15}	1619	3.36
5		4.83	6610	3.30^{15}	1691	3.51
6		4.82	6560	3.42^{15}	1614	3.35
7		4.84	6660	2.95^{15}	1495	3.47
8		4.90	7000	1.74^{15}	1072	3.72
9		4.83	6610	3.33^{15}	1595	3.35
10		4.88	6885	2.08^{15}	1240	3.96
11		4.86	6770	2.50^{15}	1370	3.59
12		4.84	6660	3.00^{15}	1470	3.35
13		4.83	6610	3.33^{15}	1595	3.33
14		4.85	6710	2.72^{15}	1530	3.77
15	↓	4.84	6660	3.00^{15}	1470	3.35

TABLE E-2. TABULATION OF SHOCK-TUBE DATA FOR THE C_2 DESLANDRES-d'AZAMBUJA SYSTEM

Test	P_1, torr	V_s, km/sec	T_2, °K	N_{C_2} parts/cm^3	I_λ, W/cm^2·μ·sr	$\Sigma\|R_e/ea_o\|^2$, A.U.
			$\Delta v = -1$			
1	10.0	4.42	5290	1.11^{17}	157	0.82
2	↓	4.50	5450	8.87^{16}	100	.66
3		4.45	5350	1.03^{17}	125	1.15
4		4.47	5390	9.70^{16}	107	1.13
5		4.50	5450	8.90^{16}	120	.75
6		4.39	5235	1.18^{17}	176	1.17
7	↓	4.40	5250	1.15^{17}	218	.85
			$\Delta v = +2$			
8	5.0	4.84	6660	3.00^{15}	13	0.65
9	↓	4.86	6770	2.50^{15}	13	.79
10		4.90	7000	1.74^{15}	14	.92
11		4.83	6610	3.33^{15}	22	.99
12		4.88	6885	2.08^{15}	13	.85
13		4.86	6770	2.50^{15}	16	.97
14		4.85	6710	2.72^{15}	19	1.04
15		4.84	6660	3.00^{15}	26	1.29
16		4.83	6610	3.33^{15}	15	.69
17		4.85	6710	2.72^{15}	15	.83
18	↓	4.84	6660	3.00^{15}	19	.95

TABLE E-3. TABULATION OF SHOCK-TUBE DATA FOR THE C_2 PHILLIPS SYSTEM. $\Delta v = +2$ SEQUENCE.

Test	P_1, torr	V_s, km/sec	T_2, °K	N_{C_2}, parts/cm^3	I_λ, W/cm^2·μ·sr	$\Sigma\|R_e/ea_o\|^2$, A.U.
1	5.0	4.83	6610	3.33^{15}	7.5	0.41
2	5.0	4.84	6660	3.00^{15}	7.4	.44
3	10.0	4.42	5290	1.11^{17}	163	.38
4	↓	4.50	5450	8.90^{16}	180	.42
5		4.45	5350	1.03^{17}	61	.35
6		4.47	5390	9.70^{16}	69	.41
7		4.43	5310	1.08^{17}	64	.36
8		4.39	5235	1.18^{17}	73	.43
9		4.38	5220	1.21^{17}	65	.38

TABLE E-4. TABULATION OF SHOCK-TUBE DATA FOR THE C_2 PHILLIPS SYSTEM. $\Delta v = 0$ SEQUENCE.

Test	P_1, torr	V_s, km/sec	T_2, °K	N_{C_2}, parts/cm^3	I_λ, W/cm^2·μ·sr	$\Sigma\|R_e/ea_o\|^2$, A.U.
1	9.15	4.53	5520	6.80^{16}	102	0.38
2		4.54	5550	6.55^{16}	90	.35
3		4.56	5600	6.00^{16}	107	.46
4		4.70	6090	2.60^{16}	40	.39
5	↓	4.48	5410	8.05^{16}	129	.49
6	10.0	4.45	5400	9.15^{16}	82	.29
7		4.45	5400	9.15^{16}	82	.29
8		4.35	5205	1.17^{17}	96	.47
9		4.42	5340	9.90^{16}	164	.42
10		4.32	5160	1.22^{17}	158	.33
11	↓	4.34	5200	1.18^{17}	101	.22
12	15.0	4.28	5200	2.00^{17}	315	.40
13		4.35	5315	1.81^{17}	241	.34
14		4.35	5315	1.81^{17}	234	.33
15		4.40	5405	1.66^{17}	174	.27
16		4.35	5315	1.81^{17}	213	.30
17		4.27	5190	2.01^{17}	269	.34
18		4.36	5330	1.78^{17}	227	.32
19		4.26	5175	2.03^{17}	269	.34
20		4.38	5365	1.71^{17}	267	.40
21		4.34	5300	1.84^{17}	252	.35
22		4.31	5250	1.91^{17}	294	.39
23	↓	4.37	5350	1.75^{17}	232	.33
24	10.0	4.49	5495	8.10^{16}	164	.52
25		4.52	5565	7.20^{16}	110	.39
26		4.51	5540	7.40^{16}	93	.33
27		4.51	5540	7.40^{16}	134	.49
28	↓	4.54	5615	6.60^{16}	103	.41

TABLE E-5. TABULATION OF SHOCK-TUBE DATA FOR THE C_2 BALLIK-RAMSAY SYSTEM

Test	P_1, torr	V_s, km/sec	T_2, °K	N_{C_2}, parts/cm^3	I_λ, W/cm^2·μ·sr	$\Sigma\|R_e/ea_o\|^2$, A.U.
1	9.15	4.53	5520	6.80^{16}	59	0.54
2	↓	4.54	5550	6.55^{16}	77	.65
3		4.56	5600	6.00^{16}	55	.50
4		4.70	6090	2.60^{16}	37	.71
5		4.48	5410	8.05^{16}	72	.52
6	10.0	4.45	5400	9.15^{16}	91	.90
7	↓	4.45	5400	9.15^{16}	90	.90
8		4.35	5205	1.17^{17}	113	.90
9		4.42	5340	9.90^{16}	108	.64
10		4.32	5160	1.22^{17}	133	.65
11		4.34	5200	1.18^{17}	188	.94
12	15.0	4.28	5200	2.00^{17}	160	.49
13	↓	4.35	5315	1.81^{17}	260	.83
14		4.35	5315	1.81^{17}	235	.75
15		4.40	5405	1.66^{17}	291	1.00
16		4.35	5315	1.81^{17}	258	.82
17		4.27	5190	2.01^{17}	155	.47
18		4.36	5330	1.78^{17}	235	.76
19		4.26	5175	2.03^{17}	156	.47
20		4.38	5365	1.71^{17}	196	.66
21		4.34	5300	1.84^{17}	223	.71
22		4.31	5250	1.91^{17}	224	.69
23	↓	4.37	5350	1.75^{17}	232	.77
24	10.0	4.49	5495	8.10^{16}	65	.46
25	↓	4.52	5565	7.20^{16}	89	.69
26		4.51	5540	7.40^{16}	93	.72
27		4.51	5540	7.40^{16}	71	.55
28	↓	4.54	5615	6.60^{16}	81	.69

TABLE E-6. TABULATION OF SHOCK-TUBE DATA FOR THE C_2 FOX-HERZBERG SYSTEM

Test	P_1, torr	V_s, km/sec	T_2, °K	N_{C_2}, parts/cm^3	I_λ, W/cm^2·μ·sr	$\Sigma\|R_e/ea_o\|^2$, A.U.
1	9.15	4.67	5960	3.25^{16}	29.8	0.38
2	9.15	4.48	5410	8.05^{16}	43.8	.46
3	10.0	4.45	5400	9.15^{16}	46.9	.50
4	↓	4.38	5265	1.10^{17}	48.7	.36
5		4.42	5340	9.90^{16}	53.5	.38
6		4.45	5400	9.15^{16}	60.6	.42
7		4.32	5160	1.22^{17}	40.9	.33
8		4.34	5200	1.18^{17}	38.5	.30
9		4.37	5250	1.12^{17}	43.7	.33
10		4.49	5495	8.10^{16}	58.4	.40
11		4.52	5565	7.20^{16}	62.0	.42
12		4.51	5540	7.40^{16}	68.2	.46
13		4.51	5540	7.40^{16}	67.2	.45
14		4.54	5615	6.60^{16}	66.9	.45
15		4.52	5565	7.20^{16}	50.5	.34
16		4.54	5615	6.60^{16}	46.0	.31
17		4.44	5390	1.04^{17}	67.8	.49
18	↓	4.47	5445	8.60^{16}	55.6	.39

TABLE E-7. TABULATION OF SHOCK-TUBE DATA FOR THE C_2 MULLIKEN AND FREYMARK SYSTEMS

Test	P_1, torr	V_s, km/sec	T_2, °K	N_{C_2}, parts/cm^3	I_λ, W/cm^2·μ·sr	$\Sigma\|R_e/ea_o\|^2$, A.U.
Mulliken						
1	10.0	4.44	5380	1.04^{17}	598	0.17
2	↓	4.49	5495	8.10^{16}	407	.12
3		4.51	5540	7.40^{16}	409	.11
4	15.0	4.39	5380	1.68^{17}	705	.12
Freymark						
1	10.0	4.54	5615	6.60^{16}	59	2.82
2	↓	4.52	5565	7.20^{16}	40	1.91
3		4.50	5520	7.75^{16}	42	2.01
4		4.41	5325	1.02^{17}	38	.230

NOTATIONS

A	constant appearing in equation (3.12), = $h/8\pi^2 c I_A$
$A\ ^1\pi_u$	lower electronic state of the Deslandres-d'Azambuja, Messerle-Krauss, and Freymark systems; upper electronic state of the Phillips system
$A_{u\ell}$	Einstein A coefficient for an electronic transition, $sec^{-1} \cdot particle^{-1}$
$A_{v'v''}$	Einstein A coefficient for the (v', v'') transition, $sec^{-1} \cdot particle^{-1}$
$a\ ^3\pi_u$	lower electronic state of the Fox-Herzberg, Swan, and Ballik-Ramsay systems
B	rotational constant, cm^{-1}
B_λ	black-body emission, $W/cm^2 \cdot \mu \cdot sr$
$b\ ^3\Sigma_g^-$	upper electronic state of the Ballik-Ramsay system
$C\ ^1\pi_g$	upper electronic state of the Deslandres-d'Azambuja system
$C'\ ^1\pi_g$	upper electronic state of the Messerle-Krauss system
c	speed of light, 2.9979×10^{10} $cm \cdot sec^{-1}$
D	rotational constant, cm^{-1}
$\vec{D}$	dyadic of coordinate transformation
$D\ ^1\Sigma_u^+$	upper electronic state of the Mulliken system
d	total statistical weight or multiplicity
$d\ ^3\pi_g$	upper electronic state of the Swan system
E	energy, ev
$E\ ^1\Sigma_g^+$	upper electronic state of the Freymark system
E_ℓ^u	integrated intensity in a rotational line, $W/cm^3 \cdot sr$

E_λ	spectral emissive power due to spontaneous emission, $W/cm^3 \cdot \mu \cdot sr$
e	electronic charge, 4.80298×10^{-10} dyne$\cdot cm^2$ (esu)
ea_o	product of electronic charge and radius of first Bohr orbit, 2.5416×10^{-18} esu$\cdot$cm, unity in atomic units (A.U.)
$e\ ^3\pi_g$	upper electronic state of the Fox-Herzberg system
F	Gibbs free energy, ev
F(J)	rotational term energy, cm^{-1}
$f_{e\ell}(\lambda)$	wavelength dependent electronic absorption f number, dimensionless
$f_{v'v''}$	band oscillator strength (absorption), dimensionless
G(v)	vibrational term energy, cm^{-1}
$G(\lambda)$	radiometer calibration constant, $V(W/cm^2 \cdot sr)^{-1}$
g	"gerade" or even state
g_n	statistical weight of the level n
H	Hamiltonian operator
H_o	wavelength independent absolute strength parameter
$H(\lambda)$	spectral irradiance incident on the radiometer, $W/cm^2 \cdot \mu$
h	Planck's constant, 6.623×10^{-27} erg$\cdot$sec, or enthalpy, cal/G
$\hbar$	Planck's constant divided by 2π, 1.054×10^{-27} erg$\cdot$sec
h_i^o	heat of formation, kcal/mole
I	moment of inertia, $G \cdot cm^2$
I_λ	specific intensity, $W/cm^2 \cdot \mu \cdot sr$
J	total rotational quantum number
$\vec{J}$	total angular momentum

K	rotational quantum number without spin
$\vec{K}$	total angular momentum apart from spin
K	equilibrium constant
k	Boltzmann constant, 1.38054×10^{-16} erg·°K^{-1}
$\vec{L}$	orbital angular momentum
$L(\lambda)$	spectral irradiance from the calibration source, W/cm^2·μ
ℓ	optical path length, cm
ℓ_s	radiating gas boundary, cm
$\vec{M}$	electric dipole moment, esu·cm
M_n	mass of the nth nuclei, G
m	particle mass, G
m_e	mass of the electron, 9.1091×10^{-28} G
N	particle concentration, particles/cm^3
$\vec{N}$	nuclear rotation vector
P	pressure, atm, or rotational branch with $\Delta J = -1$
p	parity, + or -
Q	partition function, dimensionless, or rotational branch with $\Delta J = 0$
$q_{v'v''}$	Franck-Condon factor
R	rotational branch with $\Delta J = +1$
$R^{u\ell}$	transition moment, esu·cm
$\lvert R_e(\bar{r}_{v'v''})\rvert^2$	electronic transition moment squared, esu·cm, $= \Sigma \lvert R_e(r_{v'v''})\rvert^2/du$
$\Sigma \lvert R_e/ea_o\rvert^2$	sum of the squares of the electronic transition moment, A.U., often referred to as the electronic transition moment

r	internuclear separation, cm
r_e	equilibrium internuclear distance (corresponds to the minimum of the potential curve), cm
$\bar{r}_{v'v''}$	r centroid, Å
S	spin quantum number
$\vec{S}$	spin angular momentum
$S_{v'v''}$	band strength, A.U.
$S^{J'\Lambda'}_{J''\Lambda''}$	Hönl-London factor normalized to $(2S' + 1)(2J' + 1)$
$S^{uv'J'}_{\ell v''J''}$	total line strength, A.U.
T	temperature, °K
T_e	electronic term energy, cm^{-1}
$T(\lambda)$	normalized spectral response of a radiometer
U	shock velocity, km/sec
$U(r)$	molecular potential function, ev
u	"ungerade" or odd state
V	volume, cm^3
V_{ee}	electron-electron Coulombic interaction, ev
V_{ne}	electron-nucleus Coulombic interaction, ev
V_{nn}	nucleus-nucleus Coulombic interaction, ev
$V(r)$	sum of the potential energy terms, $= V_{ee} + V_{ne} + V_{nn}$, ev
$V(\lambda)$	radiometer output, volts
v	vibrational quantum number
W_g	Gaussian line width at half-height, Å
W_L	Lorentzian line width at half-height, Å
W_V	Voigt line width at half-height, Å

$X\ ^1\Sigma_g^+$	lower electronic state of the Mulliken and Phillips systems
Y	dimensionless parameter, $= A/B_v$
Z_2	dimensionless parameter defined by equation (3.81)
α_e	rotational constant, cm^{-1}
α_j	stoichiometric coefficients
α_λ	absorption coefficient, cm^{-1}
α'_λ	absorption coefficient corrected for stimulated emission, cm^{-1}
γ	splitting constant, cm^{-1}
$\delta_{o,\Lambda}$	Kronecker delta function, $\delta_{o,\Lambda} = 1$ for $\Lambda = 0$ and $= 0$ for $\Lambda \neq 0$
ε	splitting constant, cm^{-1}
θ	angle of oblique shock, deg
Λ	quantum number of the angular momentum of the electrons along the internuclear axis
$\vec{\Lambda}$	resultant orbital angular momentum of electrons along the internuclear axis
λ	wavelength, Å, or splitting constant (equation (3.43)), cm^{-1}
λ_o	band origin, Å
ν	frequency of emitted radiation, sec^{-1}
$\bar{\nu}$	wavenumber, cm^{-1}
$\bar{\nu}_m$	wavenumber of bandhead, cm^{-1}
$\bar{\nu}_o$	wavenumber of band origin, cm^{-1}
ξ	electron coordinates
ρ	density, G/cm^3

Σ	quantum number of the spin angular momentum along the internuclear axis
$\vec{\Sigma}$	component of spin angular momentum along the internuclear axis
σ	symmetry factor, = 2.0 for homonuclear molecules, 1.0 for all others
τ	radiative lifetime, sec^{-1}
ϕ	lambda doubling function, cm^{-1}
Ψ	wave function
Ω	quantum number of the resultant momentum along the internuclear axis
$\vec{\Omega}$	total angular momentum along the internuclear axis, $= \vec{\Lambda} + \vec{\Sigma}$
ω_e	vibrational constant, cm^{-1}
$\omega_e x_e$	vibrational constant, cm^{-1}
$\omega_e y_e$	vibrational constant, cm^{-1}
$\omega_e z_e$	vibrational constant, cm^{-1}

Subscripts

c	calibration
e	electronic state or equilibrium position
ℓ	lower state
n	nuclear state
T	test
u	upper state
v	vibrational level

C_L	central point
1	conditions ahead of shock wave
2	conditions behind incident shock wave
4	conditions in the driver tube

Superscripts

'	upper state
''	lower state
u	upper state
ℓ	lower state

BIBLIOGRAPHY

Aller, L. H., 1963, Astrophysics, The Atmospheres of the Sun and Stars, The Ronald Press Co., New York, 2nd edition

Angström, A. J., and Thalen, T. R., 1875, Nova Acta Reg. Soc. Sci. Uppsala 9, 3

Arnold, J. O., 1968, JQSRT 8, 1781

_____, Whiting, E. E., and Lyle, G. C., 1969, JQSRT 9, 775

_____, Nicholls, R. W., 1972, JQSRT 12, 1435

_____, 1973, JQSRT 13, 115

_____, 1972, Ph. D. Dissertation, York University, Toronto, Canada

Ballik, E. A., and Ramsay, D. A., 1959, J. Chem. Phys. 31, 1128

_____, 1963, Astrophys. J. 137, 61

_____, 1963, Astrophys. J. 137, 84

Borucki, W. J., Cooper, D. M., and Page, W. A., 1969, Proc. 7 International Shock Tube Symposium

_____, 1970, App. Optics 9, 259

Brewer, L., Gilles, P. W., and Jenkins, F. A., 1948, J. Chem. Phys. 16, 797

_____, Hicks, W. T., and Krikorian, O. H., 1962, J. Chem. Phys. 36, 182

Clementi, E., 1960, Astrophys. J. 132, 898

_____, and Pitzer, K. S., 1960, J. Chem. Phys. 32, 656

Climenhaga, J. L., 1960, Publ. Dom. Ap. Obs. 11, 307

Coulson, C. A., and Lester, G. R., 1955, Trans. Faraday Soc. 51, 1605

Craig, R. A., and Davy, W. C., 1969, NASA TN D-5360

Danylewych, L. L., 1971, Ph. D. Dissertation, York University, Toronto, Canada

_____, and Nicholls, R. W., 1974, Proc. R. Soc. London A 339, 197

Deslandres, H., 1888, Compt. Rend. 106, 842

Deslandres, H., and d'Azambuja, C. R., 1905, Acad. Sci. Paris 140, 917

Diowart, J., Burns, R. P., DeMaria, G., and Inghram, J. C. P., 1959, J. Chem. Phys. 31, 1131

Fairbairn, A. R., 1966, JQSRT 6, 325

Fink, E. H., and Welge, K. H., 1967, J. Chem. Phys. 46, 4315

Fougere, P. F., and Nesbet, R. K., 1966, J. Chem. Phys. 44, 285

Fox, J. G., and Herzberg, G., 1937, Phys. Rev. 52, 638

Fraser, P. A., 1954, Canad. J. Phys. 32, 515

_____, Jarmain, W. R., and Nicholls, R. W., 1954, Astrophys. J. 119, 286

Freymark, H., 1951, Ann. Phys. 8, 221

Fujita, Y., 1970, Interpretation of Spectra and Atmospheric Structure in Cool Stars, University Park Press, Baltimore, Maryland

Gaydon, A. G., and Hurle, I. R., 1963, The Shock Tube in High-Temperature Chemical Physics, Reinhold Publishing Corp., New York

_____, 1968, Dissociation Energies and Spectra of Diatomic Molecules, Chapman and Hall, London, 3rd edition

Gruszczynski, J. S., 1968, AIAA Paper 68-665

Hagen, L. G., 1963, Ph. D. Dissertation, UCRL Report 10620, University of California

Harrington, J. A., Modica, H. D., and Libby, D. R., 1966, J. Chem. Phys. 44, 3380

Herzberg, G., 1946, Phys. Rev. 70, 762

_____, 1950, Molecular Spectra and Molecular Structure. I. Spectra of Diatomic Molecules, 2nd edition, Van Nostrand, New York

_____, 1966, Molecular Spectra and Molecular Structure. III. Electronic Spectra and Electronic Structure of Polyatomic Molecules, Van Nostrand, New York

_____, Lagerqvist, A., and Malberg, C., 1969, Can. J. Phys. 47, 2734

Hicks, W. T., 1957, UCRL Report 3696, University of California

Horton, T. E., and Menard, W. A., 1969, JPL Technical Report 32-1350

James, T. C., 1966, J. Mol. Spectry. 20, 77

Jeunehomme, M., and Schwenker, R. P., 1965, J. Chem. Phys. 42, 2406

Kayser, H., 1910, Handbuch der Spektroskopie, Vol. V, Hirzel, Leipzig

King, A. S., and Birge, R. T., 1930, Astrophys. J. 72, 19

Klemsdal, H., 1973, JQSRT 13, 517

Kovacs, I., 1969, Rotational Structure in the Spectra of Diatomic Molecules, Adam Hilger Ltd., London

Landsverk, O. G., 1939, Phys. Rev. 56, 769

Liepmann, H. W., and Roshko, A., 1957, Elements of Gasdynamics, John Wiley and Sons Inc., New York

Liveing, G. D., and Dewar, J., 1880, Proc. Roy. Soc. 30, 152

Lyddane, R. H., Rogers, F. T., and Roach, F. E., 1941, Phys. Rev. 60, 281

McBride, B. J., Heimel, S., Ehlers, J. G., and Gordon, S., 1963, NASA SP-3001

_____, and Gordon, S., 1967, NASA TN D-4097

McCallum, J. C., Jarmain, W. R., and Nichools, R. W., 1970, Spectroscopic Report 1, York University, Toronto, Canada

Messerle, G., and Krauss, L., 1967, Z. Naturforch 22a, 1744

_____, 1967, Z. Naturforch 22a, 2015

_____, 1967, Z. Naturforch 22a, 2023

Mirels, H., 1963, Phys. of Fluids 6, 1201

Moore, C. E., 1949, NBS Circular 467 (Vol. I)

Mulliken, R. S., 1930, Zeits. f. Elektrochemie 36, 605

_____, 1939, Phys. Rev. 56, 778

Nicholls, R. W., and Stewart, A. L., 1962, Allowed Transitions. Atomic and Molecular Processes, Ed. D. R. Bates, Academic Press, New York

Nicholls, R. W., 1969, Physical Chemistry Vol. 3 (Chapter 6), Academic Press, New York

_____, 1974, JQSRT 14, 233

Pauling, L., and Wilson, E. B., 1935, Introduction to Quantum Mechanics, McGraw-Hill, New York

Phillips, J. G., 1948, Apl. J. 108, 434

_____, and Davis, S. P., 1968, The Berkeley Analyses of Molecular Spectra, Vol. 2, (a) The Swan System of the C_2 Molecule; (b) The Spectrum of the H_gH Molecule

Rosen, B., 1970, Spectroscopic Data Relative to Diatomic Molecules, Pergamon Press, Toronto, Canada

Schadee, A., 1964, Bull. Astr. Inst. Neth. 17, 311

_____, 1967, JQSRT 7, 169

Schull, H., 1951, Astrophys. J. 114, 546

Schuster, R., 1888, British Association Report: "On the Present State of Our Knowledge of Spectrum Analysis"

Smith, W. H., 1969, Astrophys. J. 156, 791

Smithells, A., 1901, Phil. Mag. 1, 476

Spindler, R. J., 1965, JQSRT 5, 165

Stephenson, G., 1951, Proc. Phys. Soc. 64A, 99

Stull, D. R., and Prophet, H., 1971, JANAF Thermochemical Tables, NSRDS-NBS 37

Sviridov, A. G., Sobolev, N. N., and Sutovskii, V. M., 1965, JQSRT 5, 525

_____, and Novgorodov, M. Z., 1966, JQSRT 6, 337

_____, and Arutiunova, G. A., 1966, JQSRT 6, 875

Swan, W., 1857, Trans. Roy. Soc. Edinburgh 21, 411

Tatum, J. B., 1967, Astrophys. J. S. 14, 21

Tyte, D. C., Innanen, S. H., and Nicholls, R. W., 1967, Identification Atlas of Molecular Spectra, No. 5, The C_2 A $^3\pi_g^+$ - X' $^3\pi_u$ Swan System, C.R.E.S.S., York University, Toronto, Canada

Van der Willigen, S., 1859, Pogg. Ann. 107, 473

Vincenti, W. G., and Kruger, C. H., 1965, Introduction to Physical Gas Dynamics, John Wiley and Sons, Inc., New York

Wentink, T., Jr., Marram, E. P., Isaacson, L., and Spindler, R. J., 1967, Technical Report No. AFWL-TR-67-30, Vol. 1

Whiting, E. E., Arnold, J. O., and Lyle, G. C., 1969, NASA TN D-5088

_____, Page, W. A., and Reynolds, R. M., 1973, JQSRT 13, 837

_____, 1973, NASA TN D-7268

Wiese, W. L., Smith, M. W., and Glennon, B. M., 1966, National Standard Reference Data Series, National Bureau of Standards, 4, 1

_____, and Miles, B. M., 1969, National Standard Reference Data Series, National Bureau of Standards, 22, 2

Wollaston, W. H., 1802, Phil. Trans. Roy. Soc. London 11, 365

Zel'dovich, Y. B., and Raiser, Y. P., 1966, Physics of Shock Waves and High-Temperature Hydrodynamic Phenomena, Vol. I, Academic Press, New York